Title

Keeping the Noise Down: The Role of Cellular Compartmentalization In Maintaining Robust Gene Expression

Author

Mayer, Alexander

Publication Date

2023

Peer reviewed|Thesis/dissertation

UNIVERSITY OF CALIFORNIA
Los Angeles

Keeping the Noise Down: The Role of Cellular Compartmentalization In Maintaining Robust Gene Expression

A dissertation submitted in partial satisfaction
of the requirements for the degree
Doctor of Philosophy in Mathematics

by

Alexander Jacob Mayer

2023

ABSTRACT OF THE DISSERTATION

Keeping the Noise Down: The Role of Cellular Compartmentalization In Maintaining Robust Gene Expression

by

Alexander Jacob Mayer
Doctor of Philosophy in Mathematics
University of California, Los Angeles, 2023
Professor Marcus Roper, Chair

Mathematical modeling has played a pivotal role in advancing the understanding of gene expression regulation, operating at both the molecular and cellular levels. In this dissertation, stochastic models and simulations will be employed to explore the impact of various forms of cellular compartmentalization, such as the formation of functionally distinct RNA condensates or the establishment of nuclear territories in syncytia, on the robust spatiotemporal control of gene expression within cells. The highlighted model system, multinucleated filamentous fungi, serves as a prime example of global coordination and compartmentalization within expansive cytoplasmic environments. To complement these modeling efforts, image analysis on live cell data will be employed to quantify and localize RNAs, providing a means by which key model parameters can be inferred and the model's validity can be assessed within physiologically relevant contexts.

The dissertation of Alexander Jacob Mayer is approved.

Tom Chou

Chenfanfu Jiang

Roy Wollman

Marcus Roper, Committee Chair

University of California, Los Angeles

2023

TABLE OF CONTENTS

LIST OF FIGURES

LIST OF TABLES

ACKNOWLEDGMENTS

I would like to offer my utmost thanks and gratitude to everyone who guided and supported me in this journey, which has culminated in the completion of this dissertation. You have provided me with your many insights, knowledge and compassion throughout the course of my research.

I would first like to extend my most sincere gratitude to Marcus Roper, my Ph.D. advisor, who has been my mentor, strongest supporter, and a fountain of knowledge for me throughout this process. You have opened up the world of quantitative cell biology to me, and have been so important to my development as a scientist and researcher. In addition, I am so appreciative of your gentle sense of humor, your patience and good nature.

Many thanks to everyone at the Gladfelter lab. I'd especially like to acknowledge Amy Gladfelter and Grace Mclaughlin for their invaluable contributions to my research, including manuscript revisions and additions, guidance in model development, and distribution of biological data.

I would also like to acknowledge Jiayu Li for her significant contributions in smFISH image analysis, which played a crucial role in detecting RNAs and measuring transcriptional activity relevant to the third chapter of this dissertation.

I am also thankful to the rest of my Committee- Tom Chou, Chenfanfu Jiang, and Roy Wollman for sharing their respective expertise in mathematical modeling and biology, and for providing me with valuable feedback after my ATC and defense.

Finally, I would like to thank my friends and family for their interest in and support for my work during these past six years. You have played an essential role in making this thesis possible.

VITA

2017	Bachelors of Science in Mathematics and Physics, Rensselaer Polytechnic Institute, Troy, New York
2019	Masters of Science in Applied Mathematics, UCLA, Los Angeles, California

PUBLICATIONS

Syncytial Assembly-Lines: Consequences of Multinucleate Cellular Compartments for Fungal Protein Synthesis. Featured in Syncytia: Origin, Structure, and Functions

CHAPTER 1

Introduction

Protein synthesis serves as a foundational pillar within cellular systems, conducting a myriad of functions. It propels countless enzymatic pathways, facilitating appropriate responses to external stimuli and supporting proliferation, while also playing a crucial role in shaping cellular morphology. The conversion of genetic information into functional protein products is termed *gene expression*. This complex and intrinsically stochastic process, coupled with its spatiotemporal regulation, has been a fundamental driver in molding adaptation and speciation throughout all domains of life [5]. In the span of just the last 25 years, groundbreaking cellular imaging methods like single molecule fluorescence in situ hybridization (smFISH) [6] and sequencing technologies such as RNA-Seq [7] have surfaced, providing biologists with unprecedented capabilities to characterize and study gene expression and its regulation.

The compartmentalization of the cell into the nucleus and cytoplasm represents the fundamental organizational framework governing gene expression in eukaryotes [8]. This structural adaptation enables the efficient compaction of genetic information into distinct chromosomal domains with varying condensation levels, thereby affecting accessibility to cellular machinery. It also aids in RNA splicing before cytoplasmic translation, reducing the probability of aberrant protein production [9]. Consequently, the segregation of genetic material within the nucleus promotes a wider spectrum of protein synthesis, marked by an elevated level of precision surpassing what can be achieved in an undivided cellular environment. The further sub-compartmentalization of the cytosol into membrane-enclosed organelles in

eukaryotes conferred the ability for the division of labor in metabolic processes, enhancing operational efficiency [10]. Organelle-specific macro-molecules are frequently transported to their intended locations through active mechanisms. For instance, this can be achieved using molecular motors positioned along the cytoskeletal network [11], or through molecular diffusion along a maintained concentration gradient [12]. Central to this translocation process is a balance between the energy investment required for transportation and the efficiency gains derived from the precise spatiotemporal control of gene products [13]. In addition to specialized membraned-organelles, cells contain various types of sub-compartments that lack conventional membranes and enable less restrictive exchange of components between adjacent sub-compartments. In some instances, a clear boundary exists, separating sub-compartments, as observed in the case of phase-separated biomolecular condensates [14]. In other cases, the subcompartments may delineate specific regions of influence in the cytosol, such as perinuclear spaces that are often enriched in signaling or intrinsically disordered proteins [15]. Syncytial (multinucleated) filamentous fungal cells present a captivating paradigm of sub-compartmentalization and its profound impact on robust spatiotemporal protein synthesis. Immersed within a shared cytoplasm, syncytial nuclei encounter the distinct situation of orchestrating coordinated expression while retaining a certain level of individual autonomy. In fungal, mammalian and drosophilla syncytia, nuclei have the ability to delineate individual cytoplasmic territories through the emission of repulsive microtubules that hinder clustering [16–18]. The degree of intermingling among what we term as nuclear neighborhoods is dictated by the diffusivity of the associated molecules within these specific zones. This diffusivity can also be influenced by potential interactions with microtubular networks, which could enable directed transport [19], or interactions with biomolecular condensates that might restrict diffusion beyond perinuclear regions [20].

Mathematical models play a vital role in deciphering the dynamic features observed within cells, such as circadian rhythms [21–23] or cell-cycle processes [24, 25], at a molecular level.

These models often elucidate both deterministic and stochastic features, providing a holistic understanding of cellular behavior and the associated cell-to-cell variability inherent in these processes. These models conventionally operate under the assumption of homogeneously mixed interacting species across the relevant compartments — the nucleus and the cytoplasm, often disregarding other spatial features [26–28]. Even in syncytial contexts, mathematical models tend to overlook the potential exchange of gene products between nuclei, along with their associated time scales and distributions [29, 30]. Thus, our comprehension of cellular sub-compartmentalization mechanisms and their linked spatiotemporal distributions remains in its early stages.

In this dissertation, my goal is to address these questions through the development of mathematical models of varying spatial complexities, complemented by live cell image analysis. This research will be divided into three chapters, each considering increasingly broader levels of sub-compartmentalization and their respective impact on the spatiotemporal control of gene expression. A central theme in this research is the exploration of the balance between efficiency and precision in gene expression. Our model findings illuminate that gene product diffusion into distinct sub-compartments within cells bestows expression noise tolerance, a factor unaccounted for in standard, well-mixed gene expression models.

Chapter 2 comprises a manuscript currently under review, co-authored with Grace McLaughlin, Amy Gladfelter, and Marcus Roper. Within this chapter, we explore a well-mixed model of gene expression within individual nuclear neighborhoods. In this phenomenological model, RNA molecules may phase-separate into dilute and dense phases in a concentration-dependent manner, forming distinct cytoplasmic sub-compartments with disparate kinetic parameters. A combination of analytic techniques and stochastic simulations reveal that fluctuations in the dilute abundances of RNA molecules and the proteins they encode can be suppressed by rapid diffusion of these molecules into biomolecular condensates that favor localization near nuclei in syncytia. The suppression of fluctuations permits both robust and

localized expression, which may potentially play a role in preserving independent cell cycle regulation in syncytia (Dundon et al., 2016).

Chapter 3 features a manuscript co-authored with Grace McLaughlin, Jiayu Li, Amy Gladfelter, and Marcus Roper. Within this chapter, we delve into the compartmentalization of syncytial cells into nuclear sub-compartments, which assume rapid protein exchange between adjacent sub-compartments. Our model examines the gene expression variability within nuclear sub-compartments across various nuclear distributions, unveiling a diffusive averaging mechanism. This mechanism effectively dampens protein noise, distinguishing it from mononucleated cells with equivalent expression kinetics. These results reveal a potential paradigm shift towards less investment in precise transcription in favor of efficient yet more stochastic transcription in syncytial cells. To probe this, transcription profiles derived from smFISH images of homologous genes in the closely related mononucleated cell *Saccharomyces cerevisiae* and the syncytial *Ashbya gossypii* are compared, which is broadly supportive of the hypothesis.

The final chapter incorporates the modeling sections I wrote from a collaborative review on fungal syncytia, co-authored by Grace McLaughlin, N. Louise Glass, Alexander Mela, Amy Gladfelter, and Marcus Roper. Within the mathematical models featured in this chapter, we depart from the prior assumption of well-mixed cytoplasmic environments. Our focus shifts towards understanding the influence of inherent time scale separations in protein synthesis and diffusion on the spatiotemporal protein distributions within a syncytium. These findings underscore the unique challenges that fungal syncytia face in balancing the need to coordinate the responses of nuclei in a shared cytoplasm, while still preserving nuclear autonomy and minimizing competition for shared resources.

CHAPTER 2

The Role of RNA Condensation in Reducing Gene Expression Noise

2.1 Introduction

Gene expression is a noisy process, ensuring that even genetically identical cells receiving common cues from their environment may exhibit a range of protein copy numbers. In some cases, resulting cell to cell variability might be useful [31, 32]. However, in stable environments, cells generally benefit from consistent expression of proteins, and high gene expression noise may impair cellular function [33–35]. Low mRNA copy numbers are a major contributor to protein copy noise since translation to proteins amplifies small absolute variations in mRNA copy number [36]. Yet, mRNA copy numbers are often low - at 10 mRNAs or fewer per cell, across the majority of the genome in *Saccharomyces cerevisiae* [37], and transcription rates (number of mRNAs per gene per unit time) are much smaller than translation rates (number of proteins per mRNA copy per unit time) across the genomes of yeast, mice, humans and E. coli in their fast growing phases [38]. Hausser et al [38] argue that energetics constrain transcription rates; the total energetic cost of translation is invariant if protein copy numbers are held fixed, but the energetic burden of transcription, although relatively smaller, is reduced if mRNA copy numbers are kept small. Economical transcription may also reduce transcriptional interference when two genes are simultaneously transcribed. Negative interactions between different transcriptional activities can occur, such as elongating RNA polymerases obstructing each other, repressors bound to one operon overlapping with

a second operon [39], or genome conformational changes that expose one operon but mask another [40].

In both bacteria and higher eukaryotes, the primary mode of transcription is through bursting [41–43]. During bursty transcription, mRNAs are synthesized in pulses, fluctuating in both intensity and frequency. Bursts are thought to arise as a result of the reversible interactions of the pre-initiation complex (PIC) with a gene's promoter. When the PIC is bound, the RNA polymerase's affinity for binding to the transcription start site is dramatically increased, and multiple transcription events can occur while the gene is in this "on" state [44]. Since chromatin remodeling is required for gene activation, there is a fundamental cost to fast switching between promoter states [45]. We assume efficiency is achieved by minimizing the frequency of gene activity, and allowing intense bursts when in the "on" state to meet the required mean mRNA abundance. However bursty transcription introduces additional noise into expression. In the context of infrequent, intense bursts, mRNA variability will drastically increase, which is especially pronounced in systems with small mean mRNA populations, resulting in large steady state fluctuations in protein.

For many genes, protein abundance must be tightly regulated for proper function of the cell [34, 46, 47], and there exist many regulatory mechanisms in gene expression that can mitigate fluctuations in protein abundance [48], [27]. Negative feedback has been observed at each level of gene expression, resulting in gene networks that can be analyzed for their ability to control noise in expression [27]. These networks can theoretically drive expression noise below Poisson levels, but can introduce substantial deficits in the cell's energy economy [49]. For example, Lestas et al. [50] find that in systems with nonlinear real-time feedback control, signal molecules must be synthesized at rates far exceeding those of the target molecule in order to meaningfully suppress noise. In contrast, cellular compartmentalization may be an energetically efficient method for filtering expression noise if the proteins that form the

compartments are long-lived [49]. In particular, phase separation has been theorized to play a role in post-translational regulation of genes. Klosin et. al [51] provide theoretical and experimental evidence of this idea; showing that concentration-dependent phase separation of proteins can drive protein fluctuations to the minimum Poisson noise limit of the network. Deviri and Safran [52] extended this theory to multi-component phase separation, and derived criteria on their phase diagrams under which concentration buffering may occur. They hypothesized that in genes that are sensitive to noise, selective pressures may act to optimize concentration buffering, though the extent to which noise is suppressed in these systems remains less clear.

One such class of multi-component condensates are ribonucleoprotein (RNP) granules, which form as a result of multivalent interactions between mRNAs and RNA binding proteins. RNA binding proteins often contain intrinsically disordered domains, which promote RNP granule assembly and contribute to their dynamic properties [53]. RNP granules can subcompartmentalize the cytosol for regulated colocalization or segregation of interacting proteins and RNAs [54]. Notably, mRNAs that are sequestered into droplet phases may be inaccessible to translation [55], reducing effective mRNA copy numbers within the cell. Although, at first consideration, reducing mRNA copy numbers would appear to increase the noise in protein numbers, here we analyze how, by reducing fluctuations in mRNA copy numbers, phase separation may paradoxically reduce noise of gene expression.

In this chapter, we analyze several biophysical scenarios in which mRNAs are segregated into distinct phases. The central and unifying assumption in all our models will be that mRNAs in the droplet phase are translationally inert, so that only "free" mRNAs are accessible to ribosomes. Our manuscript has four main parts. Throughout, we approximate transcription, translation, and decay as Poisson processes, which we model via numerical simulations, or via analyical moment calculations. In Part 1, we approximate the dynamics of the two

mRNA state system by a random-telegraph process, and quantify noise repression with exact and asymptotic results, providing baseline results with which to compare systems in which phase-separation is incorporated. In Part 2, we discuss several models that incorporate nonlinear transition rates to phenomenologically emulate the physics of phase separation. The models will chiefly be differentiated by the way in which phase separation affects mRNA stability. Presence of RNPs may either decrease or increase mRNA lifetimes; even when homologous RNA/protein pairs are expressed in closely related species. For example, in the yeast *Saccharomyces cerevisiae* and in the genetically similar filamentous fungus *Ashbya gossypii*, the mRNA *CLN3* is known to form phase separated droplets with a protein partner Whi3. When Whi3 is deleted in *S. cerevisiae*, *CLN3* lifetimes increase [56], suggesting that phase separated mRNAs turnover more quickly than dilute mRNAs in cytosol. Conversely, *A. gossypii*, phase separation increases *CLN3* lifetimes [57]. To address both of these functions of RNP bodies, we separately consider cases where mRNA decay primarily occurs in the cytoplasm and in the dense phase. In both models, we run stochastic simulations to determine how these mechanisms influence noise in gene expression, with particular focus on gene networks with infrequent, bursty transcription. Similar to previous modeling approaches [51], in Part 2, we consider a deterministic critical concentration of mRNA to trigger the onset of phase separation. However, in Part 3, we introduce a phenomenological model of time fluctuation phase separation thresholds and through simulations and analytical results, show that robust suppression of protein noise remains possible, even when the threshold for mRNA concentration is allowed extensive variation. Finally in Part 4, to support our theoretical findings, we perform analysis on existing smFISH data on the distribution of *CLN3* mRNA transcripts within cells of the model filamentous fungus, *Ashbya gossypii*.

2.2 Materials and methods

2.2.1 Analytical Methods for Quantifying Noise

For a well-mixed, chemically reacting system consisting of memory-less reactions, the chemical master equation can be utilized to determine the evolution of the system in a probabilistic sense [58]. Consider a system in which s different species react, and are present, at time t, at abundances $\boldsymbol{N} = (N_1, \ldots, N_s)$. The reaction $R_i(\boldsymbol{N})$, $i = 1, 2, \ldots, n$, is defined by the population update map $\boldsymbol{N} \to \boldsymbol{N} + \boldsymbol{\eta}_i$, is assumed to have rate $a_i(\boldsymbol{N})$, which can be derived from the law of mass action. The probability $P(\boldsymbol{N}, t)$ that the system is in state $\boldsymbol{N}$ at time t satisfies the chemical master equation

$$\frac{\partial P(\boldsymbol{N}, t)}{\partial t} = \sum_{i=1}^{n} \left[a_i(\boldsymbol{N} - \boldsymbol{\eta}_i) P(\boldsymbol{N} - \boldsymbol{\eta}_i, t) - a_i(\boldsymbol{N}) P(\boldsymbol{N}, t) \right] \tag{2.1}$$

This infinite set of differential equations is not easily solved, but it is relatively simple to extract the statistical moments of the probability distribution. It can be shown [59] that for any continuously differentiable function $\psi(\boldsymbol{N}, t)$,

$$\frac{d\langle \psi(\boldsymbol{N}, t) \rangle}{dt} = \left\langle \sum_{i=1}^{n} \left[\psi(\boldsymbol{N} + \boldsymbol{\eta_i}, t) - \psi(\boldsymbol{N}, t) \right] a_i(\boldsymbol{N}) \right\rangle \tag{2.2}$$

In particular, consider $\mu_{\boldsymbol{M}}(t) = \langle N_1^{m_1} \ldots N_1^{m_1} \rangle$, which denotes the $\boldsymbol{M}$th order moment of $\boldsymbol{N}$. If all reactions a_i are linear in $\boldsymbol{N}$, then

$$\frac{d\mu_{\boldsymbol{M}}(t)}{dt} = F_{\boldsymbol{M}}(\underline{\mu}(t)), \tag{2.3}$$

where $F_{\boldsymbol{M}}$ is only a function of moments of order less than or equal to $\boldsymbol{M}$. Thus for any desired moment, we can solve a closed system of differential equations to determine its time evolution.

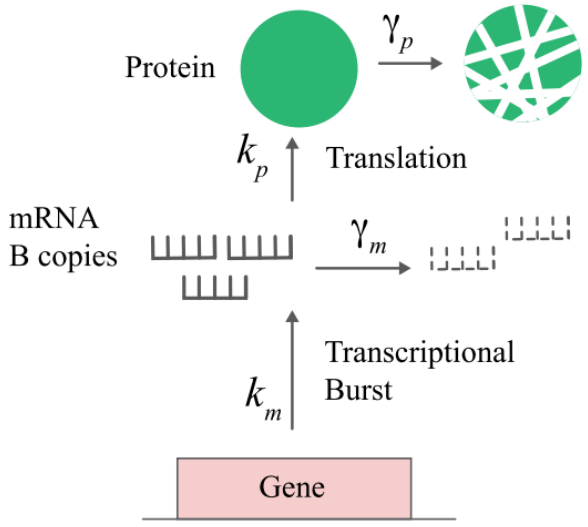

Event	Population Update	Reaction Rate
Transcription	$m(t) \to m(t) + B$	k_m
Translation	$p(t) \to p(t) + 1$	$k_p m(t)$
mRNA Decay	$m(t) \to m(t) - 1$	$\gamma_m m(t)$
Protein Decay	$p(t) \to p(t) - 1$	$\gamma_p p(t)$

(2.1) Left panel: Schematic of gene expression without mRNA state changes. A random number B of mRNAs are transcribed with rate k_m; mRNAs are tranlated into proteins at rate k_p and decay at rate γ_m. Protein decay rate is γ_p. Right panel: Reaction rates and population updates for unregulated gene expression model.

2.2.2 Analysis of gene expression without mRNA state changes

Let k_p, γ_m, and γ_p represent the rates of translation, mRNA decay, and protein decay, respectively. Additionally, we assume that transcription occurs in instantaneous bursts at a rate of k_m. During each transcription event, B mRNAs are transcribed, where B follows a geometric distribution. This model of gene expression is derived from the widely used random telegraph model [42, 60], under the assumption of infrequent gene activity (see the analysis in S1 Appendix). Roles of the kinetic constants in the update model (Eqn. 2.1) are summarized in Fig 2.1 and Table 2.1. By Equation 2.2, the moment equations of this bursting system are,

up to second order moments:

$$\begin{aligned}
\dot{\langle m\rangle} &= k_m\langle B\rangle - \gamma_m \langle m\rangle \\
\dot{\langle p\rangle} &= k_p \langle m\rangle - \gamma_p \langle p\rangle \\
\dot{\langle m^2\rangle} &= k_m \left(2\langle B\rangle^2 - \langle B\rangle\right) + \left(\gamma_m + 2k_m\langle B\rangle\right)\langle m\rangle - 2\gamma_m \left\langle m^2\right\rangle \\
\dot{\langle p^2\rangle} &= k_p \langle m\rangle + \gamma_p \langle p\rangle + 2k_p \langle mp\rangle - 2\gamma_p \left\langle p^2\right\rangle \\
\dot{\langle mp\rangle} &= k_p \left\langle m^2\right\rangle + k_m\langle B\rangle \langle p\rangle - \left(\gamma_m + \gamma_p\right)\langle mp\rangle
\end{aligned} \tag{2.4}$$

From the first two equations, we immediately find that

$$\begin{aligned}
\overline{\langle m\rangle} &= \frac{k_m\langle B\rangle}{\gamma_m} \\
\overline{\langle p\rangle} &= \frac{k_p\overline{\langle m\rangle}}{\gamma_p},
\end{aligned} \tag{2.5}$$

where $\overline{\langle\cdot\rangle}$ denotes the steady-state ensemble average. The relative magnitude of fluctuations at equilibrium can be characterized by the quantity

$$CV^2 = \frac{\overline{\langle p^2\rangle} - \overline{\langle p\rangle}^2}{\overline{\langle p\rangle}^2} \tag{2.6}$$

In this elementary gene expression model, we find that

$$CV^2 = \frac{1}{\overline{\langle p\rangle}} + \frac{1}{\left(1 + \frac{\gamma_m}{\gamma_p}\right)}\frac{\gamma_m}{k_m} \tag{2.7}$$

Observe that the first term in (2.7) represents Poisson noise; it is set only by the target protein abundance and is unaffected by any of the chemical rates. By contrast, the second term is affected by the ratios of $\frac{\gamma_m}{\gamma_p}$, and $\frac{k_m}{\gamma_m}$. Focusing on the first ratio; $\frac{\gamma_m}{\gamma_p}$ is the ratio of the protein to the mRNA lifetime. Increasing this ratio decreases CV^2, since transcribing short lived mRNAs into long-lived proteins smooths out the rapid fluctuations in mRNA distribution. The second ratio $\frac{k_m}{\gamma_m}$ appears in equation (3.2). If $\langle B\rangle$ is held constant, then

$\frac{k_m}{\gamma_m}$ is proportional to $\overline{\langle m \rangle}$. Increasing this ratio decreases CV^2, since this would increase the mean mRNA abundance and thus decreases relative fluctuations in mRNAs. If $\overline{\langle m \rangle}$ is held constant, then the ratio is inversely proportional to $\langle B \rangle$. Increasing this ratio then decreases the mean burst size, decreasing the variance in burst distribution and therefore decreasing CV^2.

2.2.2.1 Numerical Simulation

Our chemical reaction model is a continuous time Markov chain. Numerical simulations were performed using Gillespie's Algorithm, which provide statistically accurate trajectories [61]. All processes, $\boldsymbol{N}(t)$, considered in this work are ergodic, meaning that the time average $\langle \boldsymbol{N} \rangle_T$ converges in squared mean to the ensemble average $\overline{\langle \boldsymbol{N} \rangle}$ as $T \to \infty$ Long time averages of multiple trajectories were computed to estimate statistical properties such as means and variances of state variables.

Reaction constants and mean molecule abundances were chosen in accordance with studies on gene expression kinetics in yeasts. In our simulations, we set $\overline{\langle m \rangle} = 20$ and $\overline{\langle p \rangle} = 2000$. These values were chosen to be consistent with the results of Gygi et al. [62] who found across a large number of genes in *Saccharomyces Cerevisiae* that mRNAs abundance ranged approximately from 1-500 copies/cell, while protein abundance varied from 10^3-10^5 copies/cell. The simulated mean abundances were specifically chosen to be small, so that relative fluctuations are large in the absence of noise suppression mechanisms. Pelechano et al. [63] found that for most genes in yeast, between 2-30 mRNAs are transcribed per minute, which, in our model, represents the net transcription rate, $k_m \langle B \rangle$, the mean number of bursts per minute times the average burst size. Unless explicitly varied, we set $k_m = .05$ mRNAs/min and $\langle B \rangle = 20$, so that the net transcription rate of 1 mRNA/min falls on the lower end of the spectrum measured by Pelechano et al. The cytoplasmic decay rate was set

Parameter	Base Value(s)
k_m (Burst frequency)	.05 min^{-1}
k_p (Translation rate)	2 Proteins$(\text{min} \cdot \text{mRNA})^{-1}$
γ_m (Cytoplasmic mRNA decay rate)	.05 min^{-1}
γ_p (Protein decay rate)	.02 min^{-1}
$\langle B \rangle$ (Mean burst size)	20
$\overline{\langle m \rangle}$ (Mean mRNA abundance)	20
$\overline{\langle p \rangle}$ (Mean protein abundance)	2000

(2.1) Base reaction rates and molecular species abundances used in numerical simulations.

to $\gamma_m = .05$ mRNAs/min, so that we achieve a mean mRNA abundance $\overline{\langle m \rangle} = 20$ while still in agreement with physiologically relevant mRNA decay rates quantitated by Chia et al. [64]. For all simulations, the protein decay rate was set to $\gamma_p = .02$ proteins/min, so that $t_{1/2} \approx 35$ minutes, consistent with the findings of Belle et al. [65] on protein half-life, across 3,751 genes in *Saccharomyces cerevisiae*. Finally we chose the translation rate $k_p = 2$ proteins/min, which ensures that $\overline{\langle p \rangle} \approx 2000$ in all of our simulations. These rates are summarized in Table (2.1).

2.2.3 FISH Methods

Wildtype *A. gossypii* were grown in 20 ml Ashbya full media (AFM) with ampicillin (100 μg/ml) in a 125 ml baffled glass flask, shaking at 30°C for $\approx$ 16 hr. The cells were then fixed with 3.7% (v/v) formaldehyde for 1 hr at 37°C. After fixation, the cells were collected by centrifugation at 300 rpm for 5 min and washed twice with DEPC treated ice cold Buffer B (1.2 M sorbitol, 0.1 M potassium phosphate, pH 7.5). The cells were next suspended in 1 ml spheroplasting buffer (10 ml buffer B, 2 mM vanadyl ribonucleoside complex) and transferred to a new RNase-free microcentrifuge tube. The cell wall was digested by incubating the cells with 1.5 mg Zymolase (Sunrise Science) at 37°C for $\approx$ 40 min until cells were phase dark.

Cells were collected by centrifuging at 2000 rpm for 2 min and washed twice with Buffer B. The cells were then incubated in 1 ml RNase free 70% EtOH at 4°C for 4 hr. Stellaris *CLN3* TAMRA RNA FISH probes were prepared by resuspending the oligonucleotide blend in 20 ul of TE buffer (10 mM TrisCl, 1 mM EDTA pH 8) to make a 250 μM solution. A 1:10 dilution was made of the probe suspension as the working concentration to add to cells. After incubation at 4°C, the cells were resuspended in 1 ml wash solution (20× SSC, 10% v/v deionized formamide) and allowed to reach room temperature. The cells were then resuspended in 100 μl hybridization buffer (1 g Dextran sulfate, 10 mg E. coli tRNA, 2 mM vanadyl ribonucleoside complex, 2 mg BSA, 20× SSC, 10% v/v deionized formamide) with 1 μl of 25 μM probe added. The cells were left to incubate in the dark at 37°C overnight. The next day, cells were washed with 1 ml wash buffer and then resuspended in 1 ml wash buffer and incubated at 37°C for 30 min in the dark. The cells were then resuspended in 500 μl wash buffer with 1 μl Hoechst at 1mg/ml (Thermo Fisher) and incubated in the dark for 15 min at room temperature. The cells were washed with 500 μl wash buffer with as much buffer removed as possible. The cells were mounted on a RNase free microscope slide with 20 μl mounting media (ProLong Gold antifade reagent, Invitrogen) and RNase free coverslip. The slide was sealed with nail polish and imaged using a Nikon Eclipse widefield microscope and a Plan Apo λ 100×/1.45 oil Ph3 DM objective. Images were taken using phase, 405 nm, and 561 nm laser sequentially through a z-stack with an Andor Zyla VSC-06258 camera.

A multi-step image analysis algorithm extracted cell boundaries and mRNAs contained within cells. Steerable filters were applied to the phase contrast image stacks, to find the edges of cells in their mid-point planes, and projected to form 2D images. The outlines of cells were traced in the projected images using Adobe Illustrator software running on an Apple iPad. From the 2D-segmentation of cells, an accurate 3D segmentation was generated by locating the optimal depth to embed the 2D mask, based on maximizing the fluorescent intensity of the 2D mask. The embedding depth of the 2D mask was allowed to vary from place to place within the mask. The mask was then swept to 3D, by skeletonizing the mask,

measuring the diameter of the 2D mask at each skeleton point, and including each 3D voxel within half a diameter from each skeleton point. We detected each mRNA within the 3D segmented hyphal volume by applying a median filter and considering each local maximum as a candidate mRNA. Signal to noise ratios were calculated by applying a minimum filter with radius $0.55\,\mu$m, to calculate the background intensity for each peak, and by dividing peak by background intensities. Spots with signal to noise ratios of less than 1.4 were discarded. Background intensities were subtracted from the image, and integrated intensities were calculated for each detected spot, as the sum of the positive background subtracted voxel intensities within 0.22μm of each detected peak. A single transcript integrated intensity was calculated for each 3D segmented hyphal volume, as the 25 percentile integrated intensity. All spots were then assigned a weight (estimated number of transcripts), by dividing them by this single transcript intensity, and rounding to the nearest integer. Simultaneously, we segmented all nuclei within the each hypha, by a two-level Otsu threshold, in which we discarded all detected objects with volumes less than $5.4\mu\text{m}^3$. Our analysis included a total of 81 3D-segmented hyphae, and 1244 nuclei, of which 263 were identified as being in active *CLN3* transcription.

2.3 Results

2.3.1 Linear Stochastic Phase Separation Model

Common to all phase separation models considered, we assume that mRNA may exist in two states outside the nucleus. In the active state, mRNAs may be translated and have a decay rate of γ_m. In the inactive state, mRNAs no longer participate in translation and may either be completely stable or decay at rate γ_a. To gain understanding of how mRNA state changes may affect protein copy number noise, and develop results that may be compared against nonlinear phase separation models, we first investigate a basic state switching model. The model is diagrammed and the reactions are summarized in in Figure 2.2. In this model,

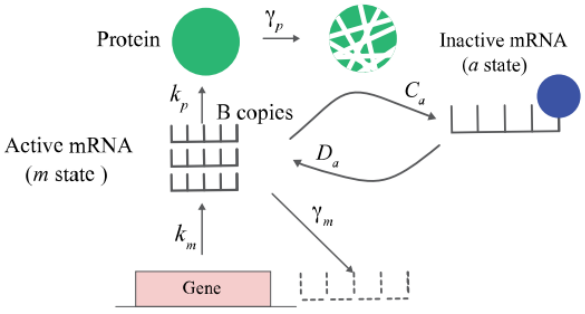

Event	Population Update	Reaction Rate
Transcription	$m(t) \to m(t) + B$	k_m
Translation	$p(t) \to p(t) + 1$	$k_p m(t)$
mRNA Decay	$m(t) \to m(t) - 1$	$\gamma_m m(t)$
Protein Decay	$p(t) \to p(t) - 1$	$\gamma_p p(t)$
Deactivation	$m(t) \to m(t) - 1$ $a(t) \to a(t) + 1$	$C_a m(t)$
Reactivation	$m(t) \to m(t) + 1$ $a(t) \to a(t) - 1$	$D_a a(t)$

(2.2) Left panel: Schematic of Stochastic State Switching Model. In addition to the gene expression processes shown in Fig 2.1, mRNAs transition from active to inactive states, and back, with respective rates C_a, D_a. Right panel: Reactions and rates for state switching model.

mRNAs spontaneously become inactive and the probabilities per unit time of switching between the two states are constant. While the linear kinetics of this system differ from those of phase separation, which is inherently nonlinear, its simplicity permits the computation of exact values for steady state coefficients of variation, which can be compared with the phase separation model. Before calculating these exact formulas, we first performed stochastic simulations on this reaction network for different values of the active-to-inactive transition rate C_a (Fig. 2.3). Qualitatively, we see that by increasing the value of C_a, we effectively shift mRNA copy number noise from the active mRNAs to the inactive mRNAs, resulting in smaller absolute variations in protein copy number, which is only sensitive to active mRNA fluctuations. We next performed exact calculations on this system to determine the extent to which state transitions reduce protein fluctuations.

Similar to the single state mRNA case, the state-switching system again defines a continuous-time Markov process, so equation (2.2) can be used to write down the moment

equations for the first and second moments:

$$
\begin{aligned}
\langle \dot{m} \rangle &= k_m \langle B \rangle - (\gamma_m + C_a) \langle m \rangle + D_a \langle a \rangle \\
\langle \dot{p} \rangle &= k_p \langle m \rangle - \gamma_p \langle p \rangle \\
\langle \dot{a} \rangle &= C_a \langle m \rangle - D_a \langle a \rangle \\
\langle \dot{m^2} \rangle &= k_m \left(2\langle B \rangle^2 - \langle B \rangle \right) + (2k_m \langle B \rangle + \gamma_m + C_a) \langle m \rangle + D_a \langle a \rangle - (2\gamma_m + 2C_a) \langle m^2 \rangle + 2D_a \langle ma \rangle \\
\langle \dot{p^2} \rangle &= k_p \langle m \rangle + \gamma_p \langle p \rangle - 2\gamma_p \langle p^2 \rangle + 2k_p \langle mp \rangle \\
\langle \dot{a^2} \rangle &= C_a \langle m \rangle + D_a \langle a \rangle - 2D_a \langle a^2 \rangle + 2C_a \langle ma \rangle \\
\langle \dot{mp} \rangle &= k_m \langle B \rangle \langle p \rangle + k_p \langle m^2 \rangle - (\gamma_m + \gamma_p + C_a) \langle mp \rangle + D_a \langle pa \rangle \\
\langle \dot{ma} \rangle &= -C_a \langle m \rangle + (k_m \langle B \rangle - D_a) \langle a \rangle + C_a \langle m^2 \rangle + D_a \langle a^2 \rangle - (\gamma_m + C_a + D_a) \langle ma \rangle \\
\langle \dot{pa} \rangle &= C_a mp + k_p \langle ma \rangle - (\gamma_p + D_a) \langle pa \rangle
\end{aligned}
\tag{2.8}
$$

where dotted quantities represent time derivatives. At equilibrium, these linear equations can be solved exactly for steady-state moments. First we find that $\overline{\langle m \rangle} = \frac{k_m \langle B \rangle}{\gamma_m}$ so, surprisingly, inactivation of mRNAs does not affect their equilibrium copy number. In particular from Equation 2.6 we find that for fixed $\overline{\langle m \rangle}, \overline{\langle a \rangle}$ and $\overline{\langle p \rangle}$

$$
\begin{aligned}
CV^2 = &\frac{1}{\overline{\langle p \rangle}} \\
&+ \frac{\gamma_p \left(D_a \left(D_a \langle B \rangle + \gamma_p \right) \overline{\langle a \rangle} + \left(D_a + \gamma_m \right) \left(D_a + \gamma_p \right) \langle B \rangle \overline{\langle m \rangle} \right)}{\left(D_a \overline{\langle a \rangle} + \left(D_a + \gamma_m \right) \overline{\langle m \rangle} \right) \left(D_a \gamma_p \overline{\langle a \rangle} + \left(D_a + \gamma_p \right) \left(\gamma_m + \gamma_p \right) \overline{\langle m \rangle} \right)}.
\end{aligned}
\tag{2.9}
$$

If state-switching is a slow process (i.e $D_a \ll \gamma_p, \gamma_m$), then equation (2.9) reduces to equation (2.7). However, in the limit that mRNA state switching is much faster than mRNA or protein decay, (i.e $D_a \gg \gamma_p, \gamma_m$), we have

$$
CV^2 \approx \frac{1}{\overline{\langle p \rangle}} + \frac{\frac{\gamma_m}{k_m}}{\frac{\overline{\langle a \rangle}}{\overline{\langle m \rangle}} + \left(1 + \frac{\gamma_m}{\gamma_p} \right)}.
\tag{2.10}
$$

Again, the first term is just the Poissonian noise of the one dimensional protein birth-death

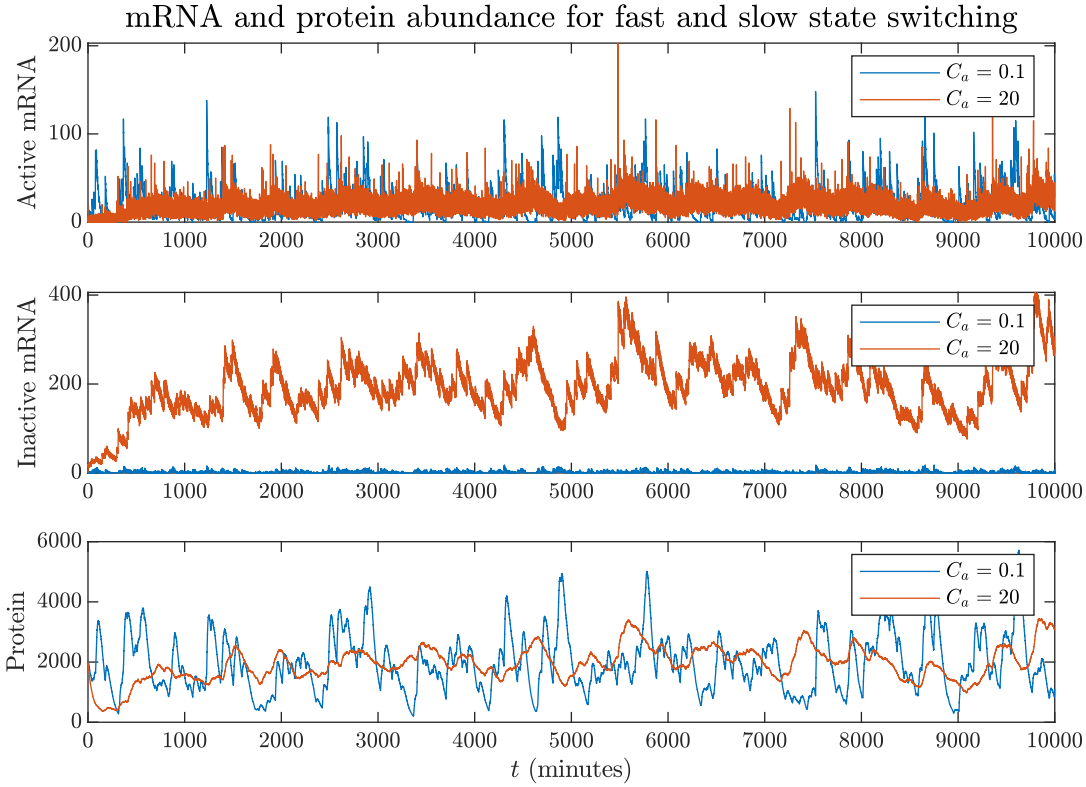

(2.3) Two sample trajectories for model in which mRNAs can stochastically switch between active and inactive states. By increasing the reaction rate for deactivation, we can decrease the magnitude of fluctuations about the common mean protein abundance of $\overline{\langle p \rangle} = 2000$. For both time series, we have $k_m = 0.05$, $k_p = 2$, $\gamma_m = 0.05$, $\gamma_p = 0.05$, $D_a = 1$, $\langle B \rangle = 20$.

process, while the second term encodes the noise due to transcription and state switching. This term shows the same dependence upon rates k_m/γ_m and γ_m/γ_p as for unregulated translation, but also decreases monotonically with the ratio $\overline{\langle a \rangle}/\overline{\langle m \rangle}$; meaning that the inactivated mRNAs decrease protein noise, for identical transcriptional burden. We see more clearly the role of mRNA modifications when we write the transcription dependent part of CV^2 as

$$CV^2_{\text{Transcription}} = \frac{\langle B \rangle}{\overline{\langle a \rangle} + \overline{\langle m \rangle}\left(1 + \frac{\gamma_m}{\gamma_p}\right)} \tag{2.11}$$

and note that the term in the denominator is close to the total (active and inactive) mRNA

copy number; inactivation of mRNAs buffers the system and creates an effectively larger pool of mRNAs, with effectively smaller Poissonian noise. Note however that only the factor $\overline{\langle m \rangle}$ in the denominator is multiplied by γ_m/γ_p, meaning that only fluctuations in transcribable mRNAs are smoothed out if the protein product is much longer lived that the mRNA. Nevertheless we observe algebraic reduction in CV^2 due to mRNA activation; for example, using our default parameters so $\overline{\langle m \rangle}$ and setting $\overline{\langle a \rangle} = 40$, we reduce CV^2 from 0.29 to 0.19 (Fig. 2.4a). At the same time, the noise continues to increase if $\overline{\langle m \rangle}$ is held constant but $\langle B \rangle$ is increased - meaning that the nucleus produces mRNAs in larger but more intermittent bursts.

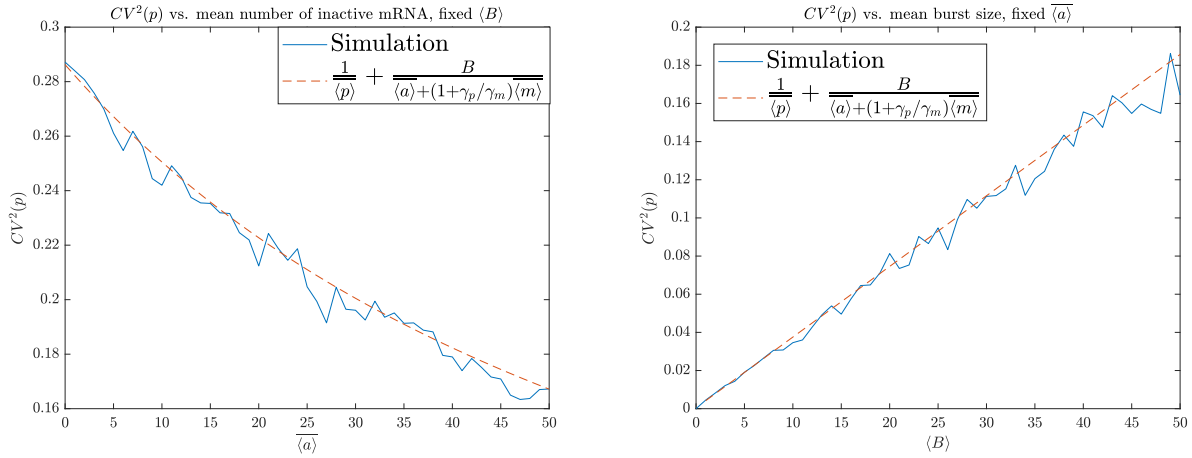

(a) $k_m = 0.05$, $k_p = 2$, $\gamma_m = 0.05$, $\gamma_p = 0.02$, $\overline{\langle m \rangle} = 20$, $\overline{\langle p \rangle} = 2000$ (b) $k_p = 2$, $\gamma_m = 0.05$, $\gamma_p = 0.02$, $\overline{\langle m \rangle} = 20$, $\overline{\langle a \rangle} = 200$, $\overline{\langle p \rangle} = 2000$

(2.4) In a model in which mRNAs transition between active and inactive states, inactive mRNAs reduce protein copy number fluctuations. (a) Increasing mean inactive mRNA abundance decreases protein CV^2. (b) Fixing mean mRNA and protein abundance and increasing mean burst size increases protein CV^2.

2.3.2 Stochastic Nonlinear Phase Separation Model

We now consider a nonlinear, stochastic model for mRNA phase separation into ribonucleoprotein (RNP) droplets. RNP droplets form as the result of multivalent RNA-RNA, RNA-protein and protein-protein interactions. These interacting systems have been shown

to exhibit concentration dependent phase transitions, conditional on both RNA and RNA-binding protein levels [66]. While RNP droplets are typically enriched with potentially many distinct RNA species [53], our model focuses on a ternary system comprising a single species of RNA and an RNA binding protein phase separating out of the cytosol. In vitro studies of similar systems have shown that at physiologically relevant concentrations of RNA-binding proteins, the presence of RNA is required to induce phase separation [66].This behavior can be analytically captured using Flory-Huggins (FH) theory, a widely employed framework for describing polymer mixing [1, 52]. The topology of the phase boundary and the equilibrium concentrations of the two species in both the dilute and dense phases are intimately linked to the relative strengths of heterotypic and homotypic interactions among the solute species. In instances where relative heterotypic interactions are sufficiently strong, FH predicts a closed loop phase boundary [1]. These loops divide the phase boundary curve into two distinct arms, representing the equilibrium concentrations of the dilute and dense phases for the respective components, connected by tie-lines. In such systems, a for a portion of RNA-binding and protein concentrations. the dilute arm of the phase boundary is almost horizontal, characterized by a nearly constant concentration of one component across a wide range of the other component's concentrations (Fig. 2.5a). Furthermore, the dilute arm of the boundary serves as the lower limit of bulk concentration of the minimally varying component for phase separation to occur [1, 52]. Building upon this free energy landscape, our model begins by assuming that the concentrations of mRNA and RNA binding proteins are confined within a specific region of phase space, encompassing the tie-lines that intersect the lower portion of the phase boundary (shaded region, Fig 2.5a). This enables us to precisely establish a threshold concentration, labeled as m_{pt}, where the dilute RNA shows minimal deviations in equilibrium concentration. In this regime, the primary factor influencing phase separation is the concentration of bulk RNA. Now, the real partitioning of mRNAs and proteins between phases can significantly diverge from what is predicted by equilibrium theory at any given moment. We additionally assume a separation of time scales between droplet dynamics

and gene expression variations [52, 67]. Under this assumption, phase separation operates in a quasi-steady state, robustly responding to gene expression variability. In this limit, we develop a stochastic model that aims to captures the temporal distribution of mRNA between phases. Our focus is primarily on the low molecule number limit, where conventional linear noise approximation methods break down [68]. Instead of explicitly modeling droplet formation and dissolution, we assume that mRNAs in both phases are well-mixed within a confined "nuclear neighborhood" surrounding the nucleus at any given time, since in numerous phase-separating systems in multinucleated cells, RNPs associated with cell-cycle or circadian rhythm mRNAs cluster near nuclei. This clustering is believed to serve as a mechanism for preserving nuclear autonomy [4, 20]. By identifying this control volume, we can regard phase separation thresholds as absolute numbers rather than concentrations, which allows us to compare our model predictions with real data.

As we did for the Linear model, we assume that only dilute mRNA m may be translated, and that the translation rate may be tuned about $m_{pt} \approx \overline{\langle m \rangle}$ to reach an optimal mean protein abundance $\overline{\langle p \rangle}$. We additionally assume that bulk RNA-binding protein fluctuations are small enough to not perturb the system from the equilibrium dilute RNA level of m_{pt}, and its influence will instead be absorbed into the stochastic transition rates of mRNA between phases. In addition to the dilute phase m, we define a to be the total number of RNA in all droplets. For the stochastic simulations we introduce the transition rates

$$\begin{aligned} C_{\text{in}} &= C\left(\sqrt{(m - m_{\text{pt}})^2 + \epsilon} + (m - m_{\text{pt}})\right)_+ \\ D_{\text{out}} &= Da. \end{aligned} \tag{2.12}$$

representing the spontaneous diffusion into and out of membraneless condensates respectively.

The phase transition of the system is characterized by the parameters m_{pt} and ϵ (see Fig. 2.6). For $\epsilon = 0$, the transition rate for mRNAs in the dilute phase to the droplet phase

reduces to

$$C_{in} = C\left(m - m_{\mathrm{pt}}\right)_{+}, \tag{2.13}$$

so that transition into the droplet phase only occurs for $m > m_{\mathrm{pt}}$. Rather than explicitly modeling the RNA binding protein, we use the parameter ϵ to influence how sharply the rate of condensate forming increases around $m \approx m_{\mathrm{pt}}$. We test the sensitivity of our results to ϵ. We take C to be larger than the rate constants for translation and mRNA decay, so that state transitions dominate the dynamics of the system, occurring on the time scale of seconds in contrast to the minutes between typical transcription and decay events. In essence, the rapid phase separation dynamics will lead to a nearly constant population of translatable RNA, effectively suppressing stochastic effects arising from bursty transcription and decay. Using this model, we will next investigate two potential scenarios of mRNA phase separation, in the context of mRNA stability. The scenarios are shown in Fig 2.7. In the first scenario Fig 2.7a, mRNAs in the droplet phase are very long lived. We refer to this scenario as the *buffer model*, since mRNAs in the droplet phase act as a reservoir that buffers dilute phase concentration of mRNAs. In a second scenario Fig 2.7b, mRNAs in the droplet phase decay more rapidly than dilute mRNAs. We call this scenario the *filter model*, since droplets filter out excess dilute phase mRNAs.

2.3.2.1 Phase Separation - Buffering Model

For unstable dilute mRNAs, we hypothesize that phase separation maintains a population of translationally inert condensate-mRNAs that become available for translation only when dilute mRNAs have been depleted. To test this hypothesis, we performed simulations assuming that the cytosolic mRNA decay rate γ_m is the same order of magnitude as the protein decay rate γ_p, and that decay does not occur for mRNAs in the droplet phase, as diagrammed in Fig. 2.7a. We simulated protein copy number variability for different mean burst sizes (Fig. 2.8a). The CV^2 of protein copy number decrease with mean burst size, plateauing when

$B \approx m_{pt}$. The curve asymptotes at approximately $CV^2 = 0.006$, far below the CV^2 value for a system with no mRNA state changes but above the Poisson limit for protein, $\frac{1}{\langle p \rangle} = 0.0005$, which solely measures the fluctuations due to protein birth and death. Qualitatively, we see on examining simulated time traces (Fig. 2.8b) that when $\langle B \rangle$ exceeds m_{pt} excess mRNAs are quickly absorbed into the droplet phase, causing the dilute mRNA population to rapidly decrease to m_{pt}. Thereafter, the mRNAs in droplet phase are slowly depleted over time, reentering the dilute phase; maintaining the copy number of the dilute mRNAs close to m_{pt}. To test the sensitivity of the model to ϵ in equation (2.12), we reproduced Fig. 2.8a with values of ϵ ranging from 0.01 to 1 and found no significant qualitative differences between the CV^2 curves (Fig. 2.9).

2.3.2.2 Phase Separation: Filter Model

In a second scenario, mRNA stability is decreased by interactions with RNPs [56]. Accordingly, we investigate whether decay of mRNA within protein aggregates filters cytosolic mRNA abundance and reduces fluctuations. For example, in yeasts the presence of the RNA-binding protein Whi3 reduces the half life of its target, the cyclin *CLN3*, presumably by interacting with deadenylation complexes that promote turnover [56]. Thus phase separation can serve to facilitate mRNA decay. We hypothesize that RNP droplets may then act as a filter, causing excess mRNAs within the cytosol to be quickly degraded and recycled. This process ensures that mRNA decay primarily occurs when bulk concentrations exceed the threshold for phase separation, allowing for precise regulation of dilute RNA abundance. To model this situation, depicted in Fig. 2.7b, we will introduce a new reaction $a \rightarrow a - 1$ with rate $\gamma_a a$ to our stochastic simulation, and assume that the cytoplasmic decay rate is much smaller than other decay rates, i.e $\gamma_m \ll \gamma_a, \gamma_p$, so that phase separation is the dominant decay mechanism of RNAs. While the decay process mediated by droplets may involve multiple steps and might not explicitly occur within the droplets, we assume that it proceeds rapidly enough to be

approximated as a single reaction taking place within the droplet.

We perform stochastic simulations of the filter model, varying γ_a and holding all other parameters fixed, and measure CV^2 as a function of $\frac{\gamma_a}{\gamma_m}$ (Fig. 2.10a). We observe that CV^2 values are far smaller than in the system with no RNA state changes over all assayed values of γ_a/γ_m. Since cytoplasmic turnover of mRNAs occurs at a much slower timescale than the other processes in the system, dilute mRNAs remain essentially fixed at the phase separation threshold, only rising when a burst occurs (Fig 2.10b, all left panels). In our model excess mRNAs rapidly transition between condensate and dilute phases, and filtering allows the cytosol to quickly reach an equilibrium in which mRNAs in the dilute phase approach the phase transition concentration. This again produces CV^2 values that approach the Poisson limit of protein synthesis, differing only due to the small noise contributions of diffusion between states and rare burst and decay events. It is interesting to note that the CV^2 curve depicted in Fig. 2.10a has a well defined minimum $\gamma_a^* \approx 0.01$, meaning that there is an optimal strength filter for reducing noise in this parameter regime. This can be explained by the trade-off between buffering and filtering. If the filter is too weak, the mean droplet mRNA population can become much larger than the phase separation threshold, so mRNAs in droplets slowly bleed back into the cytoplasmic phase and enhance noise (Fig. 2.10b, top row). In contrast, if the filter is too strong, the droplet population can be depleted on time scales faster than bursts, allowing cytoplasmic degradation to drive the dilute mRNAs copy number below the phase separation threshold (Fig. 2.10b, bottom row). By maintaining a non-zero yet small droplet mRNA population, the system can benefit from both buffering and filtering effects and minimize fluctuations of dilute mRNAs about the phase separation threshold.

We next investigated how the transition rate out of the droplet phase, D, which characterizes the system's ability to buffer dilute mRNAs, influences noise profiles. We initially assumed that mRNA had a high affinity for aggregation once $m > m_{pt}$, meaning that $C \gg D$. Increasing D weakens the buffering effect, and we see that the trade-off between buffering

and filtering breaks down - filter strength solely determines the noise suppression ability of phase separation (Fig. 2.10c). We replicated our simulations of protein-CV^2 as a function of γ_a, using different values of ϵ, the smoothing parameter. We also observe that in contrast to the buffer model (Fig. 2.9), the filter model is sensitive to ϵ, with noise increasing with ϵ. However we are still able to achieve substantial reduction in protein fluctuations compared to single mRNA state system (Fig. 2.10d). Finally, in Figure 2.10e, we observe that for $\gamma_a = 0.05 \gg \gamma_m$ and different values of the droplet-to-dilute phase transition rate D, there exists optimal mean burst sizes B^* where noise is minimized, balancing with the other rate parameters so that the mRNA copy number is maintained most steadily at m_{pt}. Increasing the diffusion rate out of the droplet phase leads to a sharper minimum that's achieved for smaller burst sizes.

2.3.3 Stochastic Phase Separation Threshold

We have assumed that the protein component of the RNP droplets remains in a region of phase space that keeps the mRNA phase boundary flat, and that aggregation and disaggregation kinetics are fast enough to make mRNA partitioning quasi-steady and the phase separation threshold constant. In live cells however, the phase separation threshold may depend on other stochastic variables, such as out of equilibrium effects, dynamic post-translational modifications, the concentration of other crowding RNAs or proteins and the temperature of the environment [69]. It is important to probe whether protein copy number noise is still reduced when we incorporate variabilities in the threshold for the onset of phase separation, m_{pt}. We model the effects of these external variables by making m_{pt} subject to stochastic fluctuations. We model the fluctuations in the phase separation threshold phenomenologically as an Ornstein-Uhlenbeck process with mean μ. The Ornstein-Uhlenbeck process satisifies the stochastic differential equation

$$dm_{pt} = \theta(\mu - m_{pt}) + \sigma dW_t. \tag{2.14}$$

The parameters θ and σ characterize the strength of mean reversion and diffusivity of the process respectively. As we noted in the previous section, the dilute mRNA abundance is highly correlated with the instantaneous phase separation threshold, so we expect $\overline{\langle m \rangle} \approx \mu$. This allows us to set $k_p = \frac{\gamma_p \overline{\langle p \rangle}}{\mu}$ in our simulations to approximate the desired mean abundance of $\overline{\langle p \rangle} = 2000$. When applied to the noise filter model, the fluctuations in the phase separation threshold will roughly determine the fluctuations in mRNA abundance due to the rapid phase separation dynamics. In order to demonstrate the connections between the two fluctuating variables, we performed stochastic simulations on the filter model, with m_{pt} allowed to evolve according to equation (2.14), and computed $CV^2(p)$ for increasing values of the Ornstein-Uhlenbeck noise parameter σ. To determine the extent to which these fluctuations determine noise in expression, we also compare our simulations with an exactly analyzable deterministic-stochastic system in which mRNA abundance exactly matches the varying phase separation threshold, and we assume that translation and protein decay are deterministic. In this idealized system, the random variables m and p satisfy the stochastic system of ODEs

$$\begin{aligned} dm &= \theta(\mu - m)dt + \sigma dW_t \\ dp &= (k_p m - \gamma_p p)dt. \end{aligned} \tag{2.15}$$

This system can be solved in terms of CV^2s of the stochastic variables, i.e

$$\begin{aligned} CV^2(m) &= \frac{\sigma^2}{2\theta\mu^2} \\ CV^2(p) &= \frac{\gamma_p}{(\gamma_p + \theta)} CV^2(m). \end{aligned} \tag{2.16}$$

We see in Fig. 2.11 that both models for fluctuating phase separation thresholds introduce a similar amount of noise in expression, suggesting that stochasticity in phase separation thresholds can not be neglected in these gene expression models. However, we see that for

sufficiently small fluctuations in m_{pt}, we can still achieve significantly reduced variation in protein abundance compared to an single mRNA state system with identical transcriptional rate and mean species abundances. Importantly, both the exact model and analyzable approximation agree in the limit where fluctuations in m_{pt} are small. The asymptotic expression (2.16) confirms that $CV^2(p)$ is proportional to $CV^2(m)$ - that is fluctuations in the phase separation threshold drive fluctuations in protein abundance. The prefactor in this expression, $\frac{1}{1+\theta/\gamma_p}$, decreases monotonically with the ratio of the protein lifetime to the timescale of fluctuations in m_{pt}, and represents the tendency of m_{pt} fluctuations to be smoothed out if mRNAs are translated into long-lived proteins, since protein abundance then averages over a long history of m_{pt} fluctuations. This smoothing is seen in Figure 2.12, in which we perform simulations where we hold $CV^2(m) = \frac{\sigma^2}{2\theta\mu^2}$ constant, and vary σ^2 and θ in proportion. We see that faster fluctuations of m_{pt} are associated with smaller fluctuations in p, though for our simulation parameters the effects are modest; with a 10-fold increase in σ associated with a factor ≈ 1.2 decrease in protein CV^2.

2.3.4 Analysis of transcript abundances for a real RNP forming system

We tested whether our modeling could be consistent with existing data on RNP-forming systems. Specifically, our simulations demonstrated that when concentration buffering occurs and bursting and mRNA decay rates are comparable, the burst only needs to reach the local threshold for phase separation in order to decrease protein copy number variation. Distributions of *CLN3* mRNA transcripts – which are translated into the cyclin Cln3 – were mapped in the filamentous fungus *Ashbya gossypii* (see Fig 2.13.) using single-molecule Fluorescence In-Situ Hybridization [57]. *CLN3* was chosen because it is known to form RNP droplets with Whi3 protein, and the specificity of *CLN3*-Whi3 RNP phase separation has been related to the presence of Whi3 binding sequences within the mRNA, and to polyQ-tract driven aggregation of Whi3 macromolecules [66].

Based on prior results about spheres of mRNA enrichment surrounding nuclei [20], we

partitioned the cytoplasm (i.e. 3D segmented hyphae, subtracting their nuclei) into spheres of radius 2.5 μm centered at nuclei centroids (nuclei and parts of the sphere that extended outside of the 3D mask were excluded, so spheres did not need to be truly spherical). Within each sphere, we measured the mRNA concentration (total number of mRNA transcripts divided by neighborhood volume), as well as the mean number of mRNAs per diffraction-limited spot (see Fig 2.14a). Spots with weight > 1 were considered to be in a condensate.To rule out spurious detection of condensates due to chance colocalization, we ran $10,000$ Monte Carlo simulations in which we distributed the measured number of RNAs uniformly within the nuclear neighborhood. Next, the mRNA molecules were clustered into distinct spots using a pairwise distance threshold of $250nm$. The mean spot intensity was then computed for each simulation and subsequently averaged across all simulations. We also detected mRNA transcripts within nuclei. A nucleus was assumed to be actively transcribing mRNAs if it contained mRNA transcripts.

In Fig. 2.14b, the binning of nuclear neighborhood data indicates a phase transition occurring at a concentration of approximately 0.092 mRNA/μm^3, as evidenced by a sharp increase in clustered RNA in contrast to the uniformly distributed scenario. The volume of a typical cytoplasmic neighborhood is $\approx 37\mu m^3$, placing the phase transition at ≈ 3.4 total mRNA transcripts. This number matches quite closely to the mean number of mRNA transcripts that were detected in actively transcribing nuclei, which we interpret as the burst size parameter (see Fig. 2.14c).

2.4 Discussion

The role of intracellular phase separation in gene expression regulation is still an emerging field of study. Here, we developed several models to examine how phase separation of mRNAs can suppress noise in protein copy numbers. We first analyzed a linearized phase separation model and demonstrated that noise can be reduced by partitioning cytosolic mRNA into

"active" and "inactive" states, even if the transition rates between states are constant. We then developed a phenomenological model for concentration-dependent phase separation, and used numerical simulations to quantify expression noise in two distinct biological scenarios consistent with RNP droplet function. The buffer model assumed that droplets act as a reservoir for inactive mRNAs, effectively extending their lifetime, while in the filter model mRNA decay happens primarily within the droplet phase. In both scenarios we demonstrated significant noise reduction, which was largely achieved due to the action of phase separation, which under reasonable conditions maintains the dilute mRNA copy number near the phase separation threshold (see Fig. 2.15). We finally introduced fluctuations into the phase separation threshold, and found that noise suppression can still be significant provided that phase separation threshold fluctuations are sufficiently rapid.

2.4.1 Efficiency in Gene Expression Regulation and Optimal Noise Suppression

Our results indicate that through phase separation of transcripts, gene expression networks can operate efficiently in the absence of any feedback or active transcriptional control, while still achieving precision in protein copy number. While infrequent transcriptional bursts can introduce a substantial amount of noise into a gene network, phase separation models show that protein abundances are largely insensitive to these large variations, so long as transitions into the droplet phase are sufficiently rapid. In fact, in the case of noise buffering, we see that in Fig. 2.8a for a fixed translation rate and phase separation threshold, that large bursts are in fact crucial in reducing noise. If burst intensities are too small, then dilute mRNAs are not maintained at the phase separation threshold, and transcriptional noise becomes significant. Due to the tradeoff between transcriptional cost and expression noise, we can imagine that selective pressures may drive burst sizes to values near the phase separation threshold, since we observe only marginal increase in noise suppression for larger bursts. In contrast, in the filter model we observe strict minima for expression noise as both a function of droplet decay rate and mean burst size. While predicting optimal values for these parameters in live cells

would require quantifying the cost of bursts and selective decay machinery and so remains an unmet challenge, these results demonstrate that kinetic parameters in phase separating systems can be tuned to effectively shift the burden of mRNA regulation from the nucleus to the cytosol.

2.4.2 Time Scale of Fluctuations

In this chapter, we were able to quantify protein abundance noise in our models through CV^2, which measures variations over many realizations of identical systems. While this quantity is well represented in current literature on gene expression noise, we note here that the time scales of protein fluctuations, which do not factor into $CV^2(p)$, may also be selected for. If, for example, copy numbers fluctuate on a time scale comparable to cell cycle length, even minor deviations from the mean protein copy number could prove to be deleterious to a cell. We can observe this to some extent in Fig. 2.3, where the small magnitude fluctuations in protein abundance are driven by slow fluctuations in in inactive mRNA. We can also see this in Fig. 2.12, where we introduced fluctuations into the phase separation threshold. Consider the red and magenta time series, where $\sigma_r < \sigma_m$, $\theta_r < \theta_m$. Although the $CV^2(p_r) < CV^2(p_m)$, fluctuations in the magenta protein copy number are significantly faster than the red protein, meaning that the magenta cell may produce more stable phenotypes if relevant processes occur at a much slower time scale than its fluctuations. These predictions suggest that the time scale of fluctuations in the phase separation threshold could prove to be an important factor in exhibiting the validity of our model, as slow variations would limit the efficacy of the buffering and filtering mechanisms.

2.4.3 Comparison with *CLN3* data

The biological data available on the *CLN3* model RNP-forming system were broadly supportive of droplets playing a role in suppressing protein fluctuations. Specifically, we observed that

phase separation occurred at a threshold abundance of approximately 0.092 RNA/μm^3 or approximately 3.4 per nuclear neighborhood. This value closely matched the burst size estimated by counting mRNAs within nuclei (2.6). While the inferred value of m_{pt} appears surprisingly small, it is consistent with in vitro findings reported by Zhang et al. [66], where phase separation was observed at concentrations as low as 0.1 RNA/μm^3. For example, the potential dimerization of RNAs may facilitate the emergence of additional binding sites essential for nucleating droplet formation. Additionally, these droplets involve not only RNA binding proteins but also numerous other RNAs that act as scaffolds [70], allowing small numbers of *CLN3* mRNAs to be drivers of phase separation. The relationship between optimal burst size and phase separation threshold is not deeply dependent upon whether condensates are filters or buffers, or equivalently whether sequestration within a condensate increases or decreases mRNA lifetimes. Indeed available experimental evidence suggests that either may be possible, including in homologous systems. For example, in data from yeast cells, which contain near-homologs of *CLN3* and Whi3, suppressing Whi3 protein expression extends the lifetimes of *CLN3* mRNAs, suggesting that condensates destabilize mRNAs. But data in the filamentous fungus *A. gossypii* indicate that RNP droplets extend the lifetime of *CLN3* mRNAs. The question of whether the droplets are functioning as buffers, or as filters, remains unanswered here, though the generality of our analysis supports noise reduction by either mechanism.

We include an additional two notes of caution here – it is not yet possible to quantitatively measure the abundance of Cln3 proteins at the scale of individual cells, so we do not offer direct proof that Cln3 protein noise is effected by RNP formation for this system. Additionally, the main assumption of our model: that mRNAs within droplets are translation-inactive, has not yet been experimentally tested. However, RNPs are assuming an ever more central role in cell biology, and there has been a corresponding expansion, in recent years, of techniques for perturbing and measuring RNP formation kinetics in live cells [71], and we expect the predictions from our mathematical model to shortly become experimentally testable.

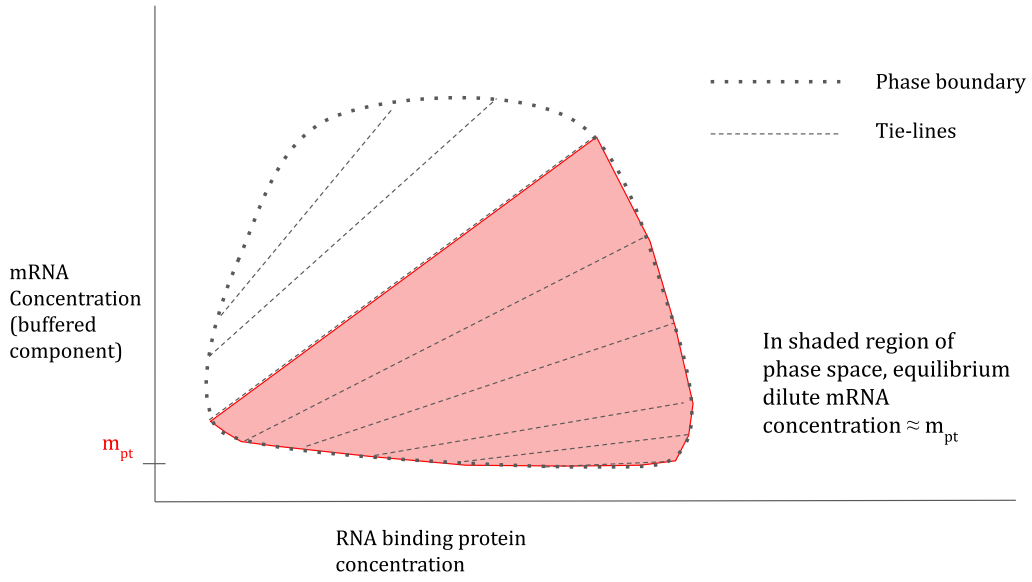

(a) Ternary Phase Diagram

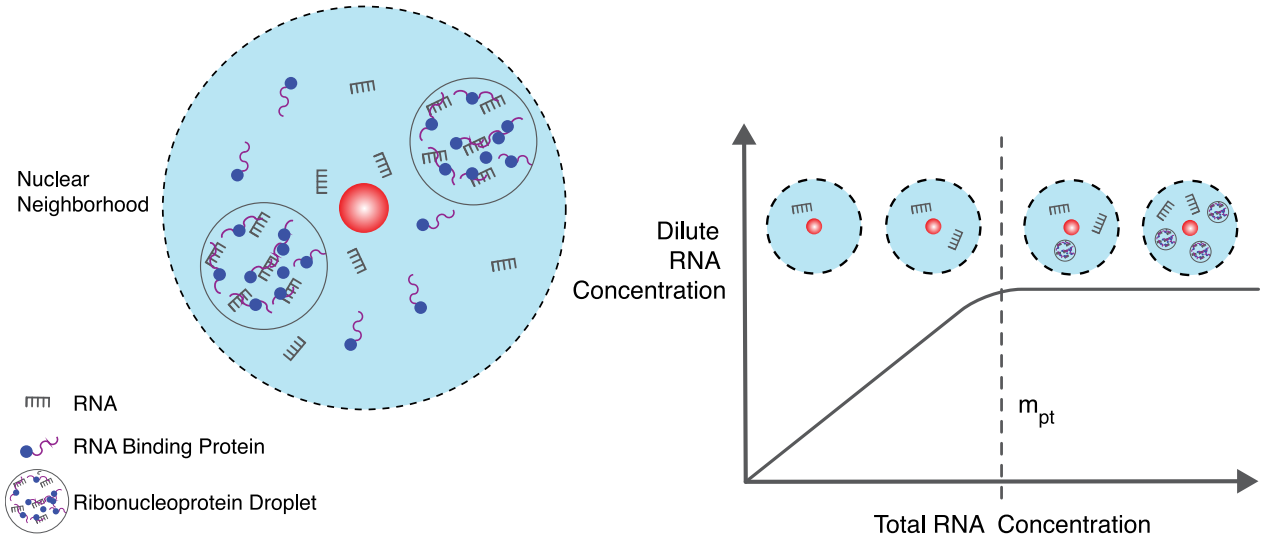

(b) (c)

(2.5) **Modeling RNA Phase Separation.** (a) The formation of RNP droplets arises from a combination of homotypic and heterotypic interactions between RNA and proteins, often leading to closed loop phase boundaries characterized by positively sloped tie-lines. Within a certain range of bulk protein concentration (shaded region), the equilibrium concentration of dilute mRNA remains close to a fixed value m_{pt}, unaffected by fluctuations in the bulk concentration of mRNA. Adapted from Seim et al. [1]. (b) In our model, we make the assumption that phase separation occurs within specific localized volumes surrounding the nucleus, which we refer to as "nuclear neighborhoods." In these regions, RNA and RNA binding proteins undergo phase separation, forming ribonucleoprotein droplets distinct from the cytosolic environment. (c) At a fixed protein concentration, any additional RNA introduced beyond m_{pt} will be sequestered into droplets, upon reaching equilibrium. Depending on the nature of the interactions and relative concentrations of molecular components, this distribution curve can persist across a range of protein concentrations, providing a robust mechanism for buffering dilute RNA concentrations precisely at m_{pt}.

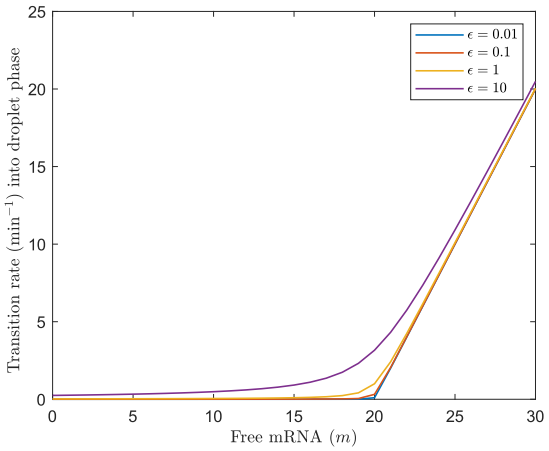

(2.6) Transition rate used to emulate a phase separation process. Droplet formation begins once $m > m_{\text{pt}} = 20$. A smoothing constant, ϵ, controls the range of dilute phase concentrations over which the phase transition may occur. Here $C = 1$, $m_{pt} = 20$, and $\epsilon = 0.01, 0.1, 1, 10$

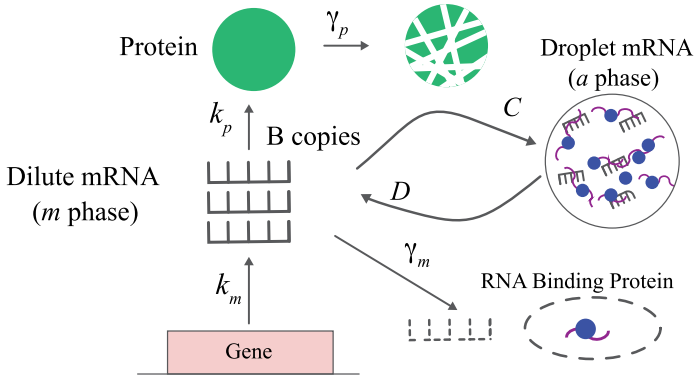

(a) "Buffering" Model

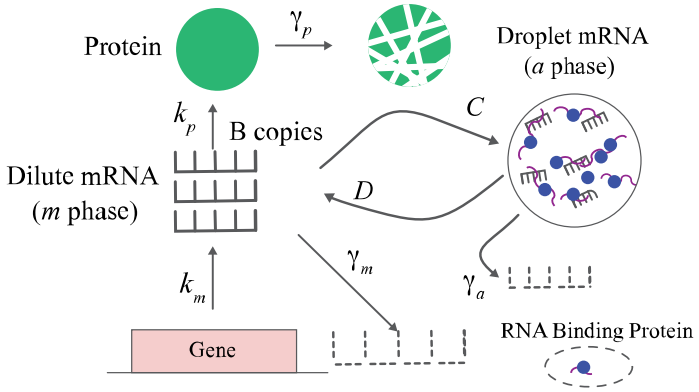

(b) "Filtering" Model

(2.7) (a) In the buffering model, mRNA may exist in two phases; the dilute phase m or the droplet phase a. Only mRNAs in the dilute phase may be translated into protein or decay. The transition function C_{in} was chosen so that the probability that a dilute mRNA transitions into the droplet phase is negligible if the dilute mRNA copy number m is below the phase separation threshold m_{pt}. mRNAs within the droplet phase can transition into the dilute phase with rate D. (b) In the filtering model, mRNAs in the droplet phase additionally may decay with rate γ_a. We assume that $\gamma_a \gg \gamma_m$ so that decay occurs primarily in the droplet phase.

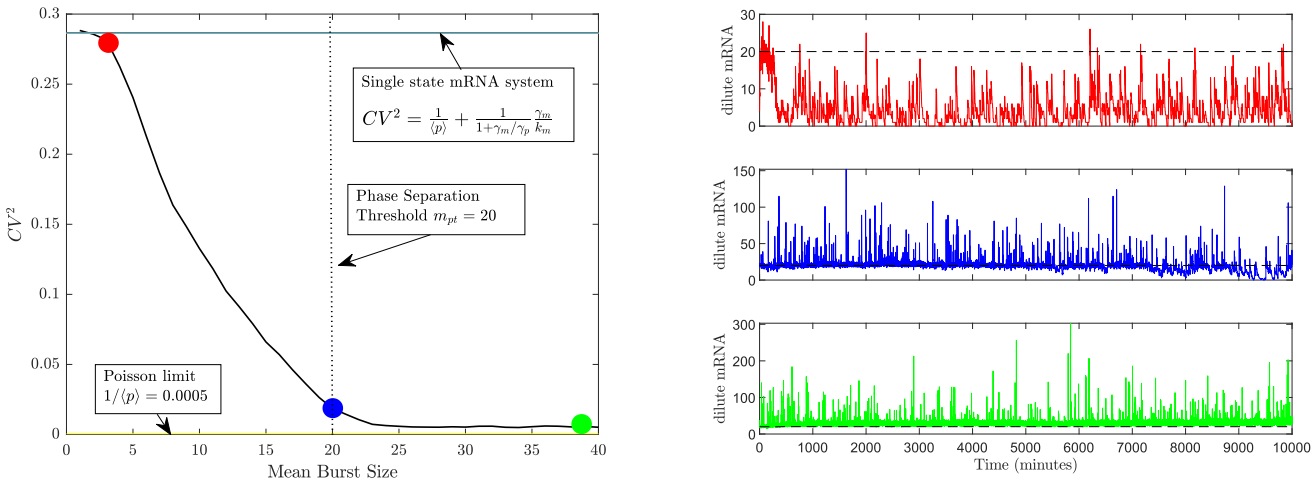

(a) (b)

(2.8) In the buffering model for phase separation with fixed phase separation threshold $m_{pt} = 20$, only mRNAs in the dilute phase are active. (a) For fixed bursting rate k_m, increasing mean burst size decreases protein CV^2 well below the CV^2 for the single mRNA state gene expression system with identical rate constants and mean protein abundance. (b) Sample trajectories of dilute mRNA population demonstrate that for a given phase separation threshold, burst intensities at or above the threshold can maintain a mean dilute mRNA abundance at m_{pt} with fluctuations that are averaged out on sufficiently large timescales. Here, $k_m = 0.05$, $k_p = 2$, $\gamma_m = 0.05$, $\gamma_p = 0.02$, $C = 1$, $D = 0.01$, $\epsilon = 0.01$, colors correspond to highlighted points in panel (a).

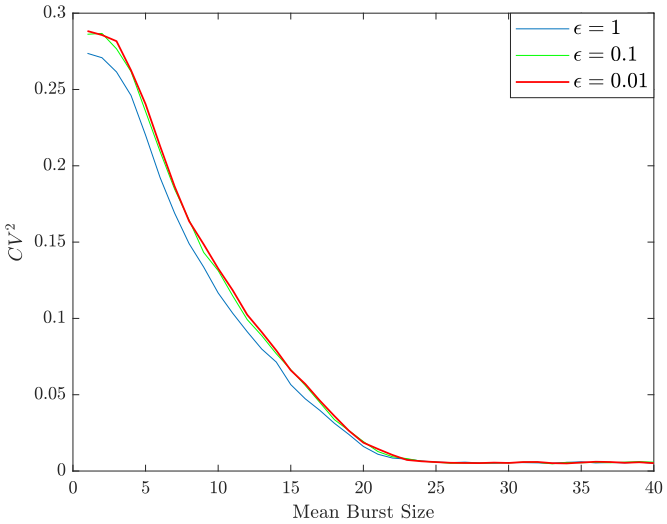

(2.9) Fig. 8a reproduced with different values of epsilon. The curves are qualitatively the same, approaching the same limiting value of CV^2 as the mean burst size is increased.

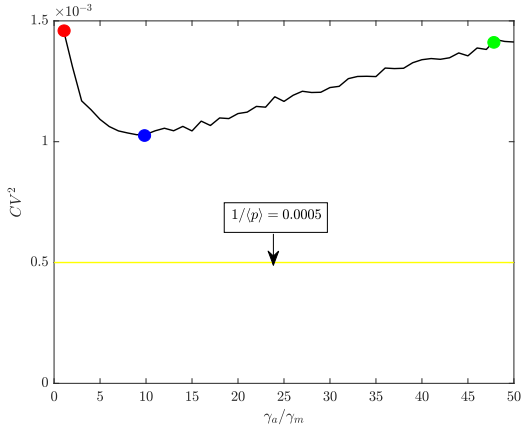

(a) **Noise suppression vs. filter strength:** $k_m = 0.05$, $\gamma_m = 0.001$, $k_p = 2$, $\gamma_p = 0.02$, $\langle B \rangle = 20$, $\epsilon = 0.01$, $C = 1$, $D = 0.01$.

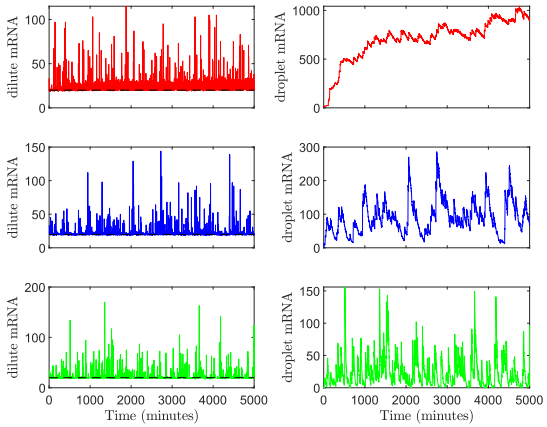

(b) **Select time series of dilute and droplet mRNA:** $k_m = 0.05$, $\gamma_m = 0.001$, $k_p = 2$, $\gamma_p = 0.02$, $\langle B \rangle = 20$, $\epsilon = 0.01$, $C = 1$, $D = 0.01$.

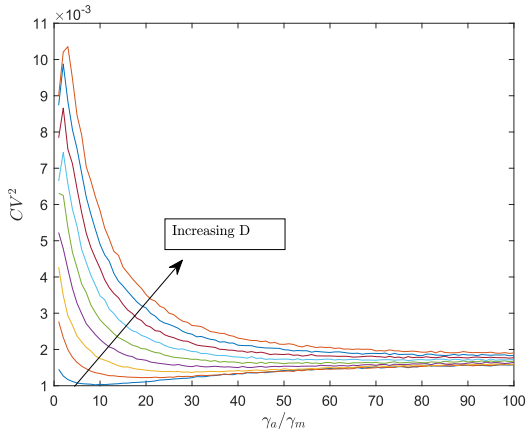

(c) **Sensitivity to D** $k_m = 0.05$, $\gamma_m = 0.001$, $k_p = 2$, $\gamma_p = 0.02$, $\langle B \rangle = 20$, $C = 1$.

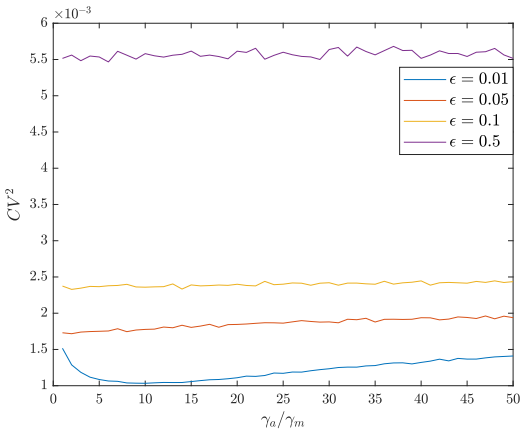

(d) **Sensitivity to ϵ:** $k_m = 0.05$, $\gamma_m = 0.001$, $k_p = 2$, $\gamma_p = 0.02$, $\langle B \rangle = 20$, $C = 1$, $D = 0.01$.

(2.10) In the filter model for phase separation of mRNAs, mRNAs within the droplet phase are unable to be translated and have a higher rate of decay. (a) Varying the droplet mRNA decay rate and keeping all other parameters constant, the CV^2 curve exhibits a well defined minimum for $\gamma_a/\gamma_m \approx 10$. Across all values of γ_a assayed, CV^2 is near the Poisson limit of protein copy number. (b) Sample trajectories of the filter model for different values of γ_a. Fluctuations in dilute mRNA copy number can be minimized by maintaining a small, but nonzero population of droplet mRNA. Colors correspond to highlighted points in panel a. (c) Figure 10a replicated with different values of D, the diffusion rate out of the droplet phase. CV^2 curves shift upwards uniformly with increasing D, due to the reduced ability of the droplet phase to filter out excess mRNA. (d) Figure 2.10a reproduced for increasing values of ϵ. CV^2 curves shift upward, but are still well below the CV^2 of the single mRNA state system.

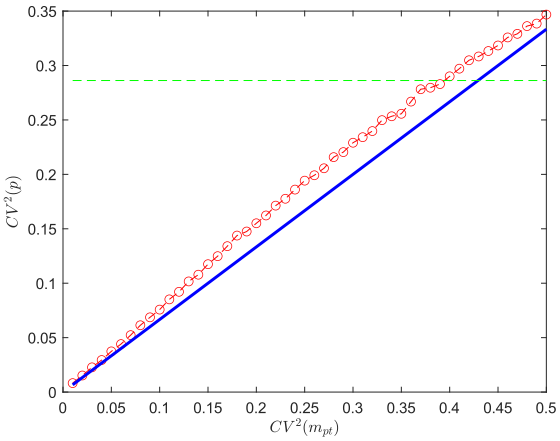

(2.11) Simulations were performed on the filter model with a phase separation threshold that evolves as an Ornstein-Uhlenbeck process. CV^2 of the protein copy number was computed for increasing values of the noise parameter σ of the Ornstein-Uhlenbeck process. Simulated $CV^2(p)$ (red) is plotted against $CV^2(m) = \frac{\sigma^2}{2\theta\mu^2}$, with $\mu = 20$. The simulated $CV^2(p)$ curve was compared to the exact CV^2 of the gene expression system with deterministic translation and protein decay, and mRNA copy number driven by an Ornstein-Uhlenbeck process (blue). The CV^2 of a single state system with the same mean mRNA and protein abundances as the red and blue systems is plotted in green. Here $k_m = 0.05$, $k_p = 2$, $\gamma_m = 0.001$, $\gamma_p = 0.02$, $C = 1$, $D = 0.01$, $\epsilon = 0.01$, $\langle B \rangle = 20$, $\theta = 0.01$.

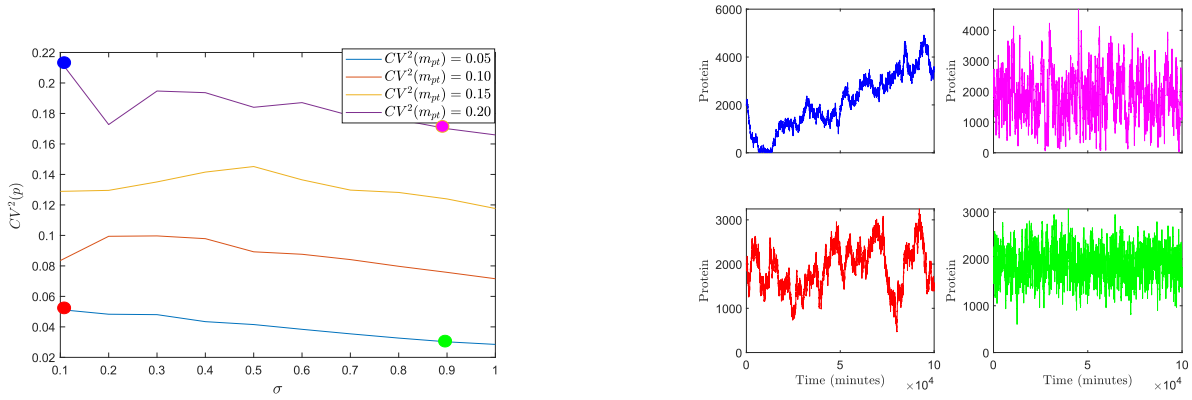

(a) (b)

(2.12) (a) $CV^2(p)$ values were computed for increasing values of σ and θ so that $CV^2(m_{pt}) = \frac{\sigma^2}{2\theta\mu^2}$ remained fixed. Curves were produced for four different values of $CV^2(m_{pt})$. (b) Sample simulations with colors corresponding to their values of σ and $CV^2(m_{pt})$ in Fig. 2.11a. Here, $k_m = 0.05$, $k_p = 2$, $\gamma_m = 0.001$, $\gamma_p = 0.02$, $\gamma_a = 0.05$, $C = 1$, $D = 0.01$, $\epsilon = 0.01$, $\langle B \rangle = 20$

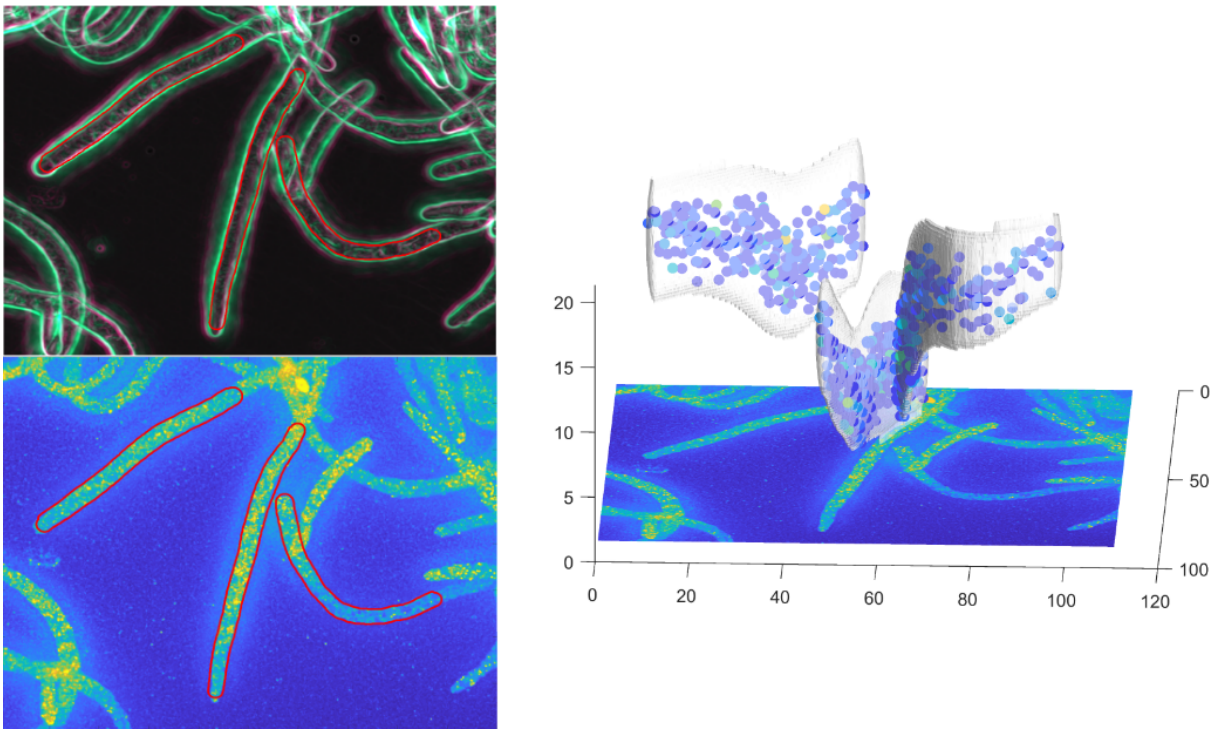

(2.13) 3D segmentation of fungal cells in *Ashbya gossypii*. Top left panel: maximum intensity projection of a stack of phase contrast images of the cells, processed using steerable filters to highlight cell boundaries. Images are false colored so that edges in the middle of the z-stack are colored green, and edges within 3μm of the top or bottom layer are colored magenta, allowing cells that are not completely contained in the z-stack to be ignored. Three hyphae are shown outlined. Bottom left panel: Fluorescence image showing the *CLN3* mRNA spots. Spots are shown in the 3D image color coded by the number of mRNAs that each is inferred to contain, ranging from 1 (blue) to 12 (yellow). Right panel: 3D reconstruction of the 3D cell surfaces, suspended above fluorescence image.

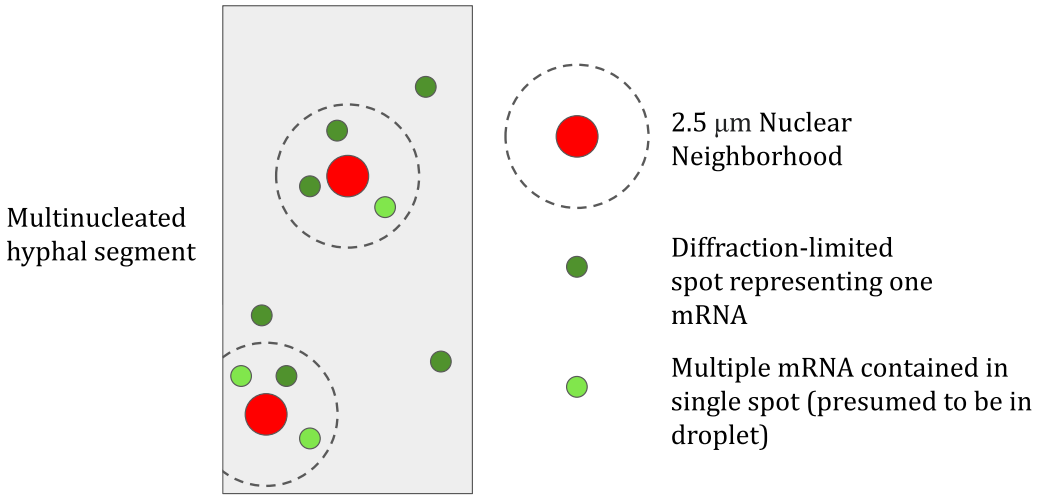

(a)

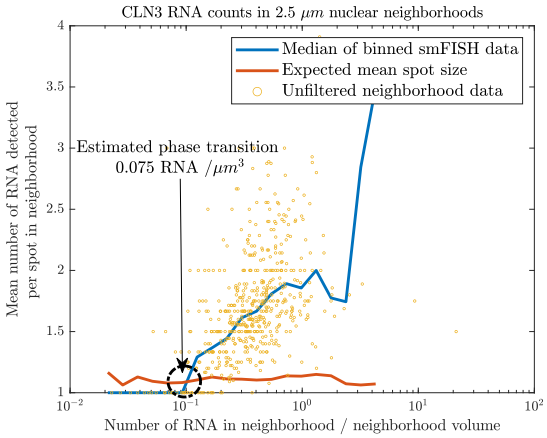

(b)

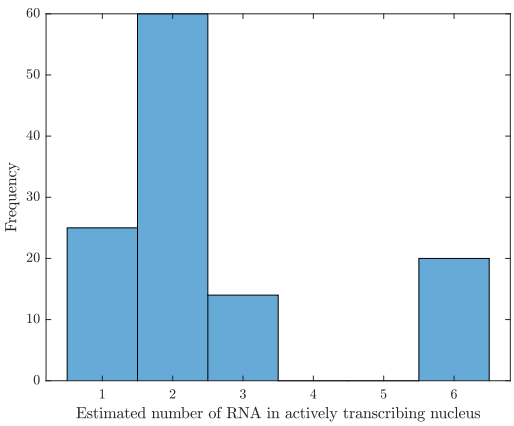

(c)

(2.14) (a) Spheres of radius 2.5μm were constructed around each nucleus to carve out cytoplasmic regions we refer to as *nuclear neighborhoods*. Each diffraction-limited spot detected was assigned a weight based on its intensity compared to a single mRNA. (b) In each nuclear neighborhood, we measured the number of mRNAs divided by the neighborhood volume, and the mean spot weight. From this we formed a scatter plot, and binned the data in 40 uniform compartments. In each bin, we measured the median mean spot weight to form the curve in blue. In order to detect clustering resulting from RNA interactions, we performed an analysis where, for each neighborhood, we calculated the anticipated mean spot weight that would be expected if the same number of RNA molecules were uniformly distributed. The resulting median filtered curve was then plotted in red to illustrate these findings. At a concentration of approximately 0.092 mRNA/μm^3, the curve derived from the smFISH data exhibits a discernible upward trend, surpassing the curve representing uniformly distributed data. This notable deviation signifies the threshold for phase separation. With a mean neighborhood volume of $\approx 37\mu m^3$, we estimate an average phase separation threshold of ≈ 3.4 mRNA per neighborhood. (c) A histogram of the number of mRNA in actively transcribing nuclei, which we use to approximate the distribution of bursts. The mean number of transcripts synthesized in a burst was estimated to be ≈ 2.6.

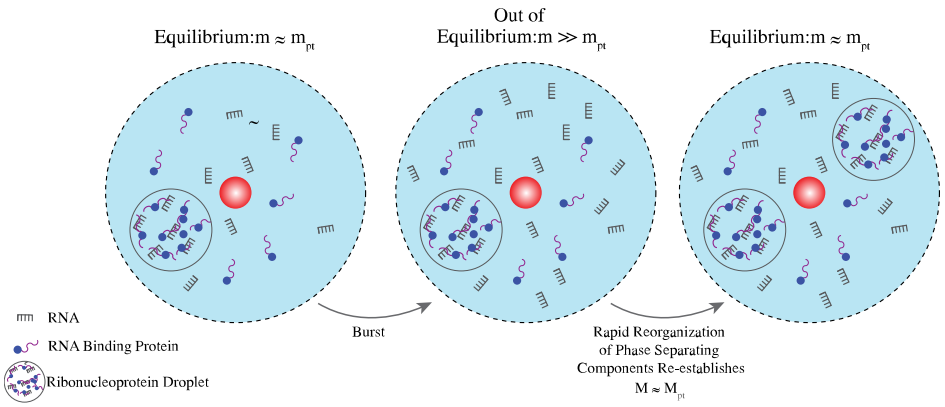

(a) *Buffer Model*

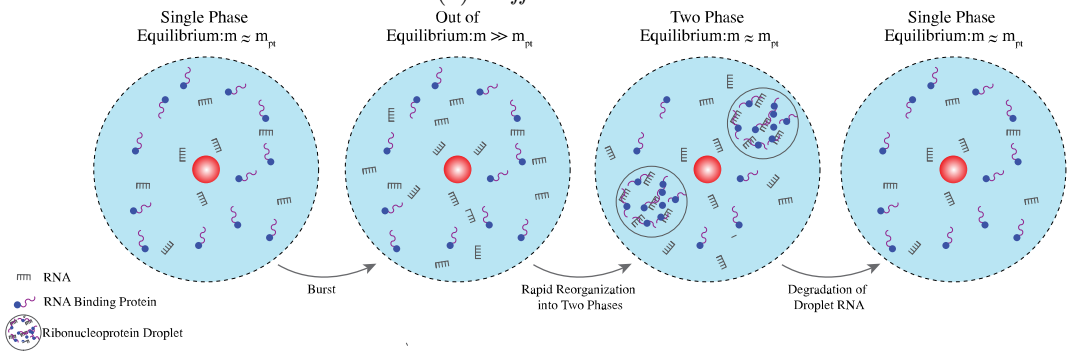

(b) *Filter Model*

(2.15) Graphical Summary of RNA Phase Separation Models. (a) Schematic of the Buffer Model. Here noise suppression is achieved through the partitioning of the cytosol between an active dilute phase and inactive droplet phase. The droplet phase acts as a reservoir for mRNAs that may have been synthesized in large bursts. So long as the net concentration of mRNAs is above the phase separation threshold, the dilute mRNA copy number remains close to the phase separation threshold with minimal fluctuations, thus reducing protein copy number noise. (b) Schematic of the Filter model. Here we assume that mRNAs are long-lived in the cytosol, and degradation primarily occurs in the droplet phase. Fluctuations due to stochastic transitions between states are reduced compared to the Buffer model, since excess mRNAs created in bursts will be quickly degraded.

CHAPTER 3

Mitigating Transcription Noise Via Rapid Protein Sharing in Syncytial Cells

3.1 Introduction

Syncytial or multinucleate cells are found across biospheres and kingdoms, including in protists, plants and animals. The syncytial cells of fungi represent the most extreme forms of this form of organization, common with cytoplasm extending for centimeters. The basic cellular unit of fungi is the hypha, a long, branching filamentous cell characterized by extreme polarity and apical growth. Hyphal growth is sustained by cytoplasmic flow, which is vital for the transport of nutrients, nuclei and other organelles to the growing hyphal tip [72]. The collective mass of branching filaments is called the mycelium. Higher order filamentous fungi have evolved porous septa which act to dynamically compartmentalize the hyphae, aiding in cellular differentiation. Porous septa permit continuous and selective cytoplasmic streaming in favorable conditions, but may be plugged via different mechanisms when a hyphal compartment is damaged, ensuring survival of the hyphal network [73, 74].

Syncytism can confer multiple selective advantages over unicellular systems. Mutations, and in some species, the potential for hyphal fusion between dissimilar strains allows a single mycellium to harbor populations of genetically different nuclei [75] Yet the sharing of proteins within compartments can shield the mycelium from deleterious mutations, endowing the whole with a remarkable tolerance for internal genetic diversity [76, 77]. The principal

benefit we explore in this chapter is that of division of labor between nuclei, specifically concerning transcription. In order to achieve a given steady-state protein abundance, a cell may combine infinite combinations of transcription, translation and molecular decay rates. In this process, for fixed protein decay rates, transcription frequency will primarily dictate the energetic cost, as the number of translation events per unit time will remain invariant of mRNA abundance [38]. Frequent transcription can incur additional fitness cost in the form of transcriptional interference, in which one transcriptional process negatively interacts with another [39]. Transcriptional frequency is also built up from the number of mRNAs transcribed in each transcriptional event and the spacing of these events in time. Mechanistically, these processes are regulated by changes changes in genome conformation associated with transcription, in which chromatin will locally decondense to expose the target operon to transcription factors. This method of chromatin remodeling results in, to an approximation, a two state system in which a gene is "active" or "inactive". The average transcription rate of a gene is thus determined by the product of the number of mRNAs synthesized per unit time in the active state and the fraction of time a gene is active. When this fraction is small, mRNAs will be synthesized in *bursts*, characterized by infrequent but intense periods of transcription. Although decondensation of chromatin is believed to be an intrinsically random event, cells may modulate burst size and deactivation rates by controlling transcription factor abundance and binding affinity respectively [78].

When considering transcriptional efficiency, burst-like production of mRNAs is advantageous compared to more Poissonian mode of transcription, as gene activation events and duration are decreased, which reduces transcriptional interference. One way transcriptional interference may arise is in a process called *promoter occlusion*, in which an elongating RNA polymerase (RNAP) encounters a downstream promoter and precludes binding of transcription factors [79]. Transcription may also interfere with DNA replication, resulting in collapsed replication forks and potential genome damage [80]. The energetic cost

of intense yet infrequent bursts is less clear. Information theoretical modeling by Huang et al. [45] hints that for a fixed RNA abundance, the slower promoter switching which is characteristic of bursty transcription consumes less energy due to decreased chromosomal conformational changes, but is offset by the energy required to synthesize enough RNA during the intermittent active periods. However, there is more clarity a about the noise trade-offs of bursty transcription: when burst frequency is on the same time scale of mRNA and protein decay, the large fluctuations in mRNAs will be transferred to the proteins they encode. For some genes, large amounts of noise may be detrimental to a cell's fitness [34].

In a syncytium, the burden of transcription may be distributed amongst the nuclei coexisting in the cytoplasm. For example, syncytism may permit the existence of robust circadian oscillators at remarkably low transcription frequencies [81]. Here, we develop several syncytial gene expression models that will quantify the extent to which protein sharing can buffer expression noise, and comment on the improvements in transcriptional efficiency in such systems. Integral to these models are the existence of *nuclear sub-compartments* which partition the cytosol of the hypha. In some syncytial organisms, neighboring nuclei repel one another via microtubules to establish quasi-independent nuclear sub-compartments [82]. Proteins may freely diffuse between sub-compartments, and nuclei can respond independently to compartmental protein concentrations, enabling operations such as asynchronous nuclear division [82]. In our models, we will extend results on protein distributions in gene expression models ([27, 42]) to multinucleate systems, and derive the fluctuations in nuclear compartmental protein abundance. The first model will consider a system in which there is a fixed number of nuclei in each hyphal compartment, approximating the distribution of nuclei in hyphal cells, where nuclear spacing is highly regular, as observed in Aspergillus nidulans [83]. Subsequent modeling will explore the effects of non-uniform distributions of nuclei, as seen in species like Neurospora crassa [84]. A second model will generalize this scenario by incorporating uncertainty into the number of nuclei per hyphal compartment.

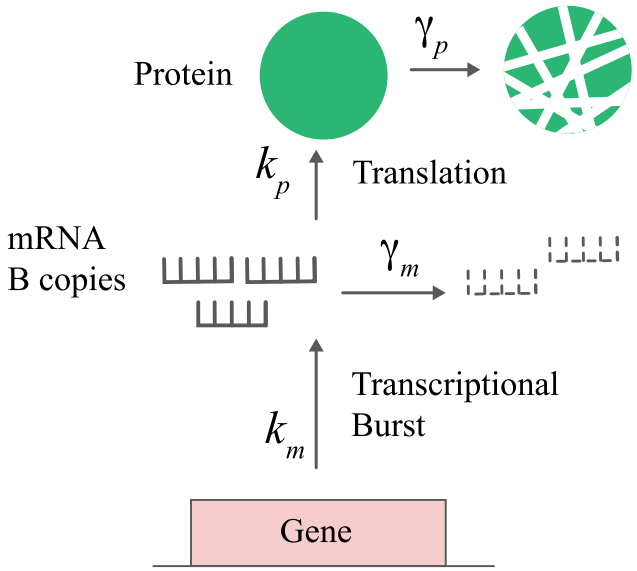

Event	Population Update	Propensity
Transcription	$m(t) \to m(t) + B$	k_m
Translation	$p(t) \to p(t) + 1$	$k_p m(t)$
mRNA Decay	$m(t) \to m(t) - 1$	$\gamma_m m(t)$
Protein Decay	$p(t) \to p(t) - 1$	$\gamma_p p(t)$

(3.1) Schematic of gene expression without mRNA state changes. A random number B ofmRNAs are transcribed with rate k_m; mRNAs are translated into proteins at rate k_p, decay at rate γ_m. Protein decay rate is γ_p.

(3.1) Reaction propensities and population updates for unregulated gene expression model.

In the third model, we will examine the scenario in which hyphal subcompartments are partitioned according to the mean number of nuclei in the hypha, and the number of nuclei is allowed to fluctuate. Finally, we will comment on how the division of labor among nuclei may permit burstier transcriptional kinetics in each nucleus, increasing transcriptional efficiency.

3.2 Materials and Methods

3.2.1 Uninucleate Gene Expression Model

To develop a syncytial model for gene expression, we will begin by introducing a model for single nucleus systems that exhibit Poissonian bursting. This model, derived in Singh [27] using the method of moments, is a special case of the common two-state random-telegraph model for transcription. In this model, the promoter undergoes alternating states of transcriptional activity, transitioning between an “on” and “off” state [85]. During the ”on” periods, bursts

of RNA are synthesized, following a geometric distribution. When the transition to the "off" state is rapid, the arrival of bursts approximates a Poisson point process [86]. Each burst results in the production of B mRNAs, where B is sampled from a geometric distribution. The parameters k_m, k_p, γ_m, and γ_p represent the burst, translation, mRNA decay, and protein decay rates, respectively. If $m(t)$ and $p(t)$ are random variables denoting the mRNA and protein abundance in the uninucleate cell at time t respectively, the time evolution of their moments may be described by the following set of differential equations:

$$\begin{aligned}
\frac{d\langle m\rangle}{dt} &= k_m\langle B\rangle - \gamma_m\langle m\rangle \\
\frac{d\langle p\rangle}{dt} &= k_p\langle m\rangle - \gamma_p\langle p\rangle \\
\frac{d\langle m^2\rangle}{dt} &= k_m\left\langle B^2\right\rangle + \left(\gamma_m + 2k_m\langle B\rangle\right)\langle m\rangle - 2\gamma_m\left\langle m^2\right\rangle \\
\frac{d\langle p^2\rangle}{dt} &= k_p\langle m\rangle + \gamma_p\langle p\rangle + 2k_p\langle p\rangle - 2\gamma_p\left\langle p^2\right\rangle \\
\frac{d\langle mp\rangle}{dt} &= k_p\left\langle m^2\right\rangle + k_m\langle B\rangle\langle p\rangle - \left(\gamma_m + \gamma_p\right)\langle p\rangle
\end{aligned} \tag{3.1}$$

From the first two equations, we immediately find that

$$\begin{aligned}
\overline{\langle m\rangle} &= \frac{k_m\langle B\rangle}{\gamma_m} \\
\overline{\langle p\rangle} &= \frac{k_p\overline{\langle m\rangle}}{\gamma_p},
\end{aligned} \tag{3.2}$$

where $\overline{\langle\cdot\rangle}$ denotes the steady-state ensemble average of a time dependent random variable. As we will only be concerned with steady state distributions, we will proceed to use $\langle\cdot\rangle \equiv \overline{\langle\cdot\rangle}$ unambiguously. To quantify the steady state relative fluctuations in our variables we will use

$$CV^2(\cdot) = \frac{\langle\cdot^2\rangle - \langle\cdot\rangle^2}{\langle\cdot\rangle^2} \tag{3.3}$$

In this single nucleus gene expression model, we find that

$$CV^2(m) = \frac{\langle B \rangle}{\overline{\langle m \rangle}} = \frac{\gamma_m}{k_m} \tag{3.4a}$$

$$CV^2(p) = \frac{1}{\overline{\langle p \rangle}} + \frac{1}{\left(1 + \frac{\gamma_m}{\gamma_p}\right)} CV^2(m). \tag{3.4b}$$

The first term in Eqn. 4b represents the Poissonian noise that arises due to the stochastic birth and deaths of proteins, and as a result depends solely on the mean protein expression level. The second term encodes the downstream contribution of stochastic mRNA production and degradation to protein noise. The size of this term is affected by the ratio $\frac{\gamma_m}{\gamma_p}$, and the relative mRNA noise $CV^2(m)$. The ratio $\frac{\gamma_m}{\gamma_p}$ represents the ratio of protein to mRNA lifetime. Increasing this ratio decreases $CV^2(p)$, since rapid fluctuations in mRNA abundance may be averaged out over a long-lived protein's lifetime. When mRNA decay rates are held constant, $CV^2(m)$ maintains a direct proportionality with the average waiting period between bursts, $\frac{1}{k_m}$, highlighting the noise penalty linked to more sporadic transcriptional bursts."

3.2.2 smFISH Analysis in *A. Gossypii*

To estimate nuclear *CLN2* mRNA distributions in *A. gossypii*, we utilized a multistage image analysis algorithm on six previously collected deconvolved hyphal image stacks, each containing smFISH-labeled *CLN2*, Hoechst-labeled nuclei, and phase-imaged hyphae with voxel size $0.1 \times 0.1 \times 0.3\mu m^3$, along with manually traced 2D segmentations of the hyphae.

To generate accurate nuclear masks, a multi-step approach was employed. Initially, Otsu thresholding was applied to the raw deconvolved Hoechst images, effectively separating the nuclei from the background. Subsequently, for each (x, y) coordinate in the image, the z index (depth) with the optimal intensity was determined. This information was then utilized to apply a standard deviation filter to identify and filter out any corona present at the nuclear boundaries. To further refine the masks and eliminate spurious detections resulting from

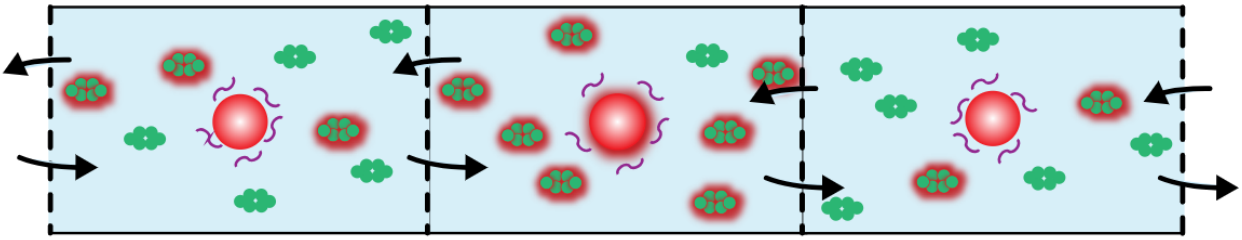

(3.2) Sample distribution of protein in a hyphal compartment subdivided into n subcompartments, (three shown here). While proteins are free to diffuse into neighboring subcompartments, mRNAs are assumed to localize near their nucleus of origin. Proteins originating from the center nucleus are highlighted in red.

deconvolution artifacts of hyphae extending beyond the imaging volume, voxels situated more than six z-slices away from the nuclear centroid were set to zero. Finally, the nuclear boundaries were smoothed by applying a dilation operation to the resulting mask, using a spherical structuring element with a radius of 2 pixels.

3D hyphal segmentations were generated using the identical procedure described by Mayer et al. [86], allowing for the subtraction of background fluorescent intensities from each raw smFISH image. In the resulting image, candidate RNAs were identified by locating the regional maxima of the median-filtered image. The identified voxels were then further refined through dilation using a 3-pixel radius spherical structuring element. Spots in close proximity were segmented by applying a watershed transformation to the image, and the mean integrated intensity of each segmented spot was calculated. Across all segmented spots in the image, the spots were binned by intensity into 30 uniformly sized bins, and the mid-point of the most populated bin was identified as the single-RNA intensity threshold.

3.3 Results

3.3.1 Deterministic Nuclear Number with Homogeneous Compartment distribution

Now, consider a cellular system containing n identical nuclei, with each nucleus defining a spatial compartment with volume $V = \frac{V_{\text{hypha}}}{n}$ (see Fig. **??**). Assume homogeneous concentrations of translational and decay protein complexes across compartments, so that k_p, γ_m, γ_p are all constant. Each nucleus will synthesize mRNA in bursts with rate k_m, and burst size is characterized by the discrete random variable B, so that the net average transcription rate per nucleus is $k_m \langle B \rangle$. Thus each compartment i is equivalent to the system described in the previous model, so that

$$\begin{aligned} \langle m_i \rangle &= \frac{k_m \langle B \rangle}{\gamma_m}, \\ \langle p_i \rangle &= \frac{k_p \langle m_i \rangle}{\gamma_p}, \end{aligned} \tag{3.5}$$

where the subscript i denotes the steady state copy number of the gene product originating from nucleus i. We can then define the random variables m_{tot}, p_{tot} to represent the total mRNA and protein abundance respectively in the syncytium, i.e $m_{\text{tot}} = \sum_i m_i$, $p_{\text{tot}} = \sum_i p_i$. If all nuclei are identical, then we can simply compute

$$\begin{aligned} \langle p_{\text{tot}} \rangle &= n \langle p_i \rangle \\ CV^2(p_{\text{tot}}) &= \frac{\text{Var}(p_{\text{tot}})}{\langle p_{\text{tot}} \rangle^2} \\ &= \frac{CV^2(p_i)}{n}. \end{aligned} \tag{3.6}$$

To better understand the benefits of compartmentalization, we will focus on expression noise per cellular compartment. This is a useful metric when considering proteins that strongly interact with nuclei, such as nuclear import proteins or cell-cycle signaling proteins. We will

notably assume that the proteins encoded by gene in consideration are highly diffusive on the time scales considered, so that proteins will instantaneously and randomly distribute themselves amongst the n compartments after each reaction with equal probability. We define the random variable p_{sub} to measure the steady state protein abundance within a single nuclear sub-compartment. For homogeneous nuclear compartment volumes, we assume that

$$p_{\text{sub}}|p_{\text{tot}} \sim \text{Bin}\left(p_{\text{tot}}, \frac{1}{n}\right) \tag{3.7}$$

since there is a $1/n$ chance a hyphal protein will reside in a given compartment. From these conditioning assumptions, we find

$$\begin{aligned}
CV^2(p_{\text{sub}}) &= \frac{\text{Var}(p_{\text{sub}})}{\langle p_{\text{sub}}\rangle^2} \\
&= \frac{\langle \text{Var}(p_{\text{sub}}|p_{\text{tot}})\rangle + \text{Var}(\langle p_{\text{sub}}|p_{\text{tot}}\rangle)}{\langle\langle p_{\text{sub}}|p_{\text{tot}}\rangle\rangle^2} \\
&= \frac{\left\langle \frac{p_{\text{tot}}(n-1)}{n^2}\right\rangle + \text{Var}\left(\frac{p_{\text{tot}}}{n}\right)}{\left\langle \frac{p_{\text{tot}}}{n}\right\rangle^2} \\
&= \frac{\frac{n-1}{n^2}\langle p_{\text{tot}}\rangle + \frac{\text{Var}(p_{\text{tot}})}{n^2}}{\frac{\langle p_{\text{tot}}\rangle^2}{n^2}} \\
&= CV^2(p_{\text{tot}}) + \frac{n-1}{\langle p_{\text{tot}}\rangle} \\
&= \frac{1}{n}\left(\frac{1}{\langle p_i\rangle} + \frac{1}{1+\frac{\gamma_m}{\gamma_p}}\frac{\gamma_m}{k_m}\right) + \frac{n-1}{n\langle p_i\rangle} \\
&= \frac{1}{\langle p_i\rangle} + \frac{1}{1+\frac{\gamma_m}{\gamma_p}}\frac{\gamma_m}{nk_m}.
\end{aligned} \tag{3.8}$$

In the second line, we use the law of total variance. Notice that $CV^2(p_{\text{sub}})$ bears resemblance to $CV^2(p_i)$ with an additional factor of $\frac{1}{n}$ multiplying the transcriptional noise term. As p_{comp} measures the effective protein abundance in each nuclear neighborhood, the benefits of

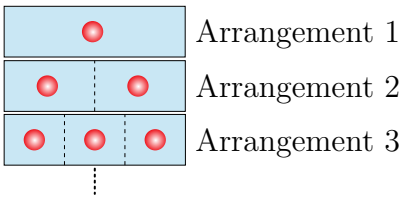

(3.3) Hyphae generally contain a variable number of nuclei. Here we assume that the number of nuclei follows a Zero-Truncated Poisson distribution with intensity parameter λ. For a given number of nuclei n, the nuclei will arrange themselves into n uniform sub-compartments, resulting in the infinite set of configurations depicted above.

protein sharing can be quantified by comparing to p_i, the steady state number of protein originating from a given nucleus:

$$\begin{aligned}\text{Percent decrease in noise} &= \frac{CV^2(p_i) - CV^2(p_{\text{sub}})}{CV^2(p_i)} \times 100 \\ &= 100 \frac{\left(\frac{n-1}{n}\right) \frac{1}{1+\frac{\gamma_m}{\gamma_p}} \frac{\gamma_m}{k_m}}{\frac{1}{\langle p_i \rangle} + \frac{1}{1+\frac{\gamma_m}{\gamma_p}} \frac{\gamma_m}{k_m}} \\ &\approx 100 \left(\frac{n-1}{n}\right).\end{aligned} \tag{3.9}$$

In the final line we assume $\frac{1}{\langle p_i \rangle} \ll \frac{1}{1+\frac{\gamma_m}{\gamma_p}} \frac{\gamma_m}{k_m}$, which is true for genes encoding highly abundant proteins [87]. For example, in the fungus *Ashbya gossypii*, where $n \approx 10$, in each hyphal compartment [88], expression noise is reduced by 90 percent under this model.

3.3.2 Random number of Nuclei with Homogeneous Compartment Size

In practice, the number of nuclei in a given hyphal compartment will generally fluctuate with time, and will vary between compartments. This may be due to asynchronous nuclear division [89], or flow through pores in the septal walls that partition the hypha into compartments [73]. To model this uncertainty in nuclear number N, we will assume that N follows a Poisson distribution with intensity parameter $\lambda > 0$, conditioned on $N > 0$, also known as the

Zero-Truncated Poisson Distribution, or ZTP. This distribution has mean and variance

$$\begin{aligned} E[N] &= \frac{\lambda}{1-e^{-\lambda}} \\ \mathrm{Var}(N) &= \frac{\lambda+\lambda^2}{1-e^{-\lambda}} - \frac{\lambda^2}{\left(1-e^{-\lambda}\right)^2} \end{aligned} \tag{3.10}$$

We need not consider the scenario when $N = 0$, since there would be no nuclear compartment to distribute proteins. Since the number of nuclei is now itself a random variable, the total number of protein in the hypha is now a random variable conditioned on N, i.e

$$p_{\mathrm{tot}}|N = \sum_{i=1}^{N} p_i. \tag{3.11}$$

We again will assume that nuclear compartments are uniformly distributed, so that $p_{\mathrm{sub}}|\left\{p_{\mathrm{tot}}, N\right\} \sim \mathrm{Bin}\left(p_{\mathrm{tot}}, \frac{1}{N}\right)$. Statistically, this means that

$$\begin{aligned} \left\langle p_{\mathrm{sub}} \middle| p_{\mathrm{tot}}, \frac{1}{N} \right\rangle &= \frac{p_{\mathrm{tot}}}{N} \\ \mathrm{Var}\left(p_{\mathrm{sub}} \middle| p_{\mathrm{tot}}, \frac{1}{N} \right) &= \frac{p_{\mathrm{tot}}(N-1)}{N^2} \end{aligned} \tag{3.12}$$

Intrinsic to this assumption is that nuclei respond instantaneously to changes in nuclear number, redistributing themselves to form uniform compartments. This approximation is valid if the time scale of nuclear fluctuations is much larger than gene expression kinetics, so that the system reaches steady state well before the number of nuclei changes again. As p_{sub} is now conditioned on two independent random variables, its variance as now given by

$$\begin{aligned} \mathrm{Var}(p_{\mathrm{sub}}) = &\left\langle \mathrm{Var}(p_{\mathrm{sub}}|p_{\mathrm{tot}}, N) \right\rangle + \left\langle \mathrm{Var}\left(\left\langle p_{\mathrm{sub}}|p_{\mathrm{tot}}, N \right\rangle |N \right) \right\rangle \\ &+ \mathrm{Var}(\left\langle p_{\mathrm{sub}}|N \right\rangle) \end{aligned} \tag{3.13}$$

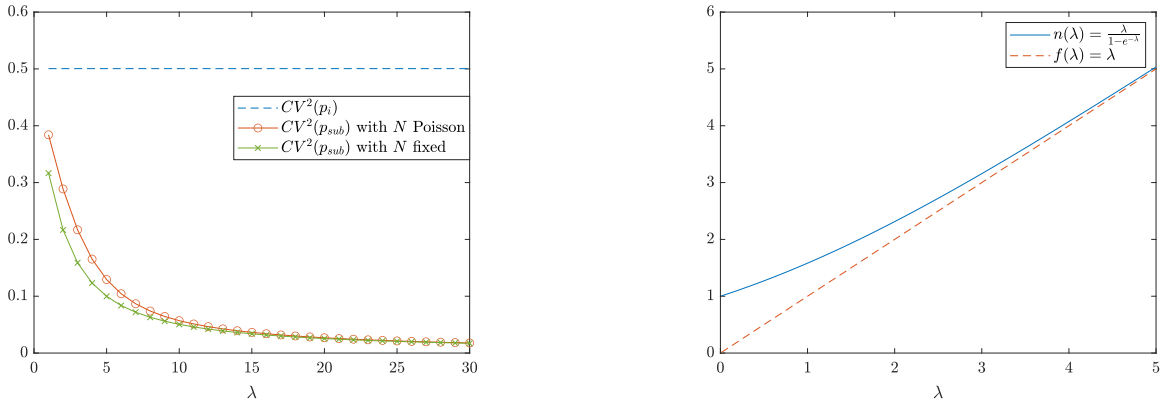

(a) (b)

(3.4) Noise suppression comparison for syncytial gene expression models with fixed number of nuclei, and stochastic number of nuclei. Here λ is the intensity parameter for the Zero-Truncated Poisson Distribution, and we use $n = \frac{\lambda}{1-e^{-\lambda}}$ in equation (10). (a) Integrating stochasticity into nuclei number minimally affects the CV^2 of the determinstic syncytial system, implying that under this range of parameters, subcompartmental protein abundances are robust to nuclei number fluctuations. (b) The intensity parameter λ closely approximates the mean number of sub-compartments n for $\lambda \gtrapprox 3$. Here we use $k_m = \gamma_m = \gamma_p = 1$, $\langle p_i \rangle = 2000$.

where we have used the general formula for variance decomposition derived in Bowsher and Swain [90]. Using equations (11) and (12), we find

$$\begin{aligned} CV^2(p_{\text{sub}}) &= \frac{1 - F(\lambda)}{\langle p_i \rangle} + F(\lambda) CV^2(p_i), \\ \text{with } F(\lambda) &= \frac{Ei(\lambda) - \ln(\lambda) - \gamma}{e^{\lambda} - 1}. \end{aligned} \tag{3.14}$$

where γ is the Euler Mascheroni Constant, and $Ei(\lambda)$ is the exponetial integral.

For fixed gene expression kinetic rates, we plot this result as a function of λ, along with equation (8), using $n = \frac{\lambda}{1-e^{-\lambda}}$. We observe that under the assumption of a random, Poisson-distributed number of nuclei, the computed CV^2 is close to equivalent to that of a compartment containing a fixed number of nuclei. Qualitatively, there is a small difference between the CV^2 values for $\lambda \leq 5$ ($n \leq 5$), but nonetheless, even when nuclear number noise is incorporated, noise is significantly reduced relative to a uninucleate cell (Fig. 3.4).

3.3.3 Compartment Size Independent of Number of Nuclei

In fast flowing hyphae such as *Neurospora crassa*, nuclear positions in sub-apical compartments are dictated primarily by bulk cytoplasmic flow, rather than by their microtubule interactions. In these systems, protein noise reduction is best assessed as a purely spatial phenomenon, using volumetric sub-compartments independent of the instantaneous number of nuclei in the hypha. As in the first model for protein sharing, we will assume that each hypha is subdivided into n uniform compartments. The number of nuclei N will again follow a Zero-Truncated Poisson distribution, with intensity parameter $\lambda(n)$ such that $\langle N \rangle = n$, so that on average, each compartment is occupied by one nucleus. Biologically, we imagine that n is the optimal number of nuclei for the hypha, so that the target number of protein in the hypha is $p^* = n \langle p_i \rangle$ Again applying the assumption that protein diffusion is rapid, we can redefine the random variable p_{sub} so that $p_{\text{sub}}|p_{\text{tot}} \sim \text{Bin}(p_{\text{tot}}, \frac{1}{n})$, and p_{tot} is defined as in equation (10). Applying equation (12) to p_{sub}, p_{tot} and N, we find

$$\begin{aligned} CV^2(p_{\text{sub}}) &= CV^2(p_{\text{sub}}|N=n) + CV^2(N) \\ &= \left[\frac{1}{E[P_i]} + \frac{1}{1+\frac{\gamma_m}{\gamma_p}} \frac{\gamma_m}{nk_m}\right] + \left[\frac{1+\lambda(n)-n}{n}\right]. \end{aligned} \tag{3.15}$$

Equation (15) can be decomposed as the sum of two contributions to noise. The first term represents the noise intrinsic to gene expression for a deterministic number of nuclei N equivalent to the number of subcompartments, which is precisely what we computed in the first model. The second term encodes the relative fluctuations of the number of nuclei in

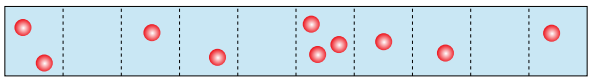

(3.5) In the filamentous fungi *Neurosporra crassa*, nuclear spacing is largely unregulated as nuclei flow through subapical compartments. We assume that there is some optimal number of nuclei n in each hypha, so that on average each spatial compartment is occupied by one nuclei. If the instantaneous number of nuclei follows a Zero-Truncated Poisson distribution with mean n, there are infinitely many occupational configurations, one such is shown above.

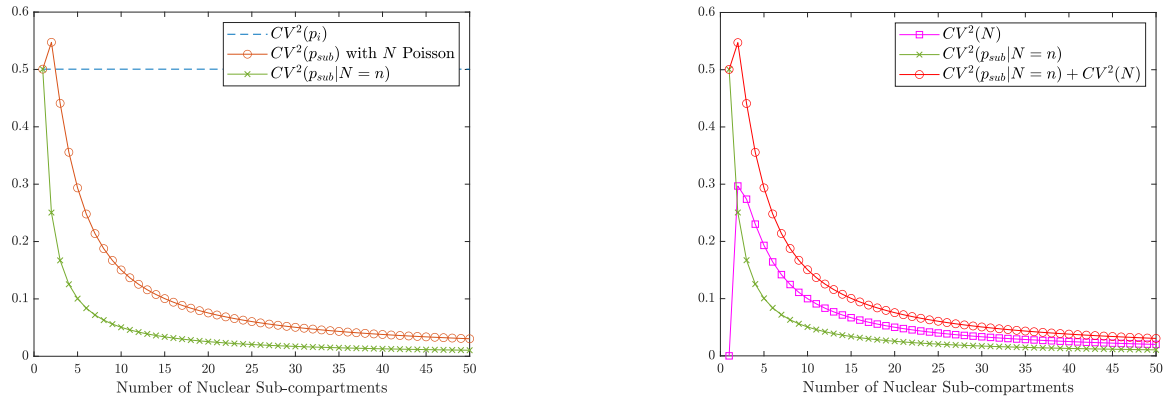

(a) (b)

(3.6) In hyphal compartments containing n nuclei on average, we define n uniform spatial subcompartments along their length. (a) Under the assumption that protein are highly diffusive, we plot CV^2 of protein within a single compartment for a fixed number of nuclei (red) and nuclei following a Zero-Truncated Poisson distribution with intensity $\lambda(n)$ (green) as we vary n. Fluctuations in the number of nuclei per hyphal compartment non-negligibly increases $CV^2(p_{\text{sub}})$ over the deterministic scenario explored in the first model, but this effect is suppressed as the mean number of nuclei n increases. (b) The total sub-compartmental noise may be decomposed into the sum of $CV^2(p_{\text{sub}}|N=n)$ (magenta) and $CV^2(N)$ (green). Both terms, and hence their sum (red) decay as $\mathcal{O}(n^{-1})$ for large n. Here we use $k_m = \gamma_m = \gamma_p = 1$, $\langle p_i \rangle = 2000$.

the hyphal compartment, which is determined from its ZTP distribution assumption. The additive effect of noise makes clear that the additional effect of varying the habitation of nuclear sub-compartment only affects noise if $CV^2(p_{\text{sub}}) \approx CV^2(N)$. Now, for large n,

$$CV^2(N) \sim \frac{1}{n}\left(1 + \mathcal{O}(e^{-n})\right), \tag{3.16}$$

so the two effects continue to contribute at the same order even as n increases. But, both decrease proportionately to $\frac{1}{n}$; and the general story that adding nuclei to a syncytium reduces protein-noise continues to hold. This result is plotted in Fig. 3.6, along with the first term of equation (15). We see that for a small number of compartments, we no longer benefit from protein sharing, as the large relative fluctuations in N dominate the noise in the network. As n increases, these relative fluctuations are suppressed and $CV^2(P_{comp})$ tends towards the CV^2 of the first model. If noise reduction is strongly selected for in syncytial

systems, we would predict that the mean number of nuclei per hyphal compartment is greater in dynamic, fast flowing hyphae like *Neurospora crassa*, in contrast to more static systems like *Ashbya gossypii*. In fact, compartmental nuclear density in *N. crassa* has been observed to exceed that of *A. gossypii* by nearly an order of magnitude [84, 91], thereby providing support for this hypothesis.

3.3.4 Fitness Costs

Our previous results have shown that, as a result of protein sharing, genes in syncytial environments are often expressed with less noise than their unicellular homologs under identical expression kinetics, even when the number of nuclei per cell is subject to fluctuations. At the onset, we have hypothesized that due to the increased precision conferred by protein sharing, syncytial nuclei may be able to operate more efficiently by increasing burst size and decreasing burst frequency. To explore this idea, we develop a rudimentary model for the fitness cost of expressing a gene at some mean abundance p^* in our model hyphal system, and determine how the fitness-optimizing burst frequency k_m depends on the number of nuclei n.

Hausser et al. [38] postulated that the total fitness cost of expressing a gene could be decomposed as

$$\Delta f_{p^*} = \Delta f_{\text{noise}} + \Delta f_{\text{trans}}, \tag{3.17}$$

where Δf_{noise} and Δf_{trans} are the fitness costs due to noise and transcription respectively. They found that $\Delta f_{\text{noise}} = \alpha CV^2(p)$, where α represents the gene's sensitivity to noise. Operating under the assumption that deleterious transcriptional interference scales solely with burst frequency, we assume that $\Delta f_{\text{trans}} = \beta k_m$, where β is a constant of proportionality whose value varies between genes. Taken together we can apply this equation to our first model to find that

$$\Delta f_{p*} = \alpha \left(\frac{1}{p*} + \frac{1}{1 + \frac{\gamma_m}{\gamma_p}} \frac{\gamma_m}{n k_m} \right) + \beta k_m \tag{3.18}$$

If we presume that $p*$, translation rate, and mRNA/protein decay rates are fixed, then the mean number of mRNAs m^* must also be fixed, where

$$m^* = \frac{k_m \langle B \rangle}{\gamma_m}, \tag{3.19}$$

so $\langle B \rangle \propto k_m^{-1}$. The cost function $\Delta f_{p*} \equiv \Delta f_{p*}(k_m)$, and will achieve a minimum when $k_m = \left(\frac{\alpha \gamma_m}{\beta \left(1 + \frac{\gamma_m}{\gamma_p}\right)} \right)^{\frac{1}{2}} \frac{1}{\sqrt{n}}$. Since the optimal burst frequency decreases monotonically with n, this finding suggests that genes adapted to multinucleate cells may experience less frequent but more intense bursts of transcription compared to their single-cell counterparts. While measurement of burst scalings in real syncytia poses great chalenges, this calculation serves to illustrate the concept that cells with the potential for protein sharing might favor more intermittent and noisier transcription events.

3.3.5 *CLN2* Transcription Profile Comparison: *S. cerevisiae* and A. Gossypii

To explore the potentially differential transcriptional noise ceilings in mononucleate and multinucleate cells, we performed a comparative analysis of the transcription profiles of the mRNAs encoding the cyclin Cln2, which plays a crucial role in promoting G1 to S phase transition, in both *Saccharomyces cerevisiae* and the filamentous fungus *Ashbya gossypii*. Aberrant expression of Cln2 in *S. cerevisiae* can lead to adverse effects, such as increased cell size [92] and delayed cell cycle progression [93], making Cln2 a candidate for protein noise reduction.

Previously, burst intensities and frequencies of genes have been estimated by fitting single-molecule fluorescence in situ hybridization (smFISH) data to random telegraph models of transcription, which implicitly assume exponential waiting times between gene activity states [41, 60, 94]. However, with the emergence of mounting evidence showcasing the non-Markovian nature of transcriptional bursting across diverse genomes [95], we adopt a different approach. Instead, we focus on nascent RNA distributions, which decouples the analysis from

downstream processes that may skew distributions, such as RNA export, post-transcriptional modifications, and decay, as noted by Choubey et al. [96]. In this study, we heuristically characterize the "burstiness" of a gene by defining a normalized measure of nascent RNA intensity at transcription sites in actively transcribing nuclei. To this end, we analyzed transcript count data collected by Maekiniemi et al. in *S. cerevisiae* [97] and compared them with six existing smFISH image stacks collected in *A. gossypii* by Dundon et al. [20], which we reanalyzed to collect data of RNA localization and quantification. After applying image filtering, single RNA thresholding, and nuclear mask segmentation (see Methods section for details), we proceeded to identify active nuclei by initially detecting transcription sites, where nascent RNAs are localized (see Fig. 3.7, left panel). To distinguish spots representing transcription sites from mature RNAs, we applied an intensity threshold of 1.4 times the intensity of mature RNAs in each image, consistent with results from Maekiniemi et al. [97]. Nuclei containing these spots (nascent RNAs) were identified as *active*, indicating that they had either recently transcribed or were currently in the process of transcribing (see Fig. 3.7, left panel). If multiple nuclear spots exceeded this threshold, we chose the brightest spot as the transcription site and recorded the number of nascent RNAs in the nucleus as the nearest integer multiple of the transcription site's intensity relative to the base RNA intensity. To measure the "burstiness" of the gene and distinguish it from constitutive expression, we compiled the distributions of nascent RNAs in active nuclei in both data sets, normalizing each by the median number of RNA per nucleus. This normalization accounts for differing transcriptional outputs between the two cell types. Across all samples, we formed histograms of this measure in both data sets (Fig. 3.7, right panel). In *S. cerevisiae*, transcription sites often constitute only a small fraction of the total nuclear content, with the top 7% of transcription sites accounting for 50% or more of the median nuclear content. In contrast, in *A. gossypii*, RNA distributions are more heavily weighted at the transcription site, with the top 55% of transcription sites accounting for $\approx 50\%$ or more of the median nuclear mRNA content, implying a more bursty transcription process.

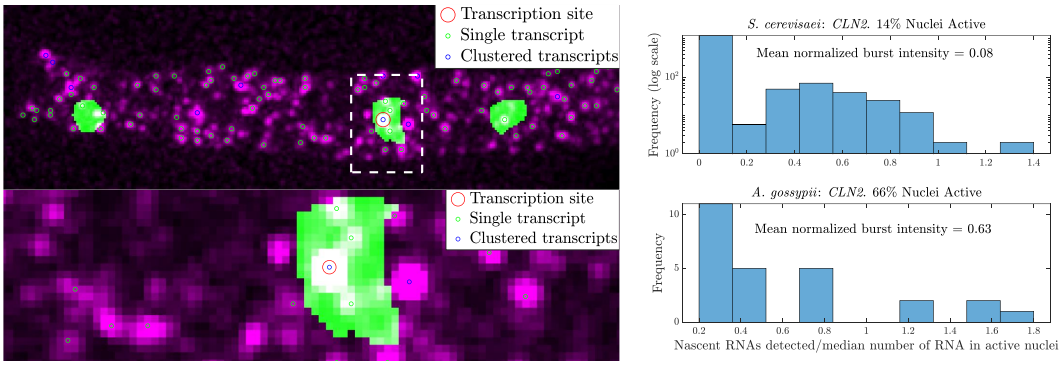

(3.7) **CLN2 RNA quantification in smFISH images of *A. gossypii*.** Left panel: Projected smFISH image after segmentation and thresholding (magenta) overlaid with projected nuclear masks (green). The threshold for single transcripts (marked by red circles) were established by binning integrated spot intensities and selecting the bin with the highest frequency, setting the threshold at the midpoint of the chosen bin. Clustered transcripts (denoted by blue circles) were assigned RNA counts based on the nearest integer multiple of the baseline RNA intensity. Transcription sites were identified as spots contained in nuclei with integrated intensity > 1.4 the base RNA intensity, (labeled in red). Right panel: Nascent RNA counts normalized by median nuclear RNA contents were compared in *S. cerevisiae* and *A. gossypii*.

3.4 Discussion

Syncytial cells possess a remarkable ability to distribute the RNA synthesis workload across multiple nuclei. In this chapter, we have extended results on gene expression noise in uninucleate cells to develop a gene expression model for the syncytium. We specifically investigated three syncytial systems that mimic the broad range of hyphal nuclei distributions observed in filamentous fungi. Central to all three models was the assumed rapid diffusion of proteins within the hypha, which effectively average out the total expression noise among the n nuclear sub-compartments partitioning the hypha. In the first scenario, nuclei were uniformly distributed so that the number of nuclei per hypha was fixed and deterministic, and our analysis revealed an n-fold reduction in protein noise due to mRNA fluctuations. We then generalized this result to consider random nuclear abundances following a Zero-Truncated Poisson distribution, and found that compartmental protein noise was robust to nuclear spacing variability. Finally, we examined the situation where the number of spatial subcompartments depended only on the average number of nuclei per hypha, and found

that the advantages of protein sharing is realized provided that the nuclear distribution N satisfies $CV^2(N) \ll CV^2(p_i)$, where $CV^2(p_i)$ is the noise level of the single nucleus system with identical gene expression kinetics.

Our presented model indicates that even in the presence of high transcriptional stochasticity, these nuclei can achieve precise protein abundances by sharing proteins through an extensive, continuous cytosol, akin to an uncoordinated assembly line. This distinguishing characteristic leads us to hypothesize that the sharing of gene products among compartments in syncytial fungi plays a significant role in facilitating robust gene expression across various cellular processes, and may provide a means to engage in more efficient transcription through bursting. Transcriptional bursting is widely recognized as a primary signature of gene expression noise, yet it simultaneously indicates a shift towards efficiency, allowing for the allocation of fewer resources towards the transcription of a given level of RNAs. In the closely related *S. cerevisiae*, to our model syncytia *A. gossypii*, predominantly exhibits constitutive transcription of mRNAs for the majority of genes currently assayed [94]. This suggests a selective pressure for consistent transcription in the face of substantial noise arising from low-copy number effects, which are omnipresent in *S. cerevisiae* genes [98].

Comparative analysis of *CLN2* distributions in *S. cerevisiae* and *A. gossypii* reveals that while mean transcription levels are similar between the two organisms, there exists a clear bias towards transcriptional bursting in *A. gossypii*, as evidenced by the high relative localization of RNAs at transcription sites. We do not have direct evidence that the Cln2 protein is shared between nuclei; indeed RNAs are observed to congregate near nuclei through liquid-liquid phase separation, possibly as a means of shielding the influence of other nuclei on cell cycle, and each may not travel far from its nucleus of origin [20]. Emerging pipelines on transcriptional activity in yeast and in the closely related *A. gossypii* are powerful tools for testing whether this instance of evolved syncytism has triggered a genome-wide selection for bursty transcription.

The immense enzyme outputs of filamentous fungi have been exploited for thousands

of years in food production, and in more recent years have made fungi into workhorses for the production of antibiotics [99–101]. Mathematical models have shed light on various aspects of fungal biology, including the transcriptional and cellular mechanisms underlying fungal circadian rhythms [23, 102], cellulase secretion [103], and catabolism [104]. Yet, few of these models have considered the syncytial context of filamentous fungus gene expression. Unraveling the efficiency gain of transcription is necessary both for the proper formulation of these models and to harnessing them to pave the way for innovative applications in the biotechnology and industrial sectors.

CHAPTER 4

The Spatiotemporal Regulation of Gene Expression in Fungal Syncytia

4.1 Introduction

Among the most diverse of all of the kingdoms of life, fungi can be found in every biosphere, from deep bedrock, to atmospheric particulates [105]. Fungal syncytism – the ability of a single fungal mycelium to harbor tens, or even millions of nuclei, bathed in a single, common cytoplasm, has shaped fungal life histories, and created distinctive routes to phenotypic plasticity, reproduction and dispersal [88]. In particular, the tolerance of the fungal syncytia for internal genetic diversity, acquired via mutation, or more rarely, through transfer of nuclei or genetic materials between genetically dissimilar mycelia, allows for levels of genetic experimentation that make pathogenic fungi formidable adversaries to their hosts, and allow fungi to adapt in real time to new niches and habitats. Their potential to rapidly adapt to new hosts inspired Buxton [106] to call fungi "the mutable and treacherous tribe" (though Caten traces the phrase back even earlier [107]). Internal genetic diversity, and fungal nuclear totipotence challenge definitions of what counts as a fungal individual, and at what level in the hierarchy from gene to mycelium selection occurs [108]. However, almost 80 years ago, Pontecorvo, one of the pioneers of microbial genetics, predicted that fungal heterokaryosis would be both a challenge and an opportunity for the then nascent science of population genetics [109]. He argued that the fluid nuclear populations present in a fungal syncytium had proportions that are set by the dynamics of competition and cooperation,

intrinsic fitness and drift [109]. Recent experiments promise to turn Pontecorvo's vision into a quantitative scientific model [88]. In particular, live cell imaging of histone-labelled nuclei allows quantification of nuclear dispersal [84], while quantitative PCR allows measurement of the number of nuclei present from different populations, and has been used to infer the presence of selection upon individual nuclear populations [110, 111], and to demonstrate that selfish nuclear populations can invade a syncytium [112, 113]. These results on the genetic dynamics of nuclei within fungal syncytia may provide a conceptual template for explaining the wide-spread appearance of syncytia across the tree of life [114].

Although syncytism has profound consequences for fungal evolution, the subject of this chapter is upon the less scrutinized question of how how syncytism has allowed fungi to evolve into remarkable factories for the production of secreted enzymes. Although secreted enzymes have direct importance in biotechnology, we will expand our focus to study nuclear coordination for protein production generally. Recent modeling has highlighted the importance of the distinctive form of syncytism adopted by fungi in enabling their prodigious cellular outputs [115]. Absence of cell walls between nuclei permits rapid translocation of resources and organelles across substrates, and allows the labor involved in multistep synthesis pathways to be divided among many nuclei – creating syncytial assembly lines – with corresponding efficiency gains. Here we will discuss evidence and ideas both from biological experiments and mathematical modeling, focusing on the adaptations that in a single mycelium allow nuclei to coordinate across an entire organism or to maintain autonomy. We will discuss the implications of sharing of mRNAs or proteins between nuclei upon the amounts of proteins that can be expressed, the stability and predictability of expression, and of the amount of labor that each nucleus must perform.

4.2 Implications of syncytial cell structure for protein synthesis

It is clear that syncytia exploit global integration and coordinated responses as well as regional and localized processes, with the ability to harbor both kinds of processes in the cell and switch between these modes depending on conditions [116–118]. How can we begin to understand the mechanistic benefits of global or local modes of coordination? In these next sections we develop several theoretical frameworks for considering the benefits of a syncytial state for conserving resources, sustainable production and minimizing noise in synthesis or signaling.

Filamentous fungi are distinguished for their use as cellular factories, capable of synthesizing and secreting a wealth of enzymes at an industrial scale [101]. A central question in the study of global gene expression in syncytia is how this vast output of enzymes is achieved while still maintaining consistent expression of housekeeping proteins, which are essential for basic cell function. One potential evolutionary advantage of syncytism is through the economical division of transcriptional labor. In Hausser et al. [38], analysis of high-throughput sequencing data in several model organisms reveal a strong evolutionary bias towards combining low transcription and high translation to achieve a given protein abundance, which they attribute to cells being adapted to minimize the energetic costs of mRNA transcription. Another possible advantage towards infrequent transcription may be come from reducing transcriptional interference, which occurs when the transcription of one gene interferes with the transcription of an independently regulated gene [39]. However, transcription rates are generally prevented from being driven too low, because small mRNA copy numbers are more strongly affected by expression noise, leading to larger fluctuations in protein abundance [32]. In our recent modeling work, we have studied whether syncytism allows for even lower floors on mRNA copy numbers, and more stochastic, less frequent transcription because the dispersion of proteins between nuclear neighborhoods smooths out fluctuations in single nucleus-expression. In this section, we present a simple mathematical model of gene expression in multinucleated

cells, and illustrate how nuclear cooperation for common goods may emerge spontaneously through stochastic transcription.

Mathematical models for gene expression vary extensively in scope and methodology. In this chapter, we focus on simplified *mass-action kinetics* based models, which involve modeling the synthesis, decay, and binding of biochemical components, to form a dynamical picture of the gene network. Typically, mass-action models incorporate the transcription of RNAs, translation of proteins, and their corresponding degradation as single step reactions that occur with certain propensities. In uninucleate gene expression models, the cytoplasm is generally assumed to be well-mixed, which allows for gene networks to be studied purely temporally. The well-mixed assumption necessitates that gene products are highly diffusive in their cytoplasmic environment, allowing for spatial heterogeneities to be smoothed out. The nucleus may additionally be modeled as a well-mixed compartment within the cell, in which case each participating molecule will be prescribed nuclear import/export rates. This added layer of complexity is necessary when modeling feedback mechanisms such as the binding of transcription factors that regulate circadian clocks [119, 120].

When extending gene expression models from uninucleate cells to multinucleate syncytia, the partitioning of mRNAs and proteins becomes an important model element. To model this partitioning, we must measure or make assumptions about the spatial organization of nuclei in the cytosol, as well as the extent to which they enjoy transcriptional autonomy. Indeed, nuclear spacing is highly regulated in fungi; in *A. gossypi*, microtubule and motor protein assisted repulsion between neighboring nuclei space them regularly through the syncytium [82]. Even in syncytia in which nuclei are rapidly moved by protoplasmic flows, eddy currents can lead to formation of stable nuclear aggregates. For these reasons, we treat the cytosol has being divided into distinct *nuclear neighborhoods*, which may function as "cells-within-cells" [89].

In syncytia, nuclei can exhibit different degrees of nuclear cooperation and nuclear autonomy. Nuclear cooperation refers to the situation where nuclei within the syncytium express

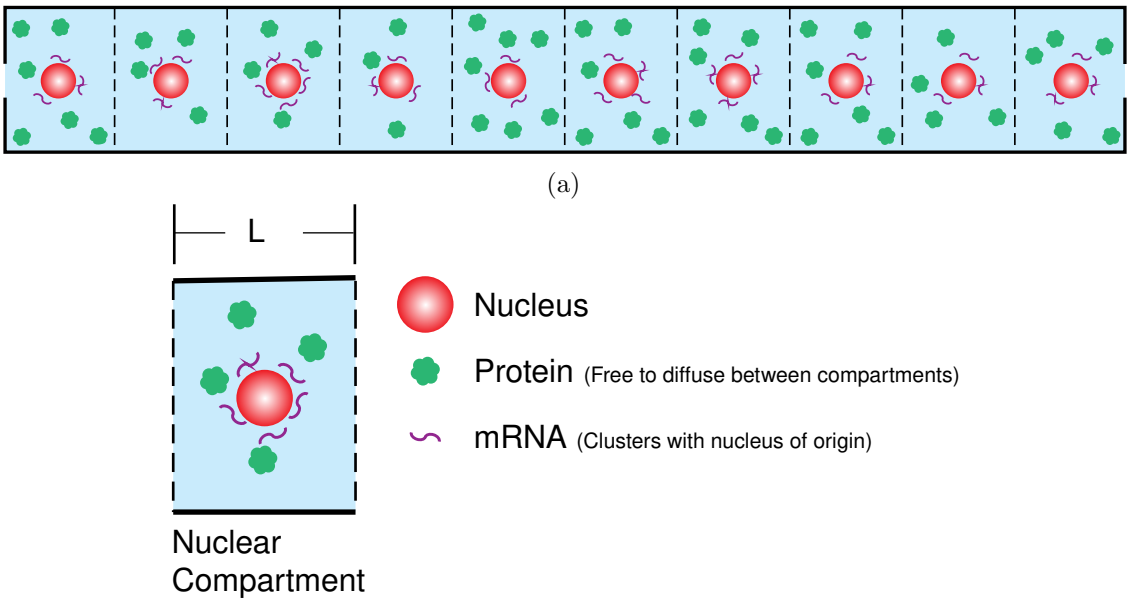

(4.1) Modeling RNA and protein distributions in a syncytial cell. (a) Linear arrangement of N identical nuclear compartments. (b) A single nuclear compartment with characteristic length L.

the same set of genes, potentially in a synchronous fashion, and work together to control the overall function of the syncytium. Conversely, in the case of transcriptional autonomy, nuclei are shielded from the influence of one another, and exhibit distinct transcriptional programs [121].

Nuclear cooperation may emerge spontaneously, without the need for explicit programming or direct communication between nuclei. Even in genotypically identically nuclei, transcription of RNAs will generally not be precisely coordinated, due to stochastic effects, and resulting in heterogeneity in gene product levels between nuclear compartments, which is exacerbated in the case of transcriptional bursting, where mRNAs are synthesized in infrequent pulses rather than individually. However, due to the homogenizing ability of molecular diffusion, the sharing of proteins between nuclear compartments may suppress noise in compartmental protein abundance, providing the the time scale of diffusion is sufficiently fast. To illustrate this idea, we consider an elementary model for syncytial gene expression, which consists of a linear arrangement of N nuclear compartments, which we assume to be uniform in size

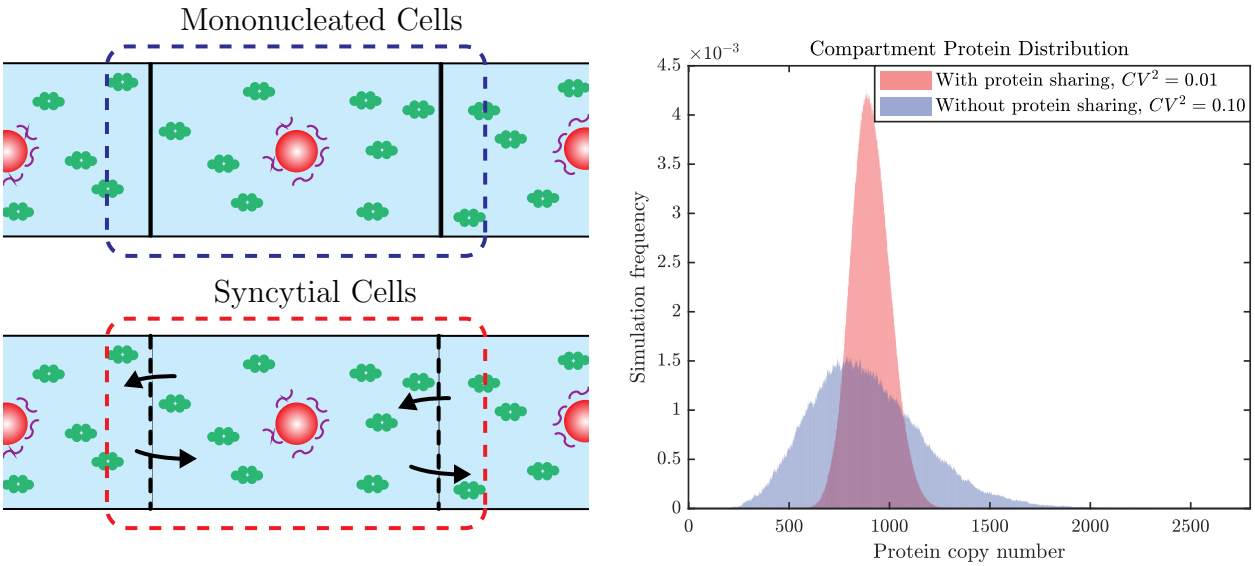

(4.2) Sharing of proteins in syncytial cells permits consistent protein expression under identical transcriptional kinetics. Left panel: In mononucleated cells (top), global protein abundance strictly depends on the synthesis rates of mRNA in the nucleus and translation rates in the cytoplasm. In syncytial cells (bottom), proteins are free to diffuse into other nuclear neighborhoods, and typically protein diffusive time scales are substantially faster than the gene expression time scales of transcription, translation, and decay. Right panel: Stochastic simulations derived from standard and syncytial models of gene expression reveal that spatial averaging of diffusive proteins results in a tighter distribution of local proteins in nuclear neighborhoods of syncytial cells. In the syncytial model, we simulate the sharing of proteins among ten nuclei, all of which have identical transcription kinetics. In the limit of rapid diffusion, CV^2 is reduced by a factor of 1/10 compared to the scenario where protein sharing is prohibited.

(Figure 4.1). This model resembles the typical morphology of hyphal compartments in *A. gossypi*, which consists of $N \approx$ 8-10 nuclei spaced $L \approx$ 2-5μm apart [82, 91]. A protein, modeled as a Brownian particle with diffusivity D, will diffuse half a cell length $\frac{NL}{2}$ in time $\Delta\tau_p = \frac{N^2L^2}{4\pi^2 D}$ at which point there is roughly an even probability that it occupies any of the N compartments. Taking the protein GFP for example, which has diffusivity $D \approx 30\mu m^2/s$ in eukaryotic cytoplasm [122], the homogenization time in a hyphal compartment of *A. gossypi* is $\Delta\tau_p \approx .75s$. As the kinetics of gene expression often operates on the timescale of minutes [38], we may make the limiting assumption that at any given time t, the total protein content $p(t)$ is disseminated with uniform probability between nuclear compartments. As a reminder, in Chapter 3, we found that the magnitude of relative fluctuations of protein abundance in a

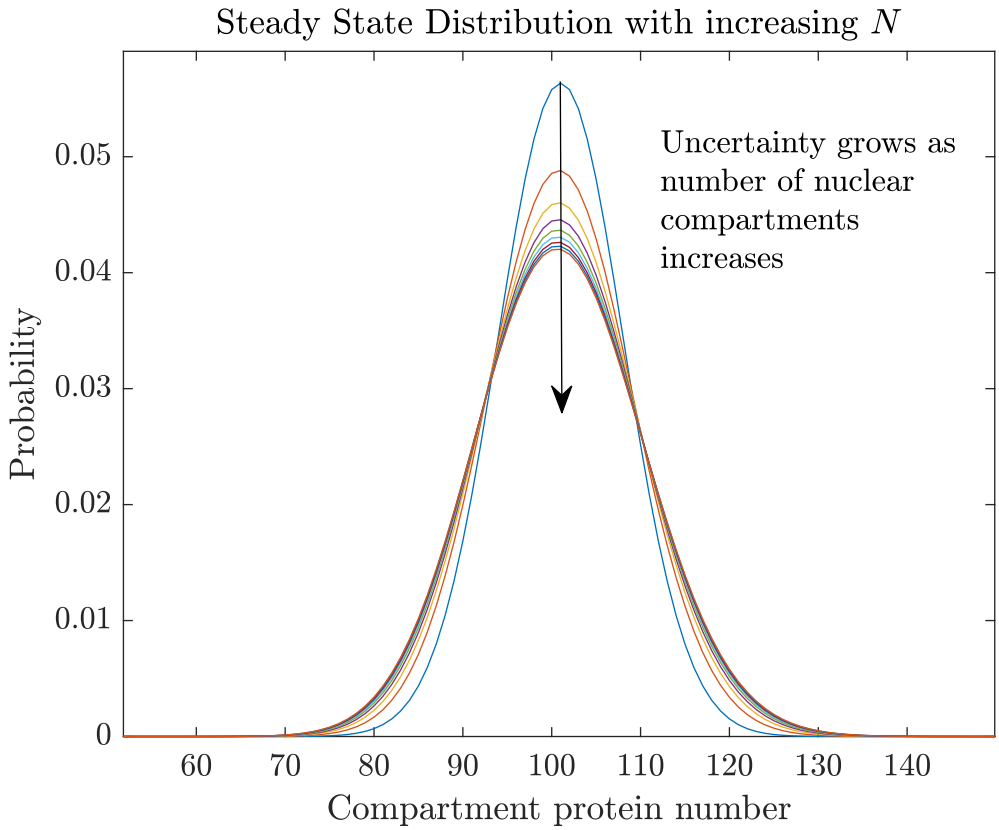

(4.3) Compartmental protein abundance is subject to poissonian diffusive noise in the limit where protein synthesis is deterministic, (i.e cellular protein abundance fixed).

compartment in this model is found to have the approximate scaling

$$CV^2(p_{sub}) \sim \frac{CV^2(p_{mono})}{N} \tag{4.1}$$

(see Figure 4.2), where p_{mono} is the distribution of protein in a mononucleated cell with identical expression kinetics, and

$$CV^2(p_{mono}) \approx \frac{\tau_B}{\tau_m + \tau_p}. \tag{4.2}$$

Here τ_m is the average mRNA lifetime, τ_p is the average protein lifetime, and τ_B is the average waiting time between transcriptional bursts. As transcription is often an energetic bottleneck

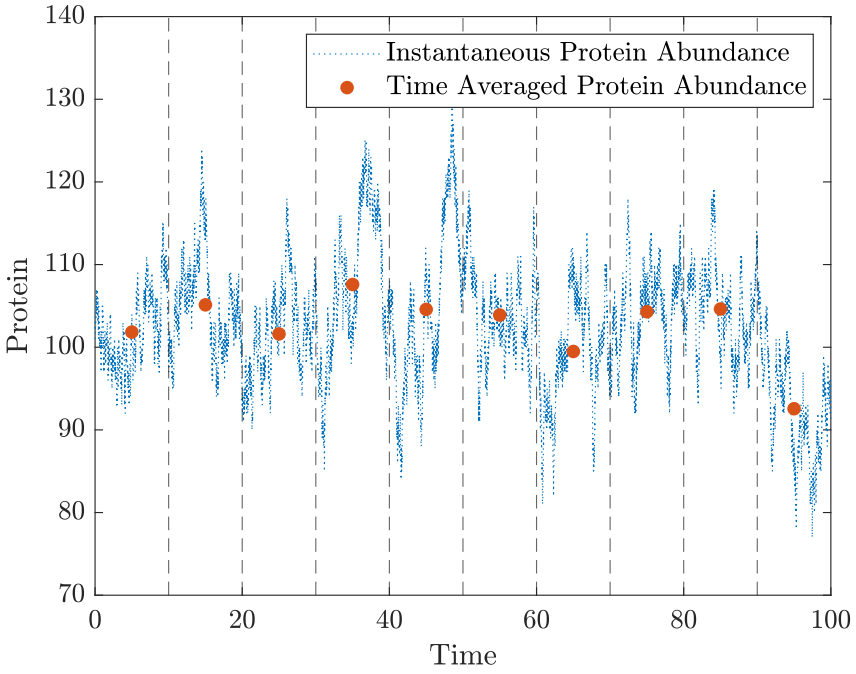

(4.4) Stochastic time series of sub-compartmental protein abundance in syncytial gene expression model with finite diffusion rate. Averaging over characteristic time periods reduces the perceived magnitude of protein copy number fluctuations.

in gene circuits [38] this result suggests that in syncytia permit more stochastic transcription (i.e larger and more infrequent bursts) before reaching a compartmental noise ceiling driven by selection. Preliminary analysis of smFISH data in *A. gossypi* on the cell cycle associated genes encoding cln2 and clb2 support this hypothesis revealing potentially divergent modes of transcription to analogous genes in the genetically similar *S. cerivisae* (Mayer et. al).

While the sharing of protein between nuclei can act to suppress fluctuations due to noisy transcription, it introduces a degree of fluctuations via the random diffusion of proteins away from their nuclei of origin. This effect is most pronounced when nuclei are each independently expressing identical numbers of proteins, which may occur if the protein's abundance is tightly regulated by nondiffusive molecules such as RNAs [27]. In our syncytial model, we assume each nucleus expresses a target protein copy number of p_{target} which provides maximum

fitness benefit per nuclear neighborhood. Given that the N sub-compartments are uniform the total number of protein in the syncytium is given by $p_{tot} = Np_{target}$. At steady state, the probability that a single protein occupies a particular compartment is simply $\frac{1}{N}$. Therefore, the distribution of proteins in a syncytium follows a multinomial distribution with a uniform compartment occupancy probability (see Figure 4.3). The number of proteins a particular nucleus has access to, p_{sub}, say through interactions with associated microtubules, follows a binomial distribution with Np_{target} trials and success probability $\frac{1}{N}$. The fluctuations in protein number per compartment is then given by

$$CV^2(p_{sub}) = \frac{1 - \frac{1}{N}}{p_{target}} \tag{4.3}$$

It can be shown that for large N, $p_{sub} \sim \text{Poisson}(p_{target})$, which sets an upper limit on the noise contribution of diffusion to $CV^2 = \frac{1}{p_{target}}$. For proteins expressed at high levels, i.e on the order of 10^2 molecules/nucleus, this degree of noise is negligible. Although little data exists on whole proteome abundances in *A. gossypii*, if it follows its near relative, the yeast *S. cerevisiae*, for which 90% of proteins are expressed with median levels over 822 per cell, then we expect protein partitioning noise to be negligible.

What about low abundance proteins, such as transcription factors? For such proteins, random diffusions can lead to very uneven distributions through the syncytium. However, even when instant-to-instant distributions of proteins may be very uneven, function may only be impaired if the protein level in a given nuclear neighborhood is persistently too low or too high [34]. If the time-varying protein in a given nuclear neighborhood is $p(t)$, then the phenotype associated with the protein likely reflects the time averaged abundance of the protein. Supposing this time averaging occurs over a characteristic time scale T (e.g. the time taken for protein recruitment to a particular organelle, which is often on the order of

seconds or 10s of seconds), then

$$p_T = \frac{1}{T}\int_{t_0}^{t_0+T} p(t)dt \tag{4.4}$$

Although $p(t)$ fluctuates on a time scale τ_P, if these fluctuations are rapid, meaning that $\tau_P \ll T$ then deviations from the mean are suppressed (see Figure 4.4 and Appendix Section 5.2 for more details).

4.3 Circadian rhythm through the lens of nuclear coordination

Although much biochemical interest in fungal syncytia is associated with secreted proteins, due to their many-fold uses in biotechnologies, specific pathways for secreted protein production are usually not understood at the level of individual nuclei. By contrast, the circadian clock in *N. crassa* is likely to provide an essential case study for understanding space and time-resolved patterns of nuclear coordination, because of recent innovations both in developing carefully parameterized models for the expression pathways that drive the clock, and innovative new cell manipulation tools allowing the contributions of individual nuclei to be systematically examined. *N. crassa* is a common model organism for studying circadian rhythm, as many of the molecules and regulatory motifs involved in its circadian rhythm are conserved in other organisms, including mammals [123, 124]. The fundamental mechanism of the circadian clock in *N. crassa* involves two interdependent feedback loops - one positive and one negative - that pivot on the phosphorylation-mediated interactions between the White Collar-Complex (WCC) and the protein *frq*. In its active state, the WCC is a transcriptional activator for *frq*, promoting the synthesis of *frq* mRNAs. Within the cytoplasm, the *frq* protein associates with the FRQ interacting RNA helicase (FRH) and the casein kinase-1a (CK1), culminating in the formation of the FRQ-FRH complex (FFC), which drives the incremental phosphorylation of *frq* and ultimately directs its degradation. During this process, the FCC may be imported into the nucleus, where it interacts with and phosphorylates the WCC, eventually leading

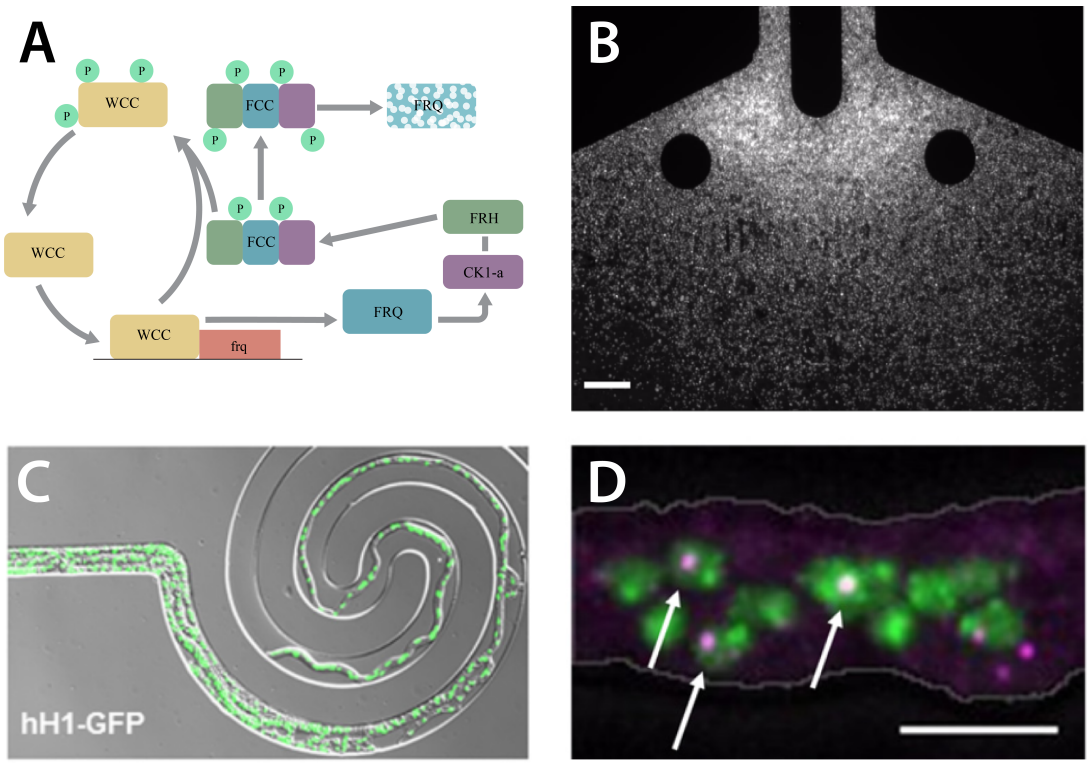

(4.5) (A) A simplified diagram of the Neurospora circadian clock. When active, the White-Collar Complex (WCC) upregulates FRQ expression. FRQ forms a component of the FRQ-FRH complex (FFC), which may inactivate WCC through a series of phosphorylations. (B) Cheong et al. [2] employed a large chamber microfluidic device to investigate the synchronization of circadian clocks in densely packed conidial cells of *N. crassa*. In the study, fluorescence intensity was used to represent the "hand" of the circadian clock. Scale bar: 50 μm (C) A microfluidic design proposed by Lee et al. [3] to perform single nucleus tracking over long time periods in hyphal *N. crassa* cells. (D) Bartholomai et al. [4] performed smFISH on N. crassa to localize the circadian clock associated mRNA frq at various time points. Maximum-intensity Z projections of composite images of frq (depicted in magenta) and nuclei (depicted in green) are presented, with arrows indicating nuclei that contain colocalized frq transcripts (scale bar, $5\mu m$).

to its inactivation (see Figure 4.8a) [23]. Due to the tractability of its principal molecular components, data-calibrated mathematical models have been created to analyze the self-sustaining and entrainable characteristics of the circadian clock [125, 126], as well as to model the circadian-linked oscillations in metabolism [29] and cell cycle [21].

The synchronization of circadian clocks is a fundamental characteristic of circadian rhythms in populations of cells. Circadian clocks in uninucleate cells distributed through a

tissue typically exhibit phase synchronization [127], but stochastic variation in gene expression hinder this synchronization [128].

Cheong et al. [2] used fluorescent imaging of a mCherry labeled clock-associated promoter to study the spatial scales over which synchronization among N. crassa nuclei that were not cytoplasmically connected: They packed unfused N. crassa conidial cells into two specialized microfluidic devices: a large chamber that simulated an artificial tissue (Figure 4.8b), and a microwell device which inhibited cell-to-cell contact. Cells that were packed into microwells of increasing density showed higher levels of synchronization, evidencing the presence of a quorum sensing molecule that can diffuse between individual cells. Based on the time scales over which cells became synchronized, they inferred this molecule must be protein-sized. Although only minimally syncytial (since each conidium may contain one, two or even up to 10 nuclei), the ability to track the emergence of synchrony between nuclear neighborhoods in syncytia is a tantalizing prospect for understanding how circadian clocks are assembled.

Microfluidic tools are likey to play a key role in allowing individual nuclear activities to be mointored. A recent study by Lee et al. [3] introduced a novel method for tracking single nuclei over circadian periods in *N. crassa*. To overcome the challenge posed by the fungus's rapid growth rate, which could cause nuclei to migrate outside of the imaging region, the researchers utilized a microfluidic device with a spiral design that effectively held nuclei within specified regions of interest (see Fig. 4.8c). smFISH (single-molecule fluorescence in situ hybridization), already exploited in yeast, and to study fungal cell cycle, is a powerful and flexible tool for creating static snap shots of the coronae of mRNAs surrounding each nucleus. Bartholomai et al. [4] used it to quantify and locate *frq* mRNA at various points in the circadian cycle. They discovered regular clustering of *frq* mRNA near nuclei (Figure 4.8d), mediated by interactions with the RNA-binding protein PRD-2. Surprisingly, *frq* mRNA levels were found to not exceed single digits per nucleus during a cycle, and only a small fraction of nuclei were found to be actively transcribing at any given time, despite being synchronized to the same oscillator. These low copy numbers are quantitatively discordant

with existing mathematical models that tend to require much higher transcription rates. They also suggest that circadian rhythm may be one of the first direct test beds for the general result, given in the previous section, that syncytia can stably and economically operate with more stochastic and lower transcription rates than uninucleate cells.

To probe whether syncytism allows for robust circadian clocks with low, noisy transcription rates, Zinn et al. [81] employed a syncytial gene expression model for linked nuclear neighborhoods, akin to the model outlined in Figure 4.1. This simplified model only encompassed the negative arm of the transcription-translation feedback loop, simplifying the circuit to the level of a solitary protein controlling its own transcriptional inhibition. This single feedback model closely mimics the circadian oscillations of *per* proteins observed in mammals, as modeled by Wang and Peskin [129], but with the added capability of the hypothetical clock protein to diffuse freely between different nuclear neighborhoods. Stochastic simulations on this system demonstrated that the sharing of clock proteins between neighborhoods facilitated precise and synchronized oscillations with a period of 24 hours at transcription rates nearly 1000-fold slower than a uninucleate system with comparable oscillatory precision. As discussed in Section 4.2, this noise insensitivity is due to the averaging of proteins between nuclear neighborhoods. Importantly, the mathematical models exposed how the labor of transcription is divided between nuclei; a readout that is hard to obtain from the static snapshots offered by smFISH measurements. At low transcription rates, often a single nucleus was responsible for the synthesizing the majority of mRNAs for the entire syncytial compartment, and this energy-saving division of labor occurred spontaneously and without additional mechanisms for coordination existing outside of the negative feedback loop.

4.4 Perspectives

In this chapter, we have highlighted specific adaptive characteristics that are present in fungal syncytia, allowing nuclei to coexist in a shared cytoplasm. The diverse mechanisms employed

by filamentous fungi to compartmentalize their cytosol and transport resources allow for independent nuclear behavior when required, such as with asynchronous cell division, while also facilitating coordinated responses to environmental stimuli. An essential trait found in syncytial cells is the ability to allocate the workload of RNA synthesis among multiple nuclei. We have termed this a 'syncytial assembly line', based on our presented mathematical model of gene expression in syncytia that indicates that nuclei can achieve the necessary copy number precision for a specific gene, even with increased transcriptional stochasticity, by sharing proteins across a large, continuous cytosol. The efficiency gains resulting from this division of transcriptional labor could explain the remarkable enzymatic output of filamentous fungi, enabling them to thrive in challenging environments and serve as a valuable resource for industrial protein production.

The themes of nuclear cooperation in syncytia explored in this chapter are not limited to filamentous fungi. Windner et al [130] outline a top-down system of nuclear regulation in *Drosophila* muscle cells, beginning with the global scaling of muscle cell size and number of nuclei conserved across cell types. As in some filamentous fungi, nuclei are distributed uniformly throughout the cell via microtubule repulsion [17], demarcating cytoplasmic territories which contain nuclei which may vary considerably in size and DNA content. In spite of this heterogeneity, the authors suggest that the diffusion of the nucleolar protein such as Fibrillarin across neighborhood boundaries may perform a critical role in homogenizing transcriptional activity, by regulating nucleolar-nuclear volume ratios. This mechanism suggests that the sharing of proteins between cytoplasmic territories can coordinate nuclear activity, which can help to smooth out expression heterogeneity at the cell level [130]. This global coordination of nuclei is important in tissues such as mammalian myofibers, where the nuclei work in concert to control muscle contraction [131].

Although we have highlighted circadian rhythm as a natural first place for bringing together mathematical modeling with experimental observations, we hypothesize that the sharing of gene products between compartments in syncytial fungi may contribute to robust gene

expression in a variety of cellular processes. Further research and mathematical modeling in this area is necessary to fully understand the complex mechanisms underlying fungal syncytial behavior and to identify novel strategies for enhancing protein production and optimizing biotechnological processes.

CHAPTER 5

Appendix

5.1 Transcriptional Bursting in a Two-State Gene Model

In the general two-state telegraph model of transcriptional bursting, the gene of interest stochastically transitions between an inactive and active state, characterized by switching rates k_{on} and k_{off}, respectively. During the active state, RNA is transcribed at a rate of k_0, encompassing elongation, termination, and export as a single step. Here we define a *burst* to occur if at least one RNA is transcribed during an activation period.

To understand the connection between the two-state model and Poisson bursting model used in the paper, we first consider the scenario describing a single burst, through the lens of the chemical master equation. We assume that at time $t = 0$, the gene is in the active state. Define $b \geq 0$ to be the random number of RNA transcribed before the gene turns off. The master equation for this process is given by

$$\begin{aligned} \frac{\partial P_{b,1}}{\partial t} &= k_0 \left(P_{b-1,1} - P_{b,1} \right) - k_{\text{off}} P_{b,1} \\ \frac{\partial P_{b,0}}{\partial t} &= k_{\text{off}} P_{b,1} \\ P_{0,1}(0) &= 1 \end{aligned} \tag{5.1}$$

where $P_{b,i}(t)$ represents the probability that b RNA are transcribed and the gene is in state i, where $i = 1$ and $i = 0$ represent the active and inactive state respectively. The distribution

of RNA transcribed during the active state is given by

$$\begin{aligned} P_b &= \lim_{t\to\infty} P_{b,0}(t) \\ &= \left(\frac{k_0}{k_0+k_{\text{off}}}\right)^b \left(\frac{k_{\text{off}}}{k_0+k_{off}}\right) \end{aligned} \tag{5.2}$$

Note that this is equivalent to a geometric distribution with "success" probability $\frac{k_{\text{off}}}{k_0+k_{\text{off}}}$, and b the number of "failures" before first success. The mean number of RNAs transcribed during a given activation period is then given by

$$\langle b\rangle = \frac{k_0}{k_{\text{off}}} \tag{5.3}$$

We may also consider the mean waiting time for bursts to occur, given that a gene is initially inactive. To compute this, we consider the three state master equation

$$\begin{aligned} \frac{\partial P_0}{\partial t} &= k_{\text{off}}P_1 - k_{\text{on}}P_0 \\ \frac{\partial P_1}{\partial t} &= k_{\text{on}}P_0 - (k_0+k_{\text{off}})P_1 \\ \frac{\partial P_2}{\partial t} &= k_0 P_1 \\ P_0(0) &= 1 \end{aligned} \tag{5.4}$$

Where P_0 is the initial, inactive state, P_1 is the state in which the gene is active but RNA have yet to be transcribed, and P_2 is the state in which transcription has occurred. Let T denote the waiting time distribution for the system to first transition to state 2. It follows that $Pr(T \le t) = P_2(t)$, so $Pr(T = t) = P_2'(t)$. Upon solving in mathematica, we find

$$\langle T\rangle = \frac{k_0 + k_{\text{on}} + k_{\text{off}}}{k_0 k_{\text{on}}}. \tag{5.5}$$

Thus the frequency of bursts is given by

$$\begin{aligned} k_m &= \frac{1}{\langle T \rangle} \\ &= k_{\text{on}} \frac{\frac{k_0}{k_{\text{off}}}}{1 + \frac{k_0}{k_{\text{off}}} + \frac{k_{\text{on}}}{k_{\text{off}}}}. \end{aligned} \tag{5.6}$$

To quantify the steady state distribution of RNA in the random telegraph model for gene activity, we write out the corresponding moment equations:

$$\begin{aligned} \langle \dot{G} \rangle &= k_{\text{on}} - (k_{\text{off}} + k_{\text{on}}) \langle G \rangle \\ \langle \dot{m} \rangle &= k_0 \langle G \rangle - \gamma_m \langle m \rangle \\ \langle \dot{G^2} \rangle &= k_{\text{on}} + (k_{\text{on}} + k_{\text{off}}) \langle G \rangle - 2(k_{\text{on}} + k_{\text{off}}) \left\langle G^2 \right\rangle \\ \langle \dot{m^2} \rangle &= k_0 \langle G \rangle + \gamma_m \langle m \rangle + 2k_0 \langle Gm \rangle - 2\gamma_m \left\langle m^2 \right\rangle \\ \langle \dot{Gm} \rangle &= k_{on} \langle m \rangle - (k_{\text{off}} + k_{\text{on}} + \gamma_m) \langle Gm \rangle + k_0 \left\langle G^2 \right\rangle, \end{aligned} \tag{5.7}$$

where γ_m is the cytoplasmic RNA decay rate, and we introduce the discrete variable G to represent gene state, taking the value 0 when the gene is inactive and 1 when the gene is active. Upon solving these equations, we find

$$\begin{aligned} \langle m \rangle &= \frac{k_0}{k_{\text{off}}} \frac{\frac{k_{\text{on}}}{\gamma_m}}{1 + \frac{k_{\text{on}}}{k_{\text{off}}}} \\ CV^2(m) &= \frac{1}{\langle m \rangle} + \frac{\frac{\gamma_m}{k_{\text{on}}}}{1 + \frac{\gamma_m}{k_{\text{off}}} + \frac{k_{\text{on}}}{k_{\text{off}}}}. \end{aligned} \tag{5.8}$$

In the limit where the gene spends the majority of the time in the inactive state, and the RNA lifetime is much greater than gene activation time, we have $\frac{\gamma_m}{k_{\text{off}}} \ll 1$ and $\frac{k_{\text{on}}}{k_{\text{off}}} \ll 1$. We may consequently approximate bursts as instantaneous, arriving with frequency

$$k_m \approx k_{\text{on}} \frac{\frac{k_0}{k_{\text{off}}}}{1 + \frac{k_0}{k_{\text{off}}}} \tag{5.9}$$

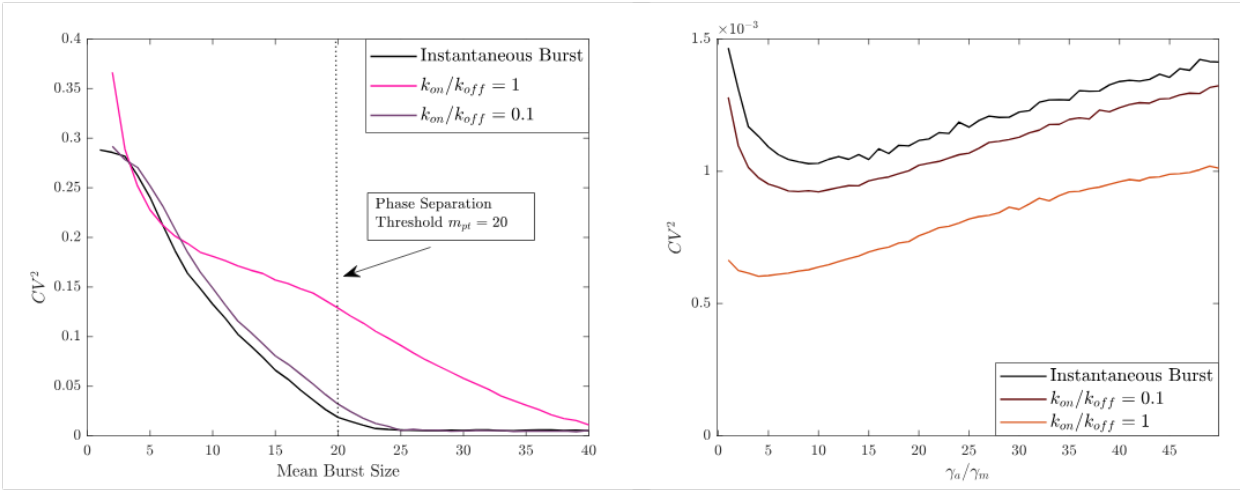

Figure 5.1 Stochastic Simulation Results With General Bursting Model. Left panel: Fig. 8a reproduced with $k_{\text{on}}/k_{\text{off}} = \{0.1, 1.0\}$. $CV^2(p)$ qualitatively deviates from the Poisson bursting model when $(k_{\text{on}}/k_{\text{off}} = 1)$, but still decreases monotonically with burst size. Right panel: Fig. 10a reproduced with $k_{\text{on}}/k_{\text{off}} = 0.1$ and $k_{\text{on}}/k_{\text{off}} = 1$. As $k_{\text{on}}/k_{\text{off}}$ decreases to 0, $CV^2(p)$ tends to shift vertically to the Poisson bursting curve in black.

and distributed by the positive geometric random variable $B = 1 + b$, where

$$\langle B \rangle = 1 + \frac{k_0}{k_{\text{off}}}. \tag{5.10}$$

It can be shown that in terms of these limiting parameters,

$$\begin{aligned} \langle m \rangle &= \frac{k_m \langle B \rangle}{\gamma_m} \\ CV^2(m) &= \frac{\langle B \rangle}{\langle m \rangle}, \end{aligned} \tag{5.11}$$

which is what we use in the main text.

In Figure , we investigate the impact of explicitly modeling gene activity on noise suppression in the buffering and filtering models. We selected parameters to ensure that the effective bursting frequency (Eq. 5.9) and burst size (Eq. 5.10) matched those of the instantaneous bursting model, resulting in an equivalent number of transcripts per unit time. The results demonstrate that, for a $k_{\text{on}}/k_{\text{off}} = 0.1$, the coefficient of variation squared ($CV^2(p)$) exhibits minimal deviation from the noise curve computed in Figures 8a and 10a, validating our approximation. In scenarios where genes spend an equal amount of time in either state, noise is amplified in the buffering scenario but reduced in the filtering scenario, while overall remaining qualitatively similar.

5.2 Syncytial Diffusion Time Scale

In this appendix section, we show that fluctuations in sub-compartmental protein abundance can be ignored over sufficiently large time scales in the scenario where total hyphal protein abundance is fixed. We begin by considering a hyphal system of radius R and length L consisting of M brownian particles with self-diffusivity D distributed amongst N uniform sub-compartments, as depicted in Figure 4.4. Now, consider the stochastic process

$$p(t) = \text{Number of protein in given compartment } k \text{ at time } t$$

governed by the system parameters, and let T be a characteristic measuring time scale of the system. Then

$$p_T = \frac{1}{T}\int_{t_1}^{T+t_1} p(t)dt \tag{5.12}$$

To determine how time scale averaging suppresses diffusive noise in syncytia, we compute $CV^2(p_T)$. Note first that

$$\begin{aligned}\langle p_T^2\rangle &= \left\langle \frac{1}{T^2}\int_{t_1}^{t_1+T}\int_{t_1}^{t_1+T} p(t')p(t'')dt'dt'' \right\rangle \\ &= \frac{1}{T^2}\int_{t_1}^{t_1+T}\int_{t_1}^{t_1+T} \langle p(t')p(t'')\rangle dt'dt'' \\ &= \frac{1}{T^2}\int_0^T\int_0^T G(t'-t'')dt'dt''\end{aligned} \tag{5.13}$$

where $G(\tau) = \langle p(t)p(t+\tau)\rangle$ is the autocorrelation function of $p(t)$. Now, observe that

$$\begin{aligned}p(t) &= \sum_{j=1}^{M} w_j(t) \\ w_j(t) &= \begin{cases} 1 & \text{Particle } j \text{ in compartment } k \text{ at time } t \\ 0 & \text{Otherwise}\end{cases}\end{aligned} \tag{5.14}$$

Taking this decomposition of $p(t)$ into M independent stochastic processes, we find that

$$G(\tau) = \sum_{j=1}^{M}\langle w_j(t)w_j(t+\tau)\rangle + \sum_{j\neq i}^{M}\sum_{i=1}^{M}\langle w_j(t)w_i(t+\tau)\rangle \tag{5.15}$$

Since the proteins are non-interacting

$$\sum_{i,j}\langle w_j(t)w_i(t+\tau)\rangle = \frac{M(M-1)}{N^2}, \tag{5.16}$$

and, additionally,

$$\langle w_j(t)w_j(t+\tau)\rangle = \text{Prob(Particle } j \text{ found in compartment } k \text{ at times } t \text{ and } t+\tau) \quad (5.17)$$

Now consider $u(\mathbf{x},t)$, defined as the probability density of a single protein. It's evolution satisfies the diffusion equation

$$\begin{aligned} \frac{\partial u}{\partial t} &= D\Delta^2 u \\ \frac{\partial u}{\partial n} &= 0 \text{ at hyphal boundary} \\ u(x,0) &= \begin{cases} \frac{1}{V} & \text{in compartment j} \\ 0 & \text{Otherwise} \end{cases} \end{aligned} \quad (5.18)$$

where $V = \pi R^2 L$ is the volume of compartment k. Taking $\bar{u}(t) = \frac{1}{\pi R^2}\int u dA$ to be the cross-sectional averaged probability distriubtion, we may show that

$$\begin{aligned} \frac{\partial \bar{u}}{\partial t} &= D\frac{\partial^2 \bar{u}}{\partial z^2} \\ \bar{u}(z,0) &= \begin{cases} \frac{1}{L} & \text{in compartment } k \\ 0 & \text{Otherwise} \end{cases} \\ \frac{\partial \bar{u}}{\partial z} &= 0 \quad \text{at ends of syncytium} \end{aligned} \quad (5.19)$$

Upon nondimensionalizing with $t = \frac{L^2N^2}{D}t^*$, $\bar{u} = \frac{1}{L}u^*$, $z = LNz^*$, we find

$$\begin{aligned} \frac{\partial u^*}{\partial t^*} &= \frac{\partial^2 u^*}{\partial z^{*2}} \\ u^*(z,0) &= \begin{cases} 1 & \frac{(j-1)}{N} < z < \frac{j}{N} \\ 0 & \text{Otherwise} \end{cases} \\ 0 &= \frac{\partial u}{\partial z}(0,t) = \frac{\partial u}{\partial z}(1,t) \end{aligned} \quad (5.20)$$

Solving equation (5.20) through separation of variables, we arrive at the series solution

$$\begin{aligned} u^*(z^*,t^*) &= \sum_{n=0}^{\infty} A_n e^{-\pi^2 n^2 t^*} \cos(\pi n z^*) \\ A_n &= \begin{cases} \frac{2}{\pi n}\left[\sin\left(\frac{\pi j n}{N}\right) - \sin\left(\frac{\pi(j-1)n}{N}\right)\right] & n > 0 \\ \frac{1}{N} & n = 0 \end{cases}, \end{aligned} \tag{5.21}$$

which may be approximated by neglecting modes with $n \geq 2$, i.e

$$u^*(z^*,t^*) \approx \frac{1}{N} + \frac{2}{\pi}\left[\sin\left(\frac{\pi j}{N}\right) - \sin\left(\frac{\pi(j-1)}{N}\right)\right] e^{-\pi^2 t^*} \cos(\pi z^*) \tag{5.22}$$

Take t^*, z^* to be new length scale

$$u(z,t) \approx \frac{1}{NL} + \frac{2}{\pi L}\left[\sin\left(\frac{\pi j}{N}\right) - \sin\left(\frac{\pi(j-1)}{N}\right)\right] e^{-\frac{D\pi^2 t}{L^2 N^2}} \cos\left(\frac{\pi z}{LN}\right) \tag{5.23}$$

Now,

$$\begin{aligned} \langle w_j(t) w_j(t+\tau)\rangle &= \frac{1}{N}\int_{(j-1)L}^{jL} u(z,\tau)dz \\ &= \frac{1}{N^2} + \frac{2}{\pi^2}\left[\sin\left(\frac{\pi j}{N}\right) - \sin\left(\frac{\pi(j-1)}{N}\right)\right]^2 e^{-\frac{D\pi^2|\tau|}{L^2N^2}}, \end{aligned} \tag{5.24}$$

so

$$\begin{aligned} G(\tau) &\approx \frac{M(M-1)}{N^2} + \frac{M}{N^2} + \frac{2M}{\pi^2}\left[\sin\left(\frac{\pi j}{N}\right) - \sin\left(\frac{\pi(j-1)}{N}\right)\right]^2 e^{-\frac{D\pi^2|\tau|}{L^2N^2}} \\ &= \frac{M^2}{N^2} + +\frac{2M}{\pi^2}\left[\sin\left(\frac{\pi j}{N}\right) - \sin\left(\frac{\pi(j-1)}{N}\right)\right]^2 e^{-\frac{D\pi^2|\tau|}{L^2N^2}} \end{aligned} \tag{5.25}$$

Since $G(\tau) = G(-\tau)$,

$$\begin{aligned}
\langle p_T^2 \rangle &= \frac{1}{T^2}\int_0^T \int_0^T \left(\frac{M^2}{N^2} + + \frac{2M}{\pi^2}\left[\sin\left(\frac{\pi j}{N}\right) - \sin\left(\frac{\pi(j-1)}{N}\right)\right]^2 e^{-\frac{D\pi^2|t'-t''|}{L^2N^2}} \right) dt'dt'' \\
&= \frac{M^2}{N^2} + \frac{2M}{\pi^2 T^2}\left[\sin\left(\frac{\pi j}{N}\right) - \sin\left(\frac{\pi(j-1)}{N}\right)\right]^2 \int_0^T \int_{t'=t''}^T 2e^{-\frac{D\pi^2(t'-t'')}{L^2N^2}} dt'dt'' \\
&= \frac{M^2}{N^2} + \frac{2M}{\pi^2 T^2}\left[\sin\left(\frac{\pi j}{N}\right) - \sin\left(\frac{\pi(j-1)}{N}\right)\right]^2 \left(\frac{\frac{2TD\pi^2}{L^2N^2} + 2\exp\left(-\frac{TD\pi^2}{L^2N^2}\right) - 1}{\left(\frac{D\pi^2}{L^2N^2}\right)^2} \right) \\
&= \frac{M^2}{N^2} + \frac{4M}{\pi^2}\left[\sin\left(\frac{\pi j}{N}\right) - \sin\left(\frac{\pi(j-1)}{N}\right)\right]^2 \left(\frac{x + e^{-x} - 1}{x^2} \right) \\
&\leq \frac{M^2}{N^2} + \frac{4M}{N^2}\left(\frac{\frac{x}{N^2} + e^{-x/N^2} - 1}{(x/N^2)^2} \right) \\
&= \langle p \rangle^2 + \frac{4\langle p \rangle}{N}\left(\frac{\frac{x}{N^2} + e^{-x/N^2} - 1}{(x/N^2)^2} \right)
\end{aligned} \tag{5.26}$$

$$CV^2(p_T) \leq \frac{4\langle p \rangle}{N}\left(\frac{\frac{x}{N^2} + e^{-x/N^2} - 1}{(x/N^2)^2} \right),$$

where $\langle p \rangle = \frac{M}{N}$, and $x = \frac{\pi^2 DT}{L^2}$. Consequently, the reduction factor from time averaging subcompartmental abundances is bounded by:

$$\frac{CV^2(p_T)}{CV^2(p_{comp})} \leq \frac{4}{N-1}\left(\frac{\frac{x}{N^2} + e^{-x/N^2} - 1}{(x/N^2)^2} \right) \tag{5.27}$$

For fixed $N = \mathcal{O}(10)$, if $x \gg N^2$,

$$\begin{aligned}
\frac{CV^2(p_T)}{CV^2(p_{comp})} &\approx \frac{4N}{(N-1)x} \\
&\leq \frac{8}{x} \\
&\ll 1
\end{aligned} \tag{5.28}$$

In our analysis, we find that time averaged noise level become sub-Poissonian when the temporal response window T greatly exceeds the threshold given by $T \gg \frac{L^2 N^2}{\pi^2 D}$. Within the context of our model organism, *A. gossypii*, we have estimated key parameters: $L \approx 3\mu m$, $N \approx 10$, and $D \approx 30\mu^2 m/s$. Consequently, we can infer that T should be much greater than 3 seconds for the diffusive noise to be effectively suppressed. This result implies that by averaging signal measurements over minutes, the absolute fluctuations in sub-compartmental protein abundance due strictly to diffusion are effectively mitigated in *A. gossypii*.

REFERENCES

[1] I. Seim, A. E. Posey, W. T. Snead, B. M. Stormo, D. Klotsa, R. V. Pappu, and A. S. Gladfelter, "Dilute phase oligomerization can oppose phase separation and modulate material properties of a ribonucleoprotein condensate," *Proceedings of the National Academy of Sciences*, vol. 119, no. 13, p. e2120799119, 2022.

[2] J. H. Cheong, X. Qiu, Y. Liu, A. Al-Omari, J. Griffith, H.-B. Schüttler, L. Mao, and J. Arnold, "The macroscopic limit to synchronization of cellular clocks in single cells of neurospora crassa," *Scientific Reports*, vol. 12, no. 1, p. 6750, 2022.

[3] K. K. Lee, L. Labiscsak, C. H. Ahn, and C. I. Hong, "Spiral-based microfluidic device for long-term time course imaging of neurospora crassa with single nucleus resolution," *Fungal Genetics and Biology*, vol. 94, pp. 11–14, 2016.

[4] B. M. Bartholomai, A. S. Gladfelter, J. J. Loros, and J. C. Dunlap, "PRD-2 mediates clock-regulated perinuclear localization of clock gene RNAs within the circadian cycle of Neurospora," *Proceedings of the National Academy of Sciences*, vol. 119, no. 31, p. e2203078119, 2022.

[5] I. G. Romero, I. Ruvinsky, and Y. Gilad, "Comparative studies of gene expression and the evolution of gene regulation," *Nature Reviews Genetics*, vol. 13, no. 7, pp. 505–516, 2012.

[6] A. M. Femino, F. S. Fay, K. Fogarty, and R. H. Singer, "Visualization of single rna transcripts in situ," *Science*, vol. 280, no. 5363, pp. 585–590, 1998.

[7] Z. Wang, M. Gerstein, and M. Snyder, "Rna-seq: a revolutionary tool for transcriptomics," *Nature reviews genetics*, vol. 10, no. 1, pp. 57–63, 2009.

[8] S. Clancy *et al.*, "Rna splicing: introns, exons and spliceosome," *Nature Education*, vol. 1, no. 1, p. 31, 2008.

[9] D. Görlich and U. Kutay, "Transport between the cell nucleus and the cytoplasm," *Annual review of cell and developmental biology*, vol. 15, no. 1, pp. 607–660, 1999.

[10] B. Alberts, *Molecular biology of the cell*. Garland science, 2017.

[11] S. L. Rogers and V. I. Gelfand, "Membrane trafficking, organelle transport, and the cytoskeleton," *Current opinion in cell biology*, vol. 12, no. 1, pp. 57–62, 2000.

[12] D. Görlich, "Transport into and out of the cell nucleus," *The EMBO journal*, vol. 17, no. 10, pp. 2721–2727, 1998.

[13] B. Darbani, D. B. Kell, and I. Borodina, "Energetic evolution of cellular transportomes," *BMC genomics*, vol. 19, no. 1, pp. 1–11, 2018.

[14] S. F. Banani, H. O. Lee, A. A. Hyman, and M. K. Rosen, "Biomolecular condensates: organizers of cellular biochemistry," *Nature reviews Molecular cell biology*, vol. 18, no. 5, pp. 285–298, 2017.

[15] M. J. do Amaral, I. de Andrade Rosa, S. A. Andrade, X. Fang, L. R. Andrade, M. L. Costa, and C. Mermelstein, "The perinuclear region concentrates disordered proteins with predicted phase separation distributed in a 3d network of cytoskeletal filaments and organelles," *Biochimica et Biophysica Acta (BBA)-Molecular Cell Research*, vol. 1869, no. 1, p. 119161, 2022.

[16] S. Grava, M. Keller, S. Voegeli, S. Seger, C. Lang, and P. Philippsen, "Clustering of nuclei in multinucleated hyphae is prevented by dynein-driven bidirectional nuclear movements and microtubule growth control in ashbya gossypii," *Eukaryotic cell*, vol. 10, no. 7, pp. 902–915, 2011.

[17] O. Deshpande, J. De-Carvalho, D. V. Vieira, and I. A. Telley, "Astral microtubule cross-linking safeguards uniform nuclear distribution in the drosophila syncytium," *Journal of Cell Biology*, vol. 221, no. 1, p. e202007209, 2021.

[18] E. S. Folker and M. K. Baylies, "Nuclear positioning in muscle development and disease," *Frontiers in physiology*, vol. 4, p. 363, 2013.

[19] L. S. Bigman and Y. Levy, "Tubulin tails and their modifications regulate protein diffusion on microtubules," *Proceedings of the National Academy of Sciences*, vol. 117, no. 16, pp. 8876–8883, 2020.

[20] S. E. Dundon, S.-S. Chang, A. Kumar, P. Occhipinti, H. Shroff, M. Roper, and A. S. Gladfelter, "Clustered nuclei maintain autonomy and nucleocytoplasmic ratio control in a syncytium," *Molecular biology of the cell*, vol. 27, no. 13, pp. 2000–2007, 2016.

[21] C. I. Hong, J. Zámborszky, M. Baek, L. Labiscsak, K. Ju, H. Lee, L. F. Larrondo, A. Goity, H. S. Chong, W. J. Belden, *et al.*, "Circadian rhythms synchronize mitosis in neurospora crassa," *Proceedings of the National Academy of Sciences*, vol. 111, no. 4, pp. 1397–1402, 2014.

[22] P. D. Mavroudis and W. J. Jusko, "Mathematical modeling of mammalian circadian clocks affecting drug and disease responses," *Journal of pharmacokinetics and pharmacodynamics*, vol. 48, pp. 375–386, 2021.

[23] J. Dunlap, J. Loros, H. Colot, A. Mehra, W. Belden, M. Shi, C. Hong, L. Larrondo, C. Baker, C.-H. Chen, *et al.*, "A circadian clock in neurospora: how genes and proteins cooperate to produce a sustained, entrainable, and compensated biological oscillator with a period of about a day," in *Cold Spring Harbor symposia on quantitative biology*, vol. 72, p. 57, NIH Public Access, 2007.

[24] J. C. Sible and J. J. Tyson, "Mathematical modeling as a tool for investigating cell cycle control networks," *Methods*, vol. 41, no. 2, pp. 238–247, 2007.

[25] N. T. Ingolia and A. W. Murray, "The ups and downs of modeling the cell cycle," *Current Biology*, vol. 14, no. 18, pp. R771–R777, 2004.

[26] A. Ay and D. N. Arnosti, "Mathematical modeling of gene expression: a guide for the perplexed biologist," *Critical reviews in biochemistry and molecular biology*, vol. 46, no. 2, pp. 137–151, 2011.

[27] A. Singh, "Negative feedback through mrna provides the best control of gene-expression noise," *IEEE transactions on nanobioscience*, vol. 10, no. 3, pp. 194–200, 2011.

[28] B. C. Goodwin, "Oscillatory behavior in enzymatic control processes," *Advances in enzyme regulation*, vol. 3, pp. 425–437, 1965.

[29] A. A. Dovzhenok, M. Baek, S. Lim, and C. I. Hong, "Mathematical modeling and validation of glucose compensation of the neurospora circadian clock," *Biophysical journal*, vol. 108, no. 7, pp. 1830–1839, 2015.

[30] R. J. Wimmer, Y. Liu, T. N. Schachter, D. P. Stonko, B. E. Peercy, and M. F. Schneider, "Mathematical modeling reveals modulation of both nuclear influx and efflux of foxo1 by the igf-i/pi3k/akt pathway in skeletal muscle fibers," *American Journal of Physiology-Cell Physiology*, vol. 306, no. 6, pp. C570–C584, 2014.

[31] N. Maheshri and E. K. O'Shea, "Living with noisy genes: How cells function reliably with inherent variability in gene expression," *Annu. Rev. Biophys. Biomol. Struct.*, vol. 36, pp. 413–434, 2007.

[32] J. M. Raser and E. K. O'Shea, "Noise in gene expression: origins, consequences, and control," *Science*, vol. 309, no. 5743, pp. 2010–2013, 2005.

[33] D. A. Charlebois, "Effect and evolution of gene expression noise on the fitness landscape," *Physical Review E*, vol. 92, no. 2, p. 022713, 2015.

[34] Z. Wang and J. Zhang, "Impact of gene expression noise on organismal fitness and the efficacy of natural selection," *Proceedings of the National Academy of Sciences*, vol. 108, no. 16, pp. E67–E76, 2011.

[35] R. Bahar, C. H. Hartmann, K. A. Rodriguez, A. D. Denny, R. A. Busuttil, M. E. Dollé, R. B. Calder, G. B. Chisholm, B. H. Pollock, C. A. Klein, *et al.*, "Increased cell-to-cell variation in gene expression in ageing mouse heart," *Nature*, vol. 441, no. 7096, pp. 1011–1014, 2006.

[36] C. Buccitelli and M. Selbach, "mrnas, proteins and the emerging principles of gene expression control," *Nature Reviews Genetics*, vol. 21, no. 10, pp. 630–644, 2020.

[37] F. Miura, N. Kawaguchi, M. Yoshida, C. Uematsu, K. Kito, Y. Sakaki, and T. Ito, "Absolute quantification of the budding yeast transcriptome by means of competitive pcr between genomic and complementary dnas," *BMC genomics*, vol. 9, no. 1, pp. 1–14, 2008.

[38] J. Hausser, A. Mayo, L. Keren, and U. Alon, "Central dogma rates and the trade-off between precision and economy in gene expression," *Nature communications*, vol. 10, no. 1, pp. 1–15, 2019.

[39] K. E. Shearwin, B. P. Callen, and J. B. Egan, "Transcriptional interference–a crash course," *TRENDS in Genetics*, vol. 21, no. 6, pp. 339–345, 2005.

[40] S. Kim and J. Shendure, "Mechanisms of interplay between transcription factors and the 3d genome," *Molecular cell*, vol. 76, no. 2, pp. 306–319, 2019.

[41] A. Sanchez and I. Golding, "Genetic determinants and cellular constraints in noisy gene expression," *Science*, vol. 342, no. 6163, pp. 1188–1193, 2013.

[42] N. Kumar, A. Singh, and R. V. Kulkarni, "Transcriptional bursting in gene expression: analytical results for general stochastic models," *PLoS computational biology*, vol. 11, no. 10, p. e1004292, 2015.

[43] D. Nicolas, N. E. Phillips, and F. Naef, "What shapes eukaryotic transcriptional bursting?," *Molecular BioSystems*, vol. 13, no. 7, pp. 1280–1290, 2017.

[44] H. Boeger, R. Shelansky, H. Patel, and C. R. Brown, "From structural variation of gene molecules to chromatin dynamics and transcriptional bursting," *Genes*, vol. 6, no. 3, pp. 469–483, 2015.

[45] L. Huang, Z. Yuan, J. Yu, and T. Zhou, "Fundamental principles of energy consumption for gene expression," *Chaos: An Interdisciplinary Journal of Nonlinear Science*, vol. 25, no. 12, p. 123101, 2015.

[46] N. Barkai and S. Leibler, "Circadian clocks limited by noise," *Nature*, vol. 403, no. 6767, pp. 267–268, 2000.

[47] B. Lehner, "Selection to minimise noise in living systems and its implications for the evolution of gene expression," *Molecular systems biology*, vol. 4, no. 1, p. 170, 2008.

[48] D. Tan, R. Chen, Y. Mo, S. Gu, J. Ma, W. Xu, X. Lu, H. He, F. Jiang, W. Fan, *et al.*, "Quantitative control of noise in mammalian gene expression by dynamic histone regulation," *Elife*, vol. 10, p. e65654, 2021.

[49] T. Stoeger, N. Battich, and L. Pelkmans, "Passive noise filtering by cellular compartmentalization," *Cell*, vol. 164, no. 6, pp. 1151–1161, 2016.

[50] I. Lestas, G. Vinnicombe, and J. Paulsson, "Fundamental limits on the suppression of molecular fluctuations," *Nature*, vol. 467, no. 7312, pp. 174–178, 2010.

[51] A. Klosin, F. Oltsch, T. Harmon, A. Honigmann, F. Jülicher, A. A. Hyman, and C. Zechner, "Phase separation provides a mechanism to reduce noise in cells," *Science*, vol. 367, no. 6476, pp. 464–468, 2020.

[52] D. Deviri and S. A. Safran, "Physical theory of biological noise buffering by multicomponent phase separation," *Proceedings of the National Academy of Sciences*, vol. 118, no. 25, p. e2100099118, 2021.

[53] D. Tauber, G. Tauber, and R. Parker, "Mechanisms and regulation of RNA condensation in RNP granule formation," *Trends in biochemical sciences*, vol. 45, no. 9, pp. 764–778, 2020.

[54] E. M. Langdon and A. S. Gladfelter, "A new lens for RNA localization: liquid-liquid phase separation," *Annual Review of Microbiology*, vol. 72, pp. 255–271, 2018.

[55] B. Tsang, J. Arsenault, R. M. Vernon, H. Lin, N. Sonenberg, L.-Y. Wang, A. Bah, and J. D. Forman-Kay, "Phosphoregulated fmrp phase separation models activity-dependent translation through bidirectional control of mrna granule formation," *Proceedings of the National Academy of Sciences*, vol. 116, no. 10, pp. 4218–4227, 2019.

[56] Y. Cai and B. Futcher, "Effects of the yeast RNA-binding protein Whi3 on the half-life and abundance of CLN3 mRNA and other targets," *PloS one*, vol. 8, no. 12, p. e84630, 2013.

[57] C. Lee, H. Zhang, A. E. Baker, P. Occhipinti, M. E. Borsuk, and A. S. Gladfelter, "Protein aggregation behavior regulates cyclin transcript localization and cell-cycle control," *Developmental cell*, vol. 25, no. 6, pp. 572–584, 2013.

[58] R. B. Ash and M. F. Gardner, *Topics in Stochastic Processes: Probability and Mathematical Statistics: A Series of Monographs and Textbooks*, vol. 27. Academic press, 2014.

[59] J. P. Hespanha, "A model for stochastic hybrid systems with application to communication networks," *Nonlinear Analysis: Theory, Methods & Applications*, vol. 62, no. 8, pp. 1353–1383, 2005.

[60] R. D. Dar, B. S. Razooky, A. Singh, T. V. Trimeloni, J. M. McCollum, C. D. Cox, M. L. Simpson, and L. S. Weinberger, "Transcriptional burst frequency and burst size are equally modulated across the human genome," *Proceedings of the National Academy of Sciences*, vol. 109, no. 43, pp. 17454–17459, 2012.

[61] D. T. Gillespie, "Exact stochastic simulation of coupled chemical reactions," *The journal of physical chemistry*, vol. 81, no. 25, pp. 2340–2361, 1977.

[62] S. P. Gygi, Y. Rochon, B. R. Franza, and R. Aebersold, "Correlation between protein and mRNA abundance in yeast," *Molecular and cellular biology*, vol. 19, no. 3, pp. 1720–1730, 1999.

[63] V. Pelechano, S. Chavez, and J. E. Perez-Ortin, "A complete set of nascent transcription rates for yeast genes," *PloS one*, vol. 5, no. 11, p. e15442, 2010.

[64] L.-L. Chia and C. McLaughlin, "The half-life of mRNA in Saccharomyces cerevisiae," *Molecular and General Genetics MGG*, vol. 170, no. 2, pp. 137–144, 1979.

[65] A. Belle, A. Tanay, L. Bitincka, R. Shamir, and E. K. O'Shea, "Quantification of protein half-lives in the budding yeast proteome," *Proceedings of the National Academy of Sciences*, vol. 103, no. 35, pp. 13004–13009, 2006.

[66] H. Zhang, S. Elbaum-Garfinkle, E. M. Langdon, N. Taylor, P. Occhipinti, A. A. Bridges, C. P. Brangwynne, and A. S. Gladfelter, "Rna controls PolyQ protein phase transitions," *Molecular cell*, vol. 60, no. 2, pp. 220–230, 2015.

[67] A. A. Hyman, C. A. Weber, and F. Jülicher, "Liquid-liquid phase separation in biology," *Annual review of cell and developmental biology*, vol. 30, pp. 39–58, 2014.

[68] P. Thomas, H. Matuschek, and R. Grima, "How reliable is the linear noise approximation of gene regulatory networks?," *BMC genomics*, vol. 14, pp. 1–15, 2013.

[69] S. Alberti, "Phase separation in biology," *Current Biology*, vol. 27, no. 20, pp. R1097–R1102, 2017.

[70] J. Luo, L. Qu, F. Gao, J. Lin, J. Liu, and A. Lin, "Lncrnas: architectural scaffolds or more potential roles in phase separation," *Frontiers in Genetics*, vol. 12, p. 626234, 2021.

[71] E. M. Langdon, Y. Qiu, A. Ghanbari Niaki, G. A. McLaughlin, C. A. Weidmann, T. M. Gerbich, J. A. Smith, J. M. Crutchley, C. M. Termini, K. M. Weeks, *et al.*, "mRNA structure determines specificity of a polyQ-driven phase separation," *Science*, vol. 360, no. 6391, pp. 922–927, 2018.

[72] M. Roper, C. Lee, P. C. Hickey, and A. S. Gladfelter, "Life as a moving fluid: fate of cytoplasmic macromolecules in dynamic fungal syncytia," *Current opinion in microbiology*, vol. 26, pp. 116–122, 2015.

[73] G. Jedd, "Fungal evo–devo: organelles and multicellular complexity," *Trends in cell biology*, vol. 21, no. 1, pp. 12–19, 2011.

[74] *Syncytia: Origin, structure, and functions*. SPRINGER INTERNATIONAL PU, 2023.

[75] N. L. Glass and I. Kaneko, "Fatal attraction: nonself recognition and heterokaryon incompatibility in filamentous fungi," *Eukaryotic cell*, vol. 2, no. 1, pp. 1–8, 2003.

[76] A. P. Mela, A. M. Rico-Ramírez, and N. L. Glass, "Syncytia in fungi," *Cells*, vol. 9, no. 10, p. 2255, 2020.

[77] A. Daskalov, J. Heller, S. Herzog, A. Fleißner, and N. L. Glass, "Molecular mechanisms regulating cell fusion and heterokaryon formation in filamentous fungi," *Microbiology Spectrum*, vol. 5, no. 2, pp. 10–1128, 2017.

[78] A. Raj, C. S. Peskin, D. Tranchina, D. Y. Vargas, and S. Tyagi, "Stochastic mrna synthesis in mammalian cells," *PLoS biology*, vol. 4, no. 10, p. e309, 2006.

[79] S. Adhya and M. Gottesman, "Promoter occlusion: transcription through a promoter may inhibit its activity," *Cell*, vol. 29, no. 3, pp. 939–944, 1982.

[80] A. M. Poveda, M. Le Clech, and P. Pasero, "Transcription and replication: breaking the rules of the road causes genomic instability," *Transcription*, vol. 1, no. 2, pp. 99–102, 2010.

[81] L. Zinn-Brooks and M. L. Roper, "Circadian rhythm shows potential for mrna efficiency and self-organized division of labor in multinucleate cells," *PLOS Computational Biology*, vol. 17, no. 8, p. e1008828, 2021.

[82] C. A. Anderson, U. Eser, T. Korndorf, M. E. Borsuk, J. M. Skotheim, and A. S. Gladfelter, "Nuclear repulsion enables division autonomy in a single cytoplasm," *Current Biology*, vol. 23, no. 20, pp. 1999–2010, 2013.

[83] A. Pantazopoulou and M. A. Penalva, "Organization and dynamics of the aspergillus nidulans golgi during apical extension and mitosis," *Molecular biology of the cell*, vol. 20, no. 20, pp. 4335–4347, 2009.

[84] M. Roper, A. Simonin, P. C. Hickey, A. Leeder, and N. L. Glass, "Nuclear dynamics in a fungal chimera," *Proceedings of the National Academy of Sciences*, vol. 110, no. 32, pp. 12875–12880, 2013.

[85] T. B. Kepler and T. C. Elston, "Stochasticity in transcriptional regulation: origins, consequences, and mathematical representations," *Biophysical journal*, vol. 81, no. 6, pp. 3116–3136, 2001.

[86] A. J. Mayer, M. Roper, A. S. Gladfelter, and G. McLaughlin, "The role of rna condensation in reducing gene expression noise," *Biophysical Journal*, vol. 122, no. 3, pp. 415a–416a, 2023.

[87] A. Bar-Even, J. Paulsson, N. Maheshri, M. Carmi, E. O'Shea, Y. Pilpel, and N. Barkai, "Noise in protein expression scales with natural protein abundance," *Nature genetics*, vol. 38, no. 6, pp. 636–643, 2006.

[88] M. Roper, C. Ellison, J. W. Taylor, and N. L. Glass, "Nuclear and genome dynamics in multinucleate ascomycete fungi," *Current biology*, vol. 21, no. 18, pp. R786–R793, 2011.

[89] A. S. Gladfelter, A. K. Hungerbuehler, and P. Philippsen, "Asynchronous nuclear division cycles in multinucleated cells," *The Journal of cell biology*, vol. 172, no. 3, pp. 347–362, 2006.

[90] C. G. Bowsher and P. S. Swain, "Identifying sources of variation and the flow of information in biochemical networks," *Proceedings of the National Academy of Sciences*, vol. 109, no. 20, pp. E1320–E1328, 2012.

[91] A. Kaufmann and P. Philippsen, "Of bars and rings: Hof1-dependent cytokinesis in multiseptated hyphae of ashbya gossypii," *Molecular and cellular biology*, vol. 29, no. 3, pp. 771–783, 2009.

[92] N. R. Adames, P. L. Schuck, K. C. Chen, T. Murali, J. J. Tyson, and J. Peccoud, "Experimental testing of a new integrated model of the budding yeast start transition," *Molecular biology of the cell*, vol. 26, no. 22, pp. 3966–3984, 2015.

[93] D. J. Lew, N. J. Marini, and S. I. Reed, "Different g1 cyclins control the timing of cell cycle commitment in mother and daughter cells of the budding yeast s. cerevisiae," *Cell*, vol. 69, no. 2, pp. 317–327, 1992.

[94] D. Zenklusen, D. R. Larson, and R. H. Singer, "Single-rna counting reveals alternative modes of gene expression in yeast," *Nature structural & molecular biology*, vol. 15, no. 12, pp. 1263–1271, 2008.

[95] S. Luo, Z. Zhang, Z. Wang, X. Yang, X. Chen, T. Zhou, and J. Zhang, "Inferring transcriptional bursting kinetics from single-cell snapshot data using a generalized telegraph model," *Royal Society Open Science*, vol. 10, no. 4, p. 221057, 2023.

[96] S. Choubey, J. Kondev, and A. Sanchez, "Deciphering transcriptional dynamics in vivo by counting nascent rna molecules," *PLoS computational biology*, vol. 11, no. 11, p. e1004345, 2015.

[97] A. Maekiniemi, R. H. Singer, and E. Tutucci, "Single molecule mrna fluorescent in situ hybridization combined with immunofluorescence in s. cerevisiae: Dataset and quantification," *Data in brief*, vol. 30, p. 105511, 2020.

[98] F. C. Holstege, E. G. Jennings, J. J. Wyrick, T. I. Lee, C. J. Hengartner, M. R. Green, T. R. Golub, E. S. Lander, and R. A. Young, "Dissecting the regulatory circuitry of a eukaryotic genome," *Cell*, vol. 95, no. 5, pp. 717–728, 1998.

[99] H. A. Wösten, "Filamentous fungi for the production of enzymes, chemicals and materials," *Current opinion in biotechnology*, vol. 59, pp. 65–70, 2019.

[100] F. Guzmán-Chávez, R. D. Zwahlen, R. A. Bovenberg, and A. J. Driessen, "Engineering of the filamentous fungus penicillium chrysogenum as cell factory for natural products," *Frontiers in microbiology*, vol. 9, p. 2768, 2018.

[101] M. Lübeck and P. S. Lübeck, "Fungal cell factories for efficient and sustainable production of proteins and peptides," *Microorganisms*, vol. 10, no. 4, p. 753, 2022.

[102] J. Cha, M. Zhou, and Y. Liu, "Mechanism of the neurospora circadian clock, a frequency-centric view," *Biochemistry*, vol. 54, no. 2, pp. 150–156, 2015.

[103] T. Matsu-Ura, A. A. Dovzhenok, S. T. Coradetti, K. R. Subramanian, D. R. Meyer, J. J. Kwon, C. Kim, N. Salomonis, N. L. Glass, S. Lim, *et al.*, "Synthetic gene network with positive feedback loop amplifies cellulase gene expression in neurospora crassa," *ACS synthetic biology*, vol. 7, no. 5, pp. 1395–1405, 2018.

[104] W. Prathumpai, J. Gabelgaard, P. Wanchanthuek, P. Van de Vondervoort, M. De Groot, M. Mcintyre, and J. Nielsen, "Metabolic control analysis of xylose catabolism in aspergillus," *Biotechnology progress*, vol. 19, no. 4, pp. 1136–1141, 2003.

[105] B. Kendrick, *The fifth kingdom*. Hackett Publishing, 2017.

[106] E. Buxton, "Heterokaryosis, saltation and adaptation," *Plant pathology*, vol. 2, no. S 359, p. 405, 1960.

[107] C. Caten, "The mutable and treacherous tribe revisited," *Plant Pathology*, vol. 45, no. 1, pp. 1–12, 1996.

[108] L. W. Buss, *The evolution of individuality*, vol. 796. Princeton University Press, 2014.

[109] G. Pontecorvo, "Genetic systems based on hetero caryosis," in *Cold Spring Harbor Symposia on Quantitative Biology*, vol. 11, pp. 193–201, Cold Spring Harbor Laboratory Press, 1946.

[110] N. Samils, J. Oliva, and H. Johannesson, "Nuclear interactions in a heterokaryon: insight from the model neurospora tetrasperma," *Proceedings of the Royal Society B: Biological Sciences*, vol. 281, no. 1786, p. 20140084, 2014.

[111] C. Meunier, S. Hosseini, N. Heidari, Z. Maryush, and H. Johannesson, "Multilevel selection in the filamentous ascomycete neurospora tetrasperma," *The American Naturalist*, vol. 191, no. 3, pp. 290–305, 2018.

[112] E. Bastiaans, D. Aanen, A. Debets, R. Hoekstra, B. Lestrade, and M. Maas, "Regular bottlenecks and restrictions to somatic fusion prevent the accumulation of mitochondrial defects in neurospora," *Philosophical Transactions of the Royal Society B: Biological Sciences*, vol. 369, no. 1646, p. 20130448, 2014.

[113] A. A. Grum-Grzhimaylo, E. Bastiaans, J. van den Heuvel, C. Berenguer Millanes, A. J. Debets, and D. K. Aanen, "Somatic deficiency causes reproductive parasitism in a fungus," *Nature Communications*, vol. 12, no. 1, p. 783, 2021.

[114] J. Skejo, S. G. Garg, S. B. Gould, M. Hendriksen, F. D. Tria, N. Bremer, D. Franjević, N. W. Blackstone, and W. F. Martin, "Evidence for a syncytial origin of eukaryotes from ancestral state reconstruction," *Genome Biology and Evolution*, vol. 13, no. 7, p. evab096, 2021.

[115] L. L. Heaton, N. S. Jones, and M. D. Fricker, "A mechanistic explanation of the transition to simple multicellularity in fungi," *Nature communications*, vol. 11, no. 1, p. 2594, 2020.

[116] S. S. Schmieder, C. E. Stanley, A. Rzepiela, D. van Swaay, J. Sabotič, S. F. Nørrelykke, A. J. deMello, M. Aebi, and M. Künzler, "Bidirectional propagation of signals and nutrients in fungal networks via specialized hyphae," *Current Biology*, vol. 29, no. 2, pp. 217–228, 2019.

[117] L. Heaton, B. Obara, V. Grau, N. Jones, T. Nakagaki, L. Boddy, and M. D. Fricker, "Analysis of fungal networks," *Fungal Biology Reviews*, vol. 26, no. 1, pp. 12–29, 2012.

[118] G. Gerisch and U. Wick, "Intracellular oscillations and release of cyclic amp from dictyostelium cells," *Biochemical and biophysical research communications*, vol. 65, no. 1, pp. 364–370, 1975.

[119] D. B. Forger and C. S. Peskin, "A detailed predictive model of the mammalian circadian clock," *Proceedings of the National Academy of Sciences*, vol. 100, no. 25, pp. 14806–14811, 2003.

[120] D. Gonze, J. Halloy, J.-C. Leloup, and A. Goldbeter, "Stochastic models for circadian rhythms: effect of molecular noise on periodic and chaotic behaviour," *Comptes rendus biologies*, vol. 326, no. 2, pp. 189–203, 2003.

[121] M.-Y. Youn, I. Takada, Y. Imai, H. Yasuda, and S. Kato, "Transcriptionally active nuclei are selective in mature multinucleated osteoclasts," *Genes to Cells*, vol. 15, no. 10, pp. 1025–1035, 2010.

[122] J. T. Mika, P. E. Schavemaker, V. Krasnikov, and B. Poolman, "Impact of osmotic stress on protein diffusion in l actococcus lactis," *Molecular Microbiology*, vol. 94, no. 4, pp. 857–870, 2014.

[123] J. C. Dunlap and J. J. Loros, "Making time: conservation of biological clocks from fungi to animals," *Microbiology spectrum*, vol. 5, no. 3, pp. 5–3, 2017.

[124] C. H. Ko and J. S. Takahashi, "Molecular components of the mammalian circadian clock," *Human molecular genetics*, vol. 15, no. suppl_2, pp. R271–R277, 2006.

[125] A. Upadhyay, M. Brunner, and H. Herzel, "An inactivation switch enables rhythms in a neurospora clock model," *International journal of molecular sciences*, vol. 20, no. 12, p. 2985, 2019.

[126] J. Bellman, J. K. Kim, S. Lim, and C. I. Hong, "Modeling reveals a key mechanism for light-dependent phase shifts of neurospora circadian rhythms," *Biophysical Journal*, vol. 115, no. 6, pp. 1093–1102, 2018.

[127] A. E. Sgro, D. J. Schwab, J. Noorbakhsh, T. Mestler, P. Mehta, and T. Gregor, "From intracellular signaling to population oscillations: bridging size-and time-scales in collective behavior," *Molecular systems biology*, vol. 11, no. 1, p. 779, 2015.

[128] Z. Deng, S. Arsenault, C. Caranica, J. Griffith, T. Zhu, A. Al-Omari, H.-B. Schüttler, J. Arnold, and L. Mao, "Synchronizing stochastic circadian oscillators in single cells of neurospora crassa," *Scientific reports*, vol. 6, no. 1, pp. 1–18, 2016.

[129] G. Wang and C. S. Peskin, "Entrainment of a cellular circadian oscillator by light in the presence of molecular noise," *Physical Review E*, vol. 97, no. 6, p. 062416, 2018.

[130] S. E. Windner, A. Manhart, A. Brown, A. Mogilner, and M. K. Baylies, "Nuclear scaling is coordinated among individual nuclei in multinucleated muscle fibers," *Developmental cell*, vol. 49, no. 1, pp. 48–62, 2019.

[131] M. Dos Santos, S. Backer, B. Saintpierre, B. Izac, M. Andrieu, F. Letourneur, F. Relaix, A. Sotiropoulos, and P. Maire, "Single-nucleus rna-seq and fish identify coordinated transcriptional activity in mammalian myofibers," *Nature communications*, vol. 11, no. 1, p. 5102, 2020.